Radioactive Decay: Microscopic Theory

4

Abstract An unstable nucleus has excess energy and can make a transition to a more stable state through a variety of means, each subject to quantum-mechanical and energy restrictions. For diagnostic and therapeutic nuclear medicine, the transitions of major interest are those in which an α particle, β particle (electron or positron), or γ ray are emitted. Subsidiary atomic radiations or processes (electron capture, characteristic X-rays, internal conversion (IC) electrons, and Auger/Coster–Krönig electrons) are consequences of nuclear transitions. This chapter looks at the three nuclear decay schemes highlighted above. Quantum tunneling is derived and used to explain the empirical characteristics of α decay. The Fermi theory of β decay will be fundamental to understanding this type of transition and will be derived in order to predict energy spectra and allowable/forbidden transitions. Within that development, the weak interaction, which is fundamental to the existence of nuclear medicine, is introduced. Electromagnetic transitions, resulting in the emission of γ rays or IC electrons, are introduced and the theory behind them developed.

Contents

4.1 Introduction and History

The previous chapter described the characteristics that make a given nucleus stable or unstable. Clearly, for nuclear medicine purposes, one is interested in unstable or radioactive nuclei. The instability of a nucleus can be manifest in a number of ways. For example, a nucleus may be unstable to the emission of positrons or electrons (β decay) due to its having excessive numbers of protons or neutrons, respectively, for its mass. This particular instability reflects an imbalance between the Coulomb and symmetry terms of the Weizsäcker formula for the binding energy. Should the sum of the binding energies of two protons and two neutrons in a nucleus be less than the binding energy of the ^{4}He nucleus (α particle), then that nucleus is unstable to α decay, in which the α particle

B.J. McParland, *Nuclear Medicine Radiation Dosimetry*,
DOI 10.1007/978-1-84882-126-2_4, © Springer-Verlag London Limited 2010

can "quantum tunnel" through the nuclear Coulomb barrier and escape. Excited nuclei, which can be thought of as having high angular momentum or with nucleons excited to higher orbitals, can de-excite through the emission of quanta (γ decay) or by the direct transfer of nuclear energy to an atomic electron, a process known as internal conversion (IC). While there are other exotic, but rarer, cases of decay such as the spontaneous emission of a single proton or neutron or, for particularly heavy nuclei, spontaneous fission, the only radioactive decays of practical interest to diagnostic and therapeutic nuclear medicine are those of α, β and γ decay, and IC.[1]

The study of radioactivity began with Becquerel's original serendipitous discovery in 1896 of the phenomenon, using photographic emulsion as the radiation detector (Martins 1997). The stimulus for Becquerel's experimental work had been Röntgen's observation of the phosphorescence of some materials exposed to X-rays and Becquerel sought to determine if phosphorescent substances emitted similar radiations. He selected uranium as a suitable element for study due to its atomic absorption and emission spectra and noted that a uranium salt contained within an opaque covering and accidentally placed upon a photographic emulsion caused darkening of the emulsion due to radiations able to penetrate the optical cover. Even around this time, it had been noted that these radiations did not vary with time (which we would now recognize as reflecting a long half-life) and could ionize air. Shortly afterwards, the Curies began investigating the radioactivity associated with various minerals containing uranium and thorium. In particular, they determined that pitchblende was more radioactive than the chemical content of uranium or thorium would have allowed. Hypothesizing that this was due to the presence of other, but unknown, radioactive substances, the Curies chemically isolated two radioactive elements from pitchblende which they called polonium and radium. Although present in pitchblende in just trace amounts, their specific activities were some six orders-of-magnitude greater than that of uranium.

At about the same time, Rutherford, whilst at McGill University in Montréal, was also studying the radiations emitted by uranium (Wilson 1983). He had recognized that the photographic emulsion used by Becquerel was an inefficient detector and noted, as did the Curies, that the radiation-induced ionization of air had a faster response than emulsion, could be measured immediately and, moreover, could be easily quantified. This change of detector type aided Rutherford's discovery of the emanation of two types of radiation from samples of uranium compounds (uranium metal, uranium nitrate, uranium oxide, and uranium potassium sulfate) by measuring the changes in the detected ionization caused by them following their transmission through increasing thicknesses of aluminium foil. The decrease in ionization with increasing foil thickness was, at first, monotonic and indicated simple absorption of the radiation. However, the reduction in ionization with foil thickness eventually became limited until, when further foils were added, the radiation intensity began to decrease more rapidly again. Rutherford's original transmission data are shown in Fig. 4.1 in which the transmission of the ionizing radiations from uranium oxide through aluminium is plotted. The transmission of radiation dropped rapidly with absorber thickness to about 20 μm of aluminium and then remained nearly constant up to a thickness of 60 μm. This feature indicated a readily absorbed radiation, termed α radiation by Rutherford, and a more penetrating radiation, that he termed β radiation.[2] As will be seen in Chap. 7, the shorter range of the α rays indicates that they are strongly ionizing particles and are, in fact, absorbed in only a few cm of air or a few μm of soft tissue.

The nature of the α radiation was next studied through its magnetic deflection, which was first achieved by Rutherford using a 0.6 T magnetic field. This demonstrated that α radiation was massive, positively-charged particles. Further measurements of electric charge and mass suggested that these were doubly-ionized helium atoms (He^{++}). This nature of the α particle was finally confirmed by Rutherford and Royds (Rutherford and Royds 1909) in an elegant and simple experiment using an apparatus consisting of a

[1]There are other emissions often associated with radioactive decay, such as characteristic X-rays and Auger electrons. These, however, are due to relaxation processes following an excitation of the atom and are more properly considered in Chap. 6.

[2]It is interesting to note that when he repeated the experiment using thorium nitrate rather than uranium, Rutherford detected a third, more penetrating type of radiation. Thus, it would seem that this observation, now recognized to be of γ radiation, preceded the usually-credited discovery by Villard (Gerward 1999).

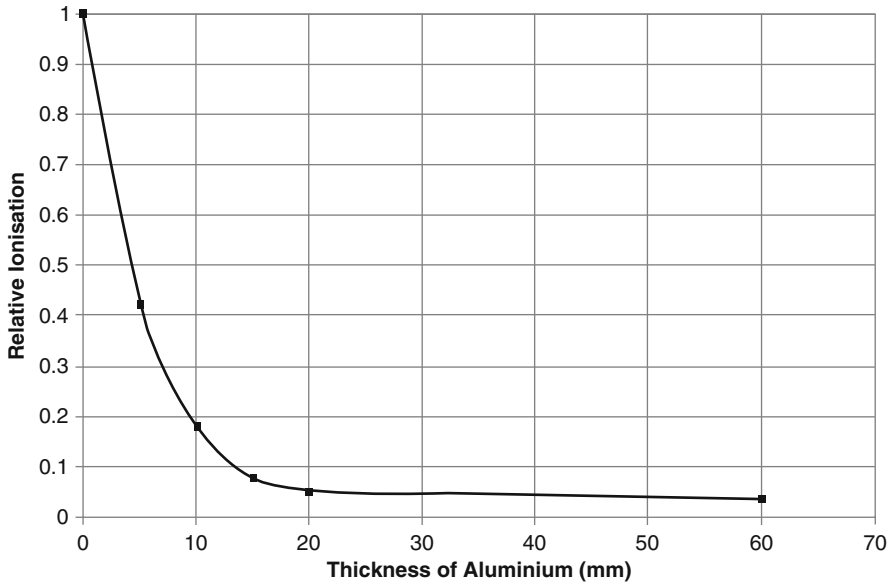

Fig. 4.1 Plot of Rutherford's original measurements of the ionization from uranium oxide following absorption by aluminium. Data points are the original data; the line is provided for guidance

volume of radon gas contained within a capillary tube with thin walls and encapsulated within an evacuated chamber. Radon is the radioactive daughter product of the α decay of radium and the α particles emitted by it came to rest within the thin wall. The He^{++} captured electrons from within the wall to form neutral atoms of helium gas which diffused through the wall into the surrounding chamber. After a sufficient amount of helium gas was formed, it was compressed and, via an electric discharge, demonstrated the characteristic emission spectrum that confirmed its nature.

Measurements by the Curies of the trajectories of the β component through a magnetic field demonstrated that it was made up of light, negatively-charged particles and studies of the β particle trajectories in combined magnetic and electric fields demonstrated that it had a charge-to-mass ratio e/m equal to that of the electron. The most elegant proof that the β particle is indeed an electron was provided by the measurements by Goldhaber and Scharff-Goldhaber (1948) of slow β particles stopped within a lead target. A low β particle energy was required to ensure that it did not eject the K-shell electron and the Pauli exclusion principle would, had β particles and electrons be the same, forbid the capture of the β particle into the full L and K shells. Had β particles and electrons been different, the β particle would cascade through orbitals, emitting X-rays, until it was eventually captured. The fact that no characteristic X-rays were detected gave unambiguous evidence of the identity of the β particle as an electron. The nuclear, rather than atomic, origin of the β particle is evident from its having a kinetic energy of a couple of MeV or less and which, from the uncertainty principle, $\Delta p\,\Delta x \approx \hbar c/2 \approx 100\,\text{MeV} \bullet \text{fm}$ and the fact that the nuclear diameter is of the order of a few fm. Nuclear β decay is the emission of a fast electron (e^-) or positron (e^+) resulting in a daughter nucleus with an atomic number of one greater or one less than the parent, respectively.[3] Associated with these is the process of electron capture in which the overlap of the wavefunctions of an atomic electron and a nuclear proton result in the capture of the electron by the proton leading to a daughter nucleus with an atomic number of one less than the parent. As such, these transitions occur between isobars and a chain of β decays will follow the mass parabola. Electron capture is a process related to β decay in which an atomic electron is "captured" by a nuclear proton to decrease the atomic number of the nucleus by one.

As noted earlier, the emission of γ-rays in nuclear decay was probably first detected from thorium by Rutherford in about 1898 but has not been greatly recognized historically as such. Villard is customarily

[3]While the term "β decay" is also sometimes used to refer to the capture of an atomic orbital electron by a proton-rich nucleus, it does not include internal conversion, a radioactive process described in the context of γ decay.

assigned recognition as the discoverer of γ rays through his measurements of the deflection by a magnetic field of the radiations emitted from radium and using photographic plates as detectors (Gerward 1999). For example, in one experiment, a collimated beam from a radium source was incident to two collinear photographic plates for which a magnetic field was placed between the collimator and the first plate to deflect the beam. The first plate demonstrated two distinctive traces of a sharp line, denoting a beam unaffected by the magnetic field, superimposed upon a second, more diffuse, trace caused by the magnetic deflect. On the second plate, which was further away, there was only the sharp trace as the charged particles creating the diffuse pattern in the first plate had been completely deflected. The undeflected beam had traversed 10 mm of glass without noticeable attenuation and even inserting a 300 μm-thick lead foil had only a slight affect upon this penetrating beam. Villard associated this penetrating and electrically-neutral radiation with Röntgen's X-rays but he did not call them γ rays. This assignation does not seem to have happened until about 1903 and was apparently due to Rutherford. Experimental study of γ rays in the early twentieth century was not as intense as were those of α and β particles and it was not until 1914 that Rutherford and Andrade established the electromagnetic nature of γ rays. Following von Laue's use in 1912 of a crystal as a space diffraction grating for X-rays, Rutherford and Andrade repeated the same approach to measure the wavelength of γ rays. Compton's later work on the elastic scatter of photons from electrons extended the wave-point duality of light photons to γ rays.

Radioactive decay is, obviously, the reason that the discipline of nuclear medicine exists. Hence, we will look at the theoretical principles behind the three major radioactive modes of interest to nuclear medicine: α decay, β decay (including electron capture) and γ emission (including IC).

4.2 α Decay

4.2.1 Introduction

α emission is a two-body process:

$$ {}^{A}_{Z}X \rightarrow {}^{A-4}_{Z-2}Y + {}^{4}_{2}He \tag{4.1} $$

The final state is that of two heavy charged particles in motion, which has significant dosimetric consequences in that, first, both rapidly lose kinetic energy to the medium in a small volume as they slow down leading to a high absorbed dose. The second consequence is that the daughter nucleus is frequently left in an excited state resulting in the subsequent emission of γ rays or conversion electrons. α decay is intrinsically linked to the high binding energy (28.3 MeV) of the α particle. Hence, a nucleus will be unstable to α decay if the sum of the binding energies of a pair or protons and a pair of neutrons within it are less than the α particle binding energy. As a result, the α emitting parent nucleus is necessarily heavy as shown in Fig. 4.2.[4] Early understanding of α decay was confounded by the failure of classical theory to provide an explanation of it even occurring – a failure shown with considerable power by consideration of the magnitude of the nuclear Coulomb potential, as shown in Fig. 4.3. Within the nucleus, the α particle is subject to the conflicting attractive strong nuclear force and the repulsive Coulomb force from the nuclear protons. Beyond the nuclear radius R_N, where the strong nuclear force is negligible, the α particle will be subject solely to the nuclear Coulomb potential. For a nucleus with atomic number Z, the Coulomb potential is,

$$ U(r) = 2\alpha\hbar c\frac{Z_Y}{r} \quad r > R_N \tag{4.2} $$

where the factor of 2 is the atomic number of the α particle. It should be noted that that the atomic number is that of the nucleus following α emission.

The Coulomb potential experienced by an α particle at this nuclear radius for a nucleus with $Z \approx 80$ and $A \approx 200$ is about 33 MeV and a classical dilemma arises from the fact that experimental measurements of the kinetic energies of the emitted α particles are typically of the order of only a few MeV, as shown

[4]Note that Fig. 4.2 shows the kinetic energy of the emitted α particle as a function of the parent nucleus' mass; the probability of the α particle occurring at all is not considered in that plot but is the focus of a later subsection.

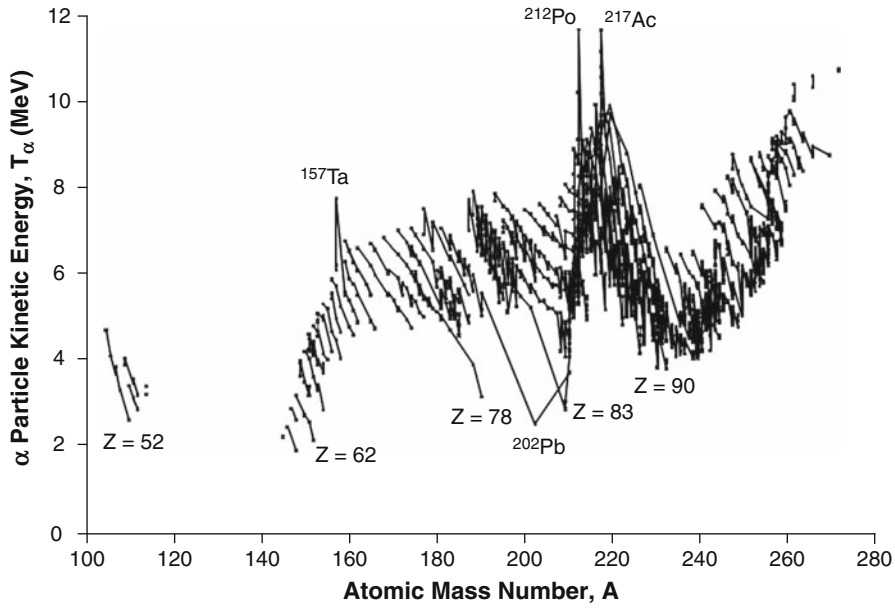

Fig. 4.2 Plot of α particle kinetic energy as a function of atomic mass number for elements between Z = 52 (tellurium) and Z = 110 (darmstadtium). Lines join isotopes. Plot is derived from data from a National Nuclear Data Center (2008) database

in Fig. 4.2.[5] Over the 2,076 α emissions represented in this figure, the mean α particle kinetic energy is 6.1 MeV, with a minimum of 2.55 MeV for ^{202}Pb and a maximum of 11.66 MeV for ^{212}Po.

4.2.2 Kinematics of α Emission

4.2.2.1 Kinetic Energy of the α Particle

The energy released in the α-emission of (4.1) is,

$$Q_\alpha = m_X - (m_Y + m_\alpha) \tag{4.3}$$

where the lower-case m's are the nuclear masses and where Q_α must be positive (i.e., (4.1) is exoergic) in order for the α decay to proceed. Both nuclei are assumed to be in their ground states (the fine structure in α particle energy spectra as a result of excited states is discussed in the following subsection) so that the

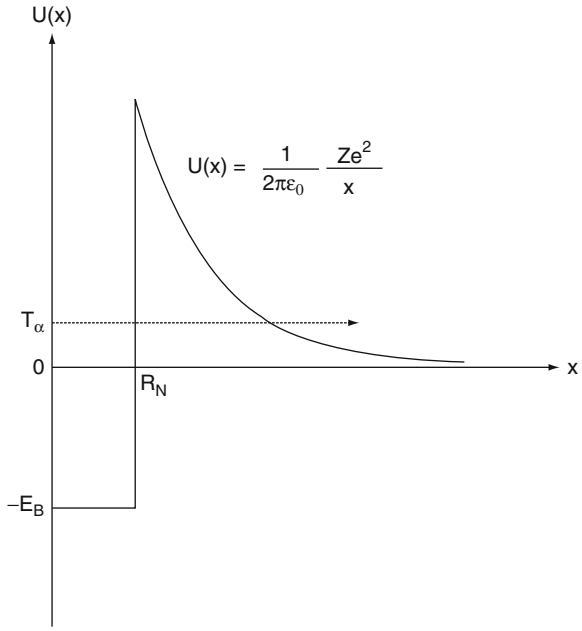

Fig. 4.3 Potential energy of a heavy nucleus for an α particle and a typical kinetic energy of an emitted α particle. Abscissa is given as x rather than r as this is a one-dimensional potential

Q_α is distributed amongst the kinetic energies of the α particle and the daughter nucleus. Because of the much larger mass of the daughter nucleus and the simultaneous conservation of linear momentum and

[5]Gamow (1928) reported that Rutherford had used the Thomson "plum pudding" model of the nucleus in an attempt to avoid this dilemma: the α particle within the nucleus was electrically-neutral as it carried two electrons. This allowed it to travel through the barrier unheeded; once out of the nucleus, the α particle somehow shed these two electrons. This hypothesis was invalidated with the demise of the Thomson model.

energy, virtually all of Q_α is taken up by the kinetic energy of the α particle. The conservation of energy is,

$$m_X = m_Y + m_\alpha + T_Y + T_\alpha. \tag{4.4}$$

As the kinetic energy of the α particle is only a few MeV, nonrelativistic kinematics are applicable and the conservation of energy can be rewritten as,

$$\frac{p_Y^2}{2m_Y} + \frac{p_\alpha^2}{2m_\alpha} = Q_\alpha. \tag{4.5}$$

Using the conservation of momentum, the recoil kinetic energy of the daughter nucleus is then obtained,

$$T_Y = \frac{Q_\alpha}{\left(1 + \frac{m_Y}{m_\alpha}\right)}. \tag{4.6}$$

As the atomic mass of the daughter nucleus is of the order of 200 or more, it is evident that only about 2% of the available energy will appear as the recoil kinetic energy of the daughter nucleus. Hence, for practical purposes, we can ignore the recoil kinetic energy whilst calculating for the α-particle kinetic energy.[6] Equation (4.6) can then be approximated by,

$$T_\alpha \approx Q_\alpha. \tag{4.7}$$

Assuming that the parent and daughter nuclei are both in their ground states, then using results from Chap. 3 and neglecting the atomic electron binding energies, the α particle kinetic energy corresponding to a parent nucleus of atomic number Z and atomic mass A can be written as,

$$\begin{aligned} T_\alpha(A,Z) &\approx Q_\alpha \\ &= M(A,Z) - M(A-4,Z-2) - M(4,2). \end{aligned} \tag{4.8}$$

where the atomic mass is given by $M(A, Z) = ZM_H + (A - Z)m_n - B(A, Z)$. The α particle kinetic energy can thus be given in terms of the nuclear binding energies of the parent, daughter, and the α particle,

$$\begin{aligned} T_\alpha(A,Z) &= B(4,2) + B(A-4,Z-2) - B(A,Z) \\ &= B(A-4,Z-2) - B(A,Z) + 28.3\,\text{MeV}. \end{aligned} \tag{4.9}$$

where the numerical value of the α particle binding energy has been inserted. The binding energies of the parent and daughter nuclei can be estimated using the Weizsäcker semi-empirical formula,

$$\begin{aligned} B(A,Z) = a_{Vol}A - a_{Surf}A^{2/3} - a_{Coul}\frac{Z^2}{A^{1/3}} \\ - a_{Sym}\frac{(A-2Z)^2}{A} - \delta(A,Z). \end{aligned}$$

Substituting this into (4.9) gives,

$$\begin{aligned} T_\alpha(A,Z) &= -4a_{Vol} - a_{Surf}\left((A-4)^{2/3} - A^{2/3}\right) \\ &\quad - a_{Coul}\left(\frac{(Z-2)^2 - Z^2}{(A-4)^{1/3} - A^{1/3}}\right) \\ &\quad - a_{Sym}\left(\frac{(A-4-2(Z-2))^2}{A-4} - \frac{(A-2Z)^2}{A}\right) \\ &\quad - \delta(A-4,Z-2) + \delta(A,Z) + 28.3\,\text{MeV} \\ &= -4a_{Vol} - a_{Surf}\left((A-4)^{2/3} - A^{2/3}\right) \\ &\quad - a_{Coul}\left(\frac{(Z-2)^2}{(A-4)^{1/3}} - \frac{Z^2}{A^{1/3}}\right) \\ &\quad - a_{Sym} - \left(\frac{(A-2Z)^2}{A-4} - \frac{(A-2Z)^2}{A}\right) \\ &\quad - \delta(A-4,Z-2) + \delta(A,Z) + 28.3\,\text{MeV} \end{aligned} \tag{4.10}$$

As α decay occurs only for heavy nuclei for which $A \gg 1$ and $Z \gg 1$, the expression can be simplified by approximating the surface, Coulomb and symmetry terms with,

$$\left((A-4)^{2/3} - A^{2/3}\right) \approx -\frac{8}{3}A^{-1/3}$$

[6] While this is acceptable for analyzing the kinematics of α decay, we cannot neglect the energy of the recoil nucleus in a dosimetry evaluation. Although its kinetic energy is small, the range of the recoil nucleus is also small, meaning that the recoil energy is deposited within a very small volume leading to a high absorbed dose. Hence, α-emitting radionuclides are important in therapeutic nuclear medicine should the α particle-emitting radiopharmaceutical be covalently-bound to the nuclear deoxyribonucleic acid.

$$\left(\frac{(Z-2)^2}{(A-4)^{1/3}}-\frac{Z^2}{A^{1/3}}\right)\approx 4Z^2A^{-1/3}\left(\frac{\frac{1}{Z}-\frac{1}{3A}}{1-\frac{4}{3A}}\right)$$

$$\left(\frac{(A-2Z)^2}{A-4}-\frac{(A-2Z)^2}{A}\right)\approx 4\left(1-\frac{2Z}{A}\right)^2.$$

Recalling that the paired nucleon term is non-zero only for odd–odd and even–even nuclei, it is retained as an explicit item. These results give,

$$\begin{aligned}T_\alpha(A,Z) = &-4a_{Vol}+\frac{8}{3}a_{Surf}A^{-1/3}\\ &+4a_{Coul}Z^2A^{-1/3}\left(\frac{\frac{1}{Z}-\frac{1}{3A}}{1-\frac{4}{3A}}\right)\\ &-4a_{Sym}\left(1-2Z/A\right)^2-\delta(A,Z)\\ &+\delta(A-4,Z-2)+28.3\,\text{MeV}.\end{aligned}\tag{4.11}$$

The fact that this expression is an approximation will not lead to an exact result of T_α but, even so, the accuracy is more than sufficient to predict the α particle kinetic energies for dosimetry purposes. For example, using (4.11) (and the values of a_{Vol}, a_{Surf}, a_{Coul}, a_{Sym}, and δ) to predict the kinetic energy of α particles emitted by ^{210}Po will yield a value of 4.26 MeV whereas the experimentally-determined value is about 4.52 MeV. This result can also be used to predict the systematics of α particle kinetic energy of Fig. 4.2. For example, for a given isotope, the α particle kinetic energy decreases with increasing atomic mass[7] which can be predicted from,

$$\begin{aligned}\Delta T_\alpha(A,A+1,Z) &= T_\alpha(A,Z)-T_\alpha(A+1,Z)\\ &=\frac{8}{3}a_{Surf}\left(A^{1/3}-(A+1)^{1/3}\right)\\ &\quad+4a_{Coul}Z^2\left(A^{1/3}\left(\frac{\frac{1}{Z}-\frac{1}{3A}}{1-\frac{4}{3A}}\right)\right.\\ &\quad\left.-(A+1)^{1/3}\left(\frac{\frac{1}{Z}-\frac{1}{3(A+1)}}{1-\frac{4}{3(A+1)}}\right)\right)\\ &\quad-8a_{Sym}Z\left(\frac{1}{A+1}-\frac{1}{A}\right)\\ &\quad-\delta(A,Z)+\delta(A+1,Z)\\ &\quad+\delta(A-4,Z-2)-\delta(A-3,Z)\end{aligned}\tag{4.12}$$

which is a negative quantity.

4.2.2.2 Energy Spectrum: Fine Structure

The discussion of the kinematics of α emission has, so far, neglected any additional energy channels which can alter Q_α. Experimentally, however, it has been observed that the α particles emitted from a single nuclide can have multiple energies occurring with different probabilities. An example is shown in Fig. 4.4 for ^{215}Po. The presence of multiple α particle kinetic energies means, from the definition of Q_α and the approximation of T_α by Q_α, that the nuclear masses of the parent and/or daughter must be multivalued, reflecting the excited states of the daughter ^{211}Pb nucleus. However, the relative intensity of each α emission (i.e., the relative probability of an α particle with that particular kinetic energy being emitted) indicates a variable "transparency" of the Coulomb barrier which impedes α emission.[8] For this example of ^{215}Po, this transparency varies by over five orders-of-magnitude.

4.2.3 Barrier Penetration

4.2.3.1 Introduction

The half-lives of α emissions vary from about 0.3 μs for ^{212}Po to 4.5×10^9 y for ^{238}U, an astonishing variation of some 23 orders-of-magnitude. This fact, combined with simple consideration of the kinematics of α emission, leads quickly to a conclusion that there

[7] This trend is broken for the conditions $209 < A < 213$ which is related to the magic proton and neutron numbers of 82 and 126, respectively.

[8] Note that, despite the different intensities among the α particles emitted, the decay probability per unit time for each is the same.

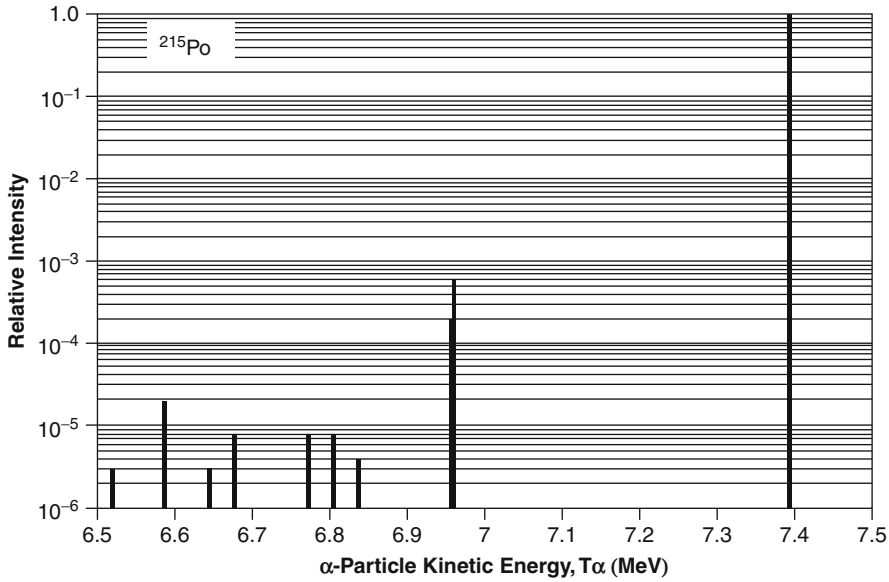

Fig. 4.4 α particle kinetic energy spectrum for ^{215}Po. Plot derived from data from National Nuclear Data Center (2008) data

exists a barrier impeding the emission of the α particle. As the kinetic energy of the α particle is a few MeV, corresponding to a speed of the order of 10^7 m/s, and the radius of a heavy nucleus is of the order of about 10 fm, the α particle should need only 10^{-21}s to traverse the nucleus. As the measured half-lives are much larger than this, there clearly must be some nature of a barrier to α emission, as was shown Fig. 4.3. However, in classical mechanics, the barrier would be completely impervious to the α particle. Gamow (1928) and, independently, Condon and Gurney (1928) showed that α emission could be explained by the quantum-mechanical tunneling of the α particle through this barrier. The solution to this problem is determined by first studying the simple case of a one-dimensional barrier.

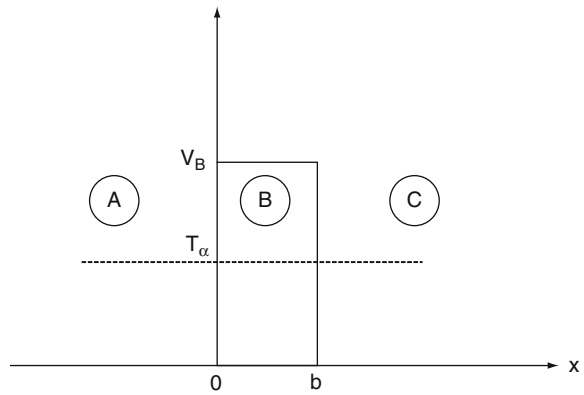

Fig. 4.5 One-dimensional potential barrier of height V_B and width b. Region A corresponds to the interior of the nucleus, B to the barrier and C to the exterior of the nucleus. The α particle has kinetic energy T_α

4.2.3.2 One-Dimensional Rectangular Barrier

The simplest potential barrier to model is the one-dimensional rectangular one of Fig. 4.5. As it is one-dimensional, angular momentum is necessarily excluded. The potential barrier is of height V_B and width b and the α particle is treated as a wave within the nucleus (Zone A) and incident to the barrier from the left. The time-independent one-dimensional Schrödinger equation is,

$$\frac{d^2\Psi}{dx^2} + \frac{2m_\alpha}{(\hbar c)^2}(T_\alpha - V(x))\Psi = 0 \tag{4.13}$$

where

$$\begin{aligned} V(x) &= V_B \quad 0 < x < b \\ &= 0 \quad \text{elsewhere.} \end{aligned} \tag{4.14}$$

Recall that the units of the α particle rest mass and its three-vector momentum are that of energy and the $\hbar c$ factor is required in the denominator to make the

equation dimensionally correct. Outside the barrier, in Zones A and C, (4.13) is,

$$\frac{d^2\Psi}{dx^2} + \frac{2m_\alpha T_\alpha}{(\hbar c)^2}\Psi = 0 \tag{4.15}$$

This is rewritten using the reduced de Broglie wavelength of the α particle,

$$\lambda\!\!\!^{-} = \frac{\hbar c}{\sqrt{2m_\alpha T_\alpha}} \tag{4.16}$$

$$\frac{d^2\Psi}{dx^2} + \frac{1}{\lambda\!\!\!^{-2}}\Psi = 0. \tag{4.17}$$

In Zone A, the solution to (4.17) is,

$$\Psi_A(x) = w_{A1}e^{i\frac{x}{\lambda\!\!\!^{-}}} + w_{A2}e^{-i\frac{x}{\lambda\!\!\!^{-}}} \quad x < 0 \tag{4.18}$$

and, similarly for Zone C,

$$\Psi_C(x) = w_{C1}e^{i\frac{x}{\lambda\!\!\!^{-}}} \quad b < x \tag{4.19}$$

where there is no reflected wave from Zone C, i.e., $w_{C2} = 0$. Within the rectangular barrier (Zone B), the Schrödinger equation is,

$$\frac{d^2\Psi}{dx^2} + \frac{2m_\alpha(T_\alpha - V_B)}{(\hbar c)^2}\Psi = 0 \quad 0 < x < b. \tag{4.20}$$

Since $T_\alpha < V_B$,

$$\frac{d^2\Psi}{dx^2} - \frac{2m_\alpha|T_\alpha - V_B|}{(\hbar c)^2}\Psi = 0 \tag{4.21}$$

with the solution,

$$\Psi_B(x) = w_{B1}e^{k_\alpha x} + w_{B2}e^{-k_\alpha x} \tag{4.22}$$

where,

$$k_\alpha = \frac{\sqrt{2m_\alpha|T_\alpha - V_B|}}{\hbar c}. \tag{4.23}$$

The probability of the wave tunneling through the barrier is defined as the transmission given by the ratio of the squared amplitudes of the wavefunction incident to and exiting the barrier,

$$\Im = \frac{|w_{C1}|^2}{|w_{A1}|^2}. \tag{4.24}$$

To solve for $\Im$, the amplitudes w_{A1} and w_{C1} are calculated in terms of the amplitudes w_{B1} and w_{B2}. The remainder of the amplitudes are determined by the boundary conditions which require that the functions and their first-derivatives be continuous at the boundaries of the potential:

$$\Psi_A(0) = \Psi_B(0) \tag{4.25}$$

$$\frac{d\Psi_A(0)}{dx} = \frac{d\Psi_B(0)}{dx} \tag{4.26}$$

$$\Psi_B(b) = \Psi_C(b) \tag{4.27}$$

$$\frac{d\Psi_B(b)}{dx} = \frac{d\Psi_C(b)}{dx}. \tag{4.28}$$

Equations (4.25) and (4.26) give,

$$w_{A1} + w_{A2} = w_{B1} + w_{B2} \tag{4.29}$$

$$\frac{i}{\lambda\!\!\!^{-}}(w_{A1} - w_{A2}) = k_\alpha(w_{B1} - w_{B2}). \tag{4.30}$$

From which, w_{A1} and w_{A2} can be solved,

$$w_{A1} = \frac{w_{B1}(1 - ik_\alpha\lambda\!\!\!^{-}) + w_{B2}(1 + ik_\alpha\lambda\!\!\!^{-})}{2} \tag{4.31}$$

$$w_{A2} = \frac{w_{B1}(1 + ik_\alpha\lambda\!\!\!^{-}) + w_{B2}(1 - ik_\alpha\lambda\!\!\!^{-})}{2}. \tag{4.32}$$

Equations (4.27) and (4.28) give,

$$w_{B1}e^{k_\alpha b} + w_{B2}e^{-k_\alpha b} = w_{C1}e^{i\frac{b}{\lambda\!\!\!^{-}}} \tag{4.33}$$

and

$$k_\alpha\left(w_{B1}e^{k_\alpha b} - w_{B2}e^{-k_\alpha b}\right) = \frac{i}{\lambda\!\!\!^{-}}w_{C1}e^{i\frac{b}{\lambda\!\!\!^{-}}}. \tag{4.34}$$

Solving for w_{B1} and w_{B2},

$$w_{B1} = \frac{w_{C1}}{2} e^{-k_\alpha b\left(1 - i/k_\alpha \hat{\lambda}\right)} \left(1 + \frac{i}{k_\alpha \hat{\lambda}}\right) \tag{4.35}$$

$$w_{B2} = \frac{w_{C1}}{2} e^{k_\alpha b\left(1 + i/k_\alpha \hat{\lambda}\right)} \left(1 - \frac{i}{k_\alpha \hat{\lambda}}\right). \tag{4.36}$$

For convenience, the reciprocal of $\Im$ is calculated,

$$\frac{1}{\Im} = \left(\frac{w_{A1}}{w_{C1}}\right)\left(\frac{w_{A1}}{w_{C1}}\right)^*. \tag{4.37}$$

Substituting (4.35) and (4.36) into (4.31) gives,

$$\begin{aligned}
\frac{w_{A1}}{w_{C1}} &= \frac{e^{-k_\alpha b\left(1 - \frac{i}{k_\alpha \hat{\lambda}}\right)}\left(1 + \frac{i}{k_\alpha \hat{\lambda}}\right)(1 - ik_\alpha \hat{\lambda}) + e^{k_\alpha b\left(1 + i/k_\alpha \hat{\lambda}\right)}\left(1 - \frac{i}{k_\alpha \hat{\lambda}}\right)(1 + ik_\alpha \hat{\lambda})}{4} \\
&= \frac{e^{ib/\hat{\lambda}}}{4} e^{-k_\alpha b}\left(1 + \frac{i}{k_\alpha \hat{\lambda}}\right)(1 - ik_\alpha \hat{\lambda}) + e^{k_\alpha b}\left(1 - \frac{i}{k_\alpha \hat{\lambda}}\right)(1 + ik_\alpha \hat{\lambda}) \\
&= e^{ib/\hat{\lambda}}\left(\frac{1 - (k_\alpha \hat{\lambda})^2}{k_\alpha \hat{\lambda}}\right)\left(\cosh k_\alpha b - \frac{i}{2}\sinh k_\alpha b\right) \\
&= \frac{e^{ib/\hat{\lambda}}}{2}\left(\frac{1 - (k_\alpha \hat{\lambda})^2}{k_\alpha \hat{\lambda}}\right)\sinh k_\alpha b\left(2\coth(k_\alpha b) - i\right).
\end{aligned} \tag{4.38}$$

It follows that,

$$\begin{aligned}
\frac{1}{\Im} &= \left(\frac{w_{A1}}{w_{C1}}\right)\left(\frac{w_{A1}}{w_{C1}}\right)^* \\
&= \frac{1}{4}\left(\frac{1 - (k_\alpha \hat{\lambda})^2}{k_\alpha \hat{\lambda}}\right)^2 \left(1 + 4\coth^2 k_\alpha b\right)\sinh^2 k_\alpha b \\
&= \frac{\left(V_B/2T_\alpha\right)^2}{\left(V_B/T_\alpha\right) - 1}\left(1 + 4\coth^2 k_\alpha b\right)\sinh^2 k_\alpha b \\
&= \frac{\left(V_B/2T_\alpha\right)^2}{\left(V_B/T_\alpha\right) - 1}\left(1 + 4\coth^2 k_\alpha b\right)\sinh^2 k_\alpha b \\
&\approx 1.94\left(1 + 4\coth^2 k_\alpha b\right)\sinh^2 k_\alpha b.
\end{aligned} \tag{4.39}$$

where a barrier height of 33 MeV and a kinetic energy of 5 MeV have been assumed in order to obtain the numerical result. Determining the product $k_\alpha b$ requires an estimation of the width of the barrier, b. To obtain this, replace the rectangular barrier with the Coulomb barrier as shown in Fig. 4.6 (with the attractive nuclear potential treated as a well potential) and use,

$$2Z\frac{\alpha\hbar c}{R_N + b} = T_\alpha. \tag{4.40}$$

Solving for b,

$$b = 2Z\left(\frac{\alpha\hbar c}{T_\alpha}\right) - R_N. \tag{4.41}$$

Using the previous example of $Z = 80$ and $R_N = 7$ fm, we calculate that for a 5 MeV α particle $b \approx 40$ fm. Hence, for $V_B = 33$ MeV, we have $k_\alpha \approx 2.3$ fm^{-1} leading to $bk_\alpha \approx 92$. For this value, approximations to the hyperbolic trigonometric functions can be used,

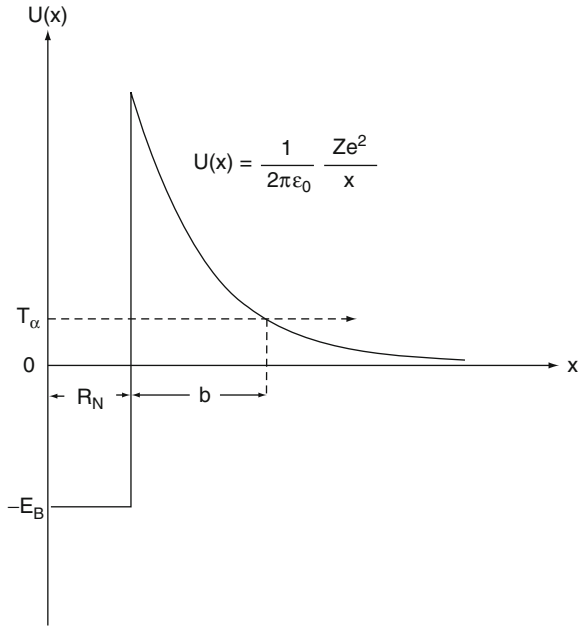

Fig. 4.6 Estimation of the barrier width for simple one-dimensional rectangular barrier calculation

$$\left(1+4\coth^2 k_\alpha b\right) = 1+\left(\frac{2\cosh k_\alpha b}{\sinh k_\alpha b}\right)^2$$
$$= 1+\left(2\frac{\left(e^{k_\alpha b}+e^{-k_\alpha b}\right)}{\left(e^{k_\alpha b}-e^{-k_\alpha b}\right)}\right)^2 \approx 5$$

and

$$\sinh^2 k_\alpha b = \frac{\left(e^{k_\alpha b}-e^{-k_\alpha b}\right)^2}{4}$$
$$\approx \frac{e^{2k_\alpha b}}{4}.$$

As the magnitude of the exponent is $\frac{1}{\Im} \approx 2.4\, e^{2k_\alpha b}$, the transmission is

$$\Im \approx 0.41\, e^{-2k_\alpha b}. \tag{4.42}$$

And, as the magnitude of the exponent is $e^{-2k_\alpha b} \approx 1.2\times 10^{-80}$, the transmission is simply written as,

$$\Im \approx e^{-2k_\alpha b}. \tag{4.43}$$

4.2.3.3 Three-Dimensional Barrier

Gamow Factor

The simple barrier model of the previous section is now extended to calculate the more realistic case of the penetration through the 1/r Coulomb barrier which is treated as a series of infinitesimal rectangular barriers with decreasing heights, as shown in Fig. 4.7. This now requires k_α to have a spatial dependence,

$$k_\alpha(x) = \frac{\sqrt{2m_\alpha|T_\alpha - V_B(x)|}}{\hbar c}. \tag{4.44}$$

Then, as $\Im \approx e^{-\frac{2x}{\hbar c}\sqrt{2m_\alpha|T_\alpha - V(x)|}}$, the differential transmission through a barrier of thickness dx is,

$$d\Im = 4e^{-\frac{2}{\hbar c}dx\sqrt{2m|T_\alpha - V(x)|}}. \tag{4.45}$$

Integrating this result gives,

$$\Im = 8e^{-2G} \tag{4.46}$$

where G is defined as the Gamow factor,

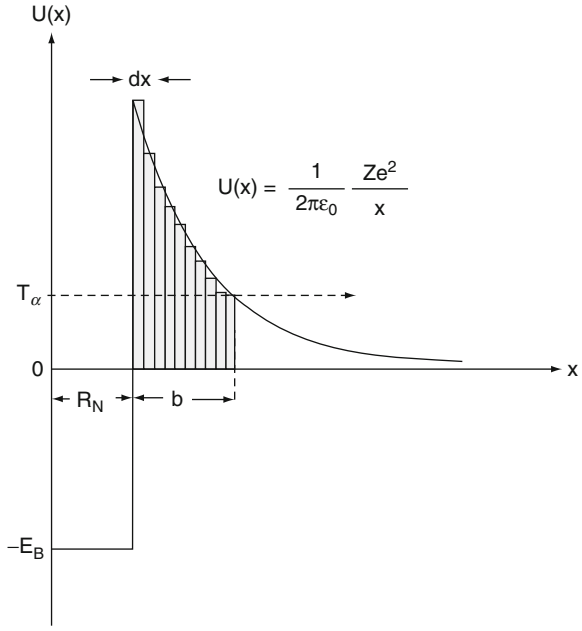

Fig. 4.7 Calculation of penetration through a one-dimensional Coulomb barrier

$$G = \frac{1}{\hbar c}\int_{R_N}^{b+R_N} dx\sqrt{2m_\alpha|T_\alpha - V_B(x)|}. \tag{4.47}$$

Hence, in order to determine the transmission, which by extension is the calculation of the decay rate constant and decay half-life, requires an explicit calculation of the Gamow factor. This is now performed for the three-dimensional case.

Changing the spatial variable from the one-dimensional x to the three-dimensional r, the Gamow factor is,

$$\begin{aligned} G &= \frac{1}{\hbar c}\int_{R_N}^{b+R_N} dr\sqrt{2m_\alpha|V_B(r) - T_\alpha|} \\ &= \frac{\sqrt{2m_\alpha}}{\hbar c}\int_{R_N}^{b+R_N} dr\sqrt{\left|2Z\left(\frac{\alpha\hbar c}{r}\right) - T_\alpha\right|} \\ &= \frac{\sqrt{2m_\alpha T_\alpha}}{\hbar c}\int_{R_N}^{b+R_N} dr\sqrt{\frac{R_N+b}{r} - 1} \\ &= \frac{\sqrt{R_N+b}}{\lambda}\int_{R_N}^{b+R_N} dr\sqrt{\frac{1}{r} - \frac{1}{R_N+b}}. \end{aligned} \tag{4.48}$$

The integral is solved via the change of variable,

$$\cos\theta = \sqrt{\frac{r}{R_N + b}}$$

which gives,

$$\sqrt{\frac{1}{r} - \frac{1}{R_N + b}} = \frac{\sin\theta}{\sqrt{r}} = \frac{\tan\theta}{\sqrt{R_N + b}}$$

and

$$dr = -2(R_N + b)\sin\theta\,\cos\theta\,d\theta.$$

Substituting these into (4.48) gives,

$$\begin{aligned} G &= \frac{\sqrt{R_N + b}}{\lambda\!\!\!^{-}} \int_{R_N}^{b+R_N} dr \sqrt{\frac{1}{r} - \frac{1}{R_N + b}} \\ &= 2\frac{R_N + b}{\lambda\!\!\!^{-}} \int_0^{\arccos\sqrt{\frac{R_N}{R_N+b}}} d\theta\,\sin^2\theta \\ &= \frac{R_N + b}{\lambda\!\!\!^{-}} \left(\arccos\left(\sqrt{\frac{R_N}{R_N + b}}\right) \right. \\ &\quad \left. - \frac{1}{2}\sin\left(2\arccos\left(\sqrt{\frac{R_N}{R_N + b}}\right)\right)\right) \\ &= \frac{R_N + b}{\lambda\!\!\!^{-}} \left(\arccos\left(\sqrt{\frac{R_N}{R_N + b}}\right) - \frac{\sqrt{R_N b}}{R_N + b}\right). \end{aligned} \tag{4.49}$$

This expression is next simplified through the use of the dimensionless quantity,

$$\xi = \frac{T_\alpha}{V_B} = \frac{R_N}{R_N + b}$$

to give,

$$\begin{aligned} G &= \frac{R_N}{\xi\lambda\!\!\!^{-}} \left(\cos^{-1}\left(\sqrt{\xi}\right) - \sqrt{\xi(1-\xi)}\right) \\ &\equiv \frac{R_N}{\xi\lambda\!\!\!^{-}} \gamma(\xi) \end{aligned} \tag{4.50}$$

By noting that $R_N \ll b$, the arccos function is expanded to first-order to give,

$$\gamma(\xi) \approx \frac{\pi}{2} - 2\sqrt{\xi} \tag{4.51}$$

allowing the Gamow factor to be written as,

$$\begin{aligned} G &= \frac{R_N}{\xi\lambda\!\!\!^{-}} \left(\frac{\pi}{2} - 2\sqrt{\xi}\right) \\ &= \frac{\pi R_N}{2\xi\lambda\!\!\!^{-}} - \frac{2R_N}{\sqrt{\xi}\lambda\!\!\!^{-}} \\ &= \frac{\sqrt{R_N + b}}{\lambda\!\!\!^{-}} \left(\frac{\pi}{2}\sqrt{R_N + b} - 2\sqrt{R_N}\right). \end{aligned} \tag{4.52}$$

Numerically, for the example of a heavy nucleus with $R_N = 7$ fm and $b \approx 40$ fm and a 5 MeV α particle, the reduced de Broglie wavelength is $\lambda\!\!\!^{-} = \hbar c/\sqrt{2m_\alpha T_\alpha} \approx 1$fm and the Gamow factor is $G \approx 37$.

Angular Momentum

Having now extended the calculation to a three-dimensional barrier, we consider the effect induced by angular momentum by using the three-dimensional Schrödinger equation as shown in Chap. 3.[9] Clearly, as this will increase the Coulomb barrier through the addition of a centrifugal term, $l(l+1)(\hbar c)^2/2m_\alpha r^2$, the angular momentum of the emitted α particle will influence the transmission of the particle through the barrier. This would arise in a step of the derivation of (4.48) in which the Gamow factor would, as a result of the centrifugal term, appear as,

$$G = \frac{\sqrt{2m_\alpha}}{\hbar c} \times \int_{R_N}^{b+R_N} dr \sqrt{\left| 2Z\left(\frac{\alpha\hbar c}{r}\right) + \frac{l(l+1)(\hbar c)^2}{2m_\alpha r^2} - T_\alpha \right|} \tag{4.53}$$

[9] As the α particle has zero spin, the angular momentum carried away is solely orbital in character.

Due to the α particle mass and the square of the radius present in the denominator of the centrifugal term, the effect of the centrifugal term to the barrier transmission will be quite limited. For an example of $Z = 80$, $r = b = 40$ fm and the high angular momentum case of $l = 4$, we find that,

$$\text{Coulomb term } 2Z\frac{\alpha\hbar c}{b} = 5.75\,\text{MeV}$$
$$\text{Centrifugal term } \frac{l(l+1)(\hbar c)^2}{2m_\alpha b^2} = 0.13\,\text{MeV}$$

Clearly for smaller l, the role of the centrifugal term within the Gamow factor can be neglected. But where the importance of the centrifugal barrier does arise is through the fact that the l values available to the emerging α particle are subject to the simultaneous conservation of angular momentum and parity.

4.2.4 Estimation of α Decay Half-Life

Consider an α particle within a spherical well potential well of radius R_N and moving with speed v_0. The rate at which the α particle will hit the "wall" is of the order of v_0/R_N times per second. The decay constant (the transition probability per unit time) for α emission is the product of this "impact rate" and the transmission factor,

$$\begin{aligned}\lambda &= \frac{v_0}{R_N}\Im \\ &= 8\frac{v_0}{R_N}e^{-2G}\end{aligned} \tag{4.54}$$

Taking logarithms of both sides, noting that $|\ln 8| \ll 2G$ and using our derived expression for the Gamow factor, we have,

$$\begin{aligned}\ln\lambda &\cong \ln\frac{v_0}{R_N} - 2G \\ &= \ln\frac{v_0}{R_N} - 2\frac{\sqrt{R_N+b}}{\lambda\!\!\!^{-}}\left(\frac{\pi}{2}\sqrt{R_N+b} - 2\sqrt{R_N}\right) \\ &= \ln\frac{v_0}{R_N} - \frac{1}{\lambda\!\!\!^{-}}\left(\pi(R_N+b) - 4\sqrt{R_N(R_N+b)}\right)\end{aligned} \tag{4.55}$$

Recalling the definition of the de Broglie wavelength, we can write,

$$\begin{aligned}\ln\lambda &= \ln\frac{v_0}{R_N} - \frac{\sqrt{2m_\alpha T_\alpha}}{\hbar c}\left(2\pi Z\frac{\alpha\hbar c}{T_\alpha} - 4\sqrt{R_N\frac{2Z\alpha\hbar c}{T_\alpha}}\right) \\ &= \ln\frac{v_0}{R_N} - \left(2\pi\alpha\sqrt{2m_\alpha}\right)\frac{Z}{\sqrt{T_\alpha}} + 8\sqrt{\frac{\alpha m_\alpha R_N}{\hbar c}}\sqrt{Z}\end{aligned} \tag{4.56}$$

As shown in the following chapter, the half-life is related to the decay constant via,

$$T_{1/2} = \frac{\ln 2}{\lambda} \tag{4.57}$$

Hence, one can write the α emission half-life as,

$$T_{1/2} = \frac{R_N \ln 2}{v_0}e^{\left(2\pi\alpha\sqrt{2m_\alpha}\right)\frac{Z}{\sqrt{T_\alpha}}}e^{-8\sqrt{\frac{\alpha m_\alpha R_N}{\hbar c}}\sqrt{Z}} \tag{4.58}$$

Because of the $T_\alpha^{-1/2}$ dependence the most energetic α particles will be associated with α decays with short half-lives. This can be seen in Fig. 4.8 which shows the very obvious tendency of the half-lives of α emitting isotopes of polonium to decrease with increasing α particle energy.

In 1911, Geiger and Nuttall reported an empirical relationship between the range of an α particle in air and the decay constant of the nuclide emitting the α particle,

$$\ln\lambda = k_1 + k_2\Re_\alpha \tag{4.59}$$

where $\Re_\alpha$ is the range of the α particle in air. For α particles with kinetic energies between 4 and 15 MeV (a range which covers most α emissions), an empirical relationship between α particle kinetic energy and its range in air is (Tsoulfanidis 1995),

$$\Re_{\text{air}} \approx (2.85 + 0.05T_\alpha)T_\alpha^{3/2} \tag{4.60}$$

where the range is in mm and the kinetic energy is in MeV. As $0.05T_\alpha > 2.85$ for the kinetic energies of interest, (4.59) can be rewritten in the form $\ln\lambda = k_1 + k_2T_\alpha^{3/2}$ leading to the Geiger–Nuttall rule relating α emission half-life to the α particle kinetic energy,

$$T_{1/2} = k_1e^{-k_2T_\alpha^{3/2}} \tag{4.61}$$

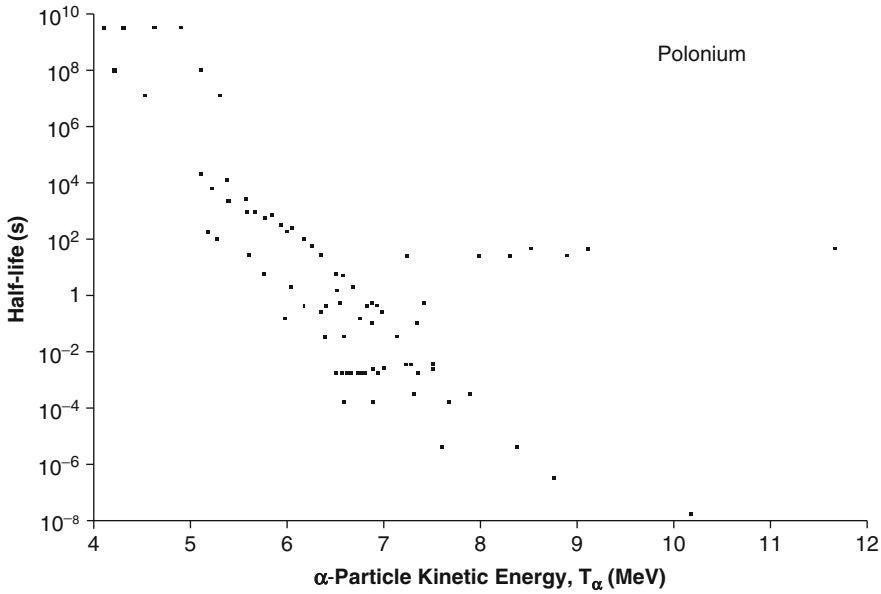

Fig. 4.8 Plot of polonium α emission half-life as a function of α particle kinetic energy. Points indicating multiple α emissions of differing kinetic energies but same half-life reflect multiple α emissions per given decay, as discussed in the text. Plot derived from data from the National Nuclear Data Center database (2008)

(note that the constants k_1 and k_2 are not the same throughout these equations). Although the empirical Geiger–Nuttall rule has $\ln T_{1/2} \propto T_\alpha^{-3/2}$ whereas the result derived from Gamow theory has $\ln T_{1/2} \propto T_\alpha^{-1/2}$, both demonstrate an association between α particles with high kinetic energies and short half-lives of the α emitters that gave rise to them.

4.3 The Weak Interaction: β Decay and Electron Capture

4.3.1 Introduction

β decay is both the most apparent manifestation of the weak force and is greatly important in nuclear medicine. Hence, it, and the weak force itself, are well-deserving of the detail provided in this section.

Early experimental studies of β decay showed that the detected final state contained only the electron and the recoiling daughter nucleus. Such a two-body decay would have required the electron to have a single well-defined kinetic energy equal to the difference between the mass of the parent nucleus and the sum of the masses of the daughter nucleus and electron (excluding any excitation energy taken up by the daughter). Using photographic emulsion as a detector, Hahn and Meitner demonstrated around 1906 that electron energy spectra associated with β decay from isotopes of thorium and actinium showed discrete peaks superimposed upon a weak, continuous background. While a well-defined electron energy was expected from the presumed two-body decay, the peaks observed were, in fact, the result of IC (a two-body final state) and the weak background was due to the electrons produced in β decay. Using a Geiger counter as a more sensitive ionization detector, Chadwick demonstrated in 1914 that the electron energy spectrum was continuous, contrary to the expectation of a two-body decay. This contradiction between the observed final state and the expected energy spectrum was problematic as the missing energy implied a failure of the law of conservation of energy. Experimental evidence demonstrated that the measured electron kinetic energy spectrum ranged in value from 0 to a value equal, to within experimental error, to the maximum dictated by a two-body final state. For example, this could be found by comparing the masses of ^{3}H and ^{3}He in the β^- decay of ^{3}H for which the mass-energy balance of $M_{^3H} = M_{^3He} + m_e + Q$ is achieved exactly by setting Q to the observed maximum electron energy in the spectrum. Another means of demonstrating this was shown by comparing the energies released in the

decay of a nucleus through alternative routes (e.g., β decay followed by α decay and vice versa) to a final nucleus. As the initial and final nuclei in the decay schemes are the same, the total energies released though all of the routes must also be the same. It was found that the sum of the α particle kinetic energies and the upper limits of the β particle energy spectra were equal in both decay branches.

Experimental data also implied the nonconservation of both angular momentum and the spin statistics of a composite system. Again, consider the β decay of ^{3}H in which there are only two observed products in the final state, the ^{3}He nucleus and the electron. Initially excluding the possibility of a non-zero orbital angular momentum, the ^{3}He angular momentum (due to the single proton in the $1p_{1/2}$ level) and the electron spin couple to form a system with a total angular momentum of either 0 or 1. In either case, the total angular momentum is an integer. Even if we were to now allow the possibility of an orbital angular momentum contribution to the final state, the total angular momentum of the final state remains an integer. The problem lies in that the angular momentum of ^{3}H in the initial state is 1/2. Thus, the ^{3}H initial state is subject to Fermi-Dirac statistics whereas the ^{3}He-e composite in the final state is subject to Bose–Einstein statistics.

These dilemmas were famously resolved by Pauli. Unable to an invitation to a meeting at Tübingen, on 4 December 1930 he wrote a letter to those attending describing his proposition:

"Dear Radioactive Ladies and Gentlemen,

As the bearer of these lines, to whom I graciously ask you to listen, will explain to you in more detail, how because of the "wrong" statistics of the N and Li^6 nuclei and the continuous beta spectrum, I have hit upon a desperate remedy to save the "exchange theorem" of statistics and the law of conservation of energy. Namely, the possibility that there could exist in the nuclei electrically-neutral particles, that I wish to call neutrons, which have spin 1/2 and obey the exclusion principle and which further differ from light quanta in that they do not travel with the velocity of light. The mass of the neutrons should be of the same order of magnitude as the electron mass and in any event not larger than 0.01 proton masses. The continuous beta spectrum would then become understandable by the assumption that in beta decay a neutron is emitted in addition to the electron such that the sum of the energies of the neutron and the electron is constant...

I agree that my remedy could seem incredible because one should have seen these neutrons much earlier if they really exist. But only the one who dare can win and the difficult situation, due to the continuous structure of the beta spectrum, is lighted by a remark of my honored predecessor, Mr Debye, who told me recently in Bruxelles: "Oh, It's well better not to think about this at all, like new taxes." From now on, every solution to the issue must be discussed. Thus, dear radioactive people, look and judge.

Unfortunately, I cannot appear in Tubingen personally since I am indispensable here in Zurich because of a ball on the night of 6/7 December. With my best regards to you, and also to Mr Back.

Your humble servant,

W. Pauli"

Following Chadwick's discovery of what is now known as the neutron (as a nucleon), Fermi later coined the word *neutrino* (ν_e)[10] to describe Pauli's proposed particle which carried away the "missing" kinetic energy.

While a succinct solution to the empirical problem, it was immediately obvious from the lack of direct evidence for its existence that the neutrino interacted very weakly with matter. Despite this, further consideration of the experimental data at these early times led to the exposition of other properties of the neutrino:

- Mass: As the maximum of the electron/positron energy spectrum was, to within experimental error, equal to the maximum set by two-body decay, the β decay kinematics demonstrated that the neutrino mass was very small or zero.[11]
- Electric charge: The observed conservation of electric charge in β decay demonstrated that the neutrino had no electric charge.
- Spin: Conservation of angular momentum requires the neutrino to be a fermion as indicated in our earlier consideration of the decay of ^{3}He.

It was not until the early 1950s that the existence of the neutrino or, to be exact, the antineutrino was confirmed experimentally. Using the antineutrino flux

[10]The e subscript signifies that the neutrino produced by β decay is associated with an electron/positron.

[11]Only in recent years has conclusive evidence for a non-zero neutrino mass been obtained from measurements of neutrinos of cosmic origin (see, e.g., Fukuda et al. 1998).

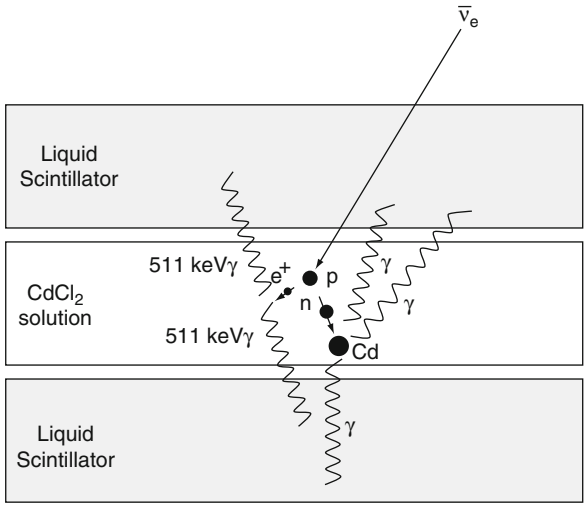

Fig. 4.9 Schematic diagram of the experimental arrangement used by Reines and Cowan to detect the existence of the electron-antineutrino. A description of the detection process is provided in the text

produced by the β decay of fission products in a nuclear reactor, Reines and Cowan (1953) (Reines 1997) detected the positron and neutron resulting from the "inverse β^+ decay" reaction of[12] $\bar{\nu}_e + p \rightarrow n + e^+$. The target consisted of $CdCl_2$ dissolved in water and sandwiched between two tanks containing liquid scintillator each viewed by photomultiplier tubes, as shown schematically in Fig. 4.9. An observed event was of an antineutrino captured by a proton of the hydrogen atom in a target water molecule to generate a positron and a neutron. The positron had a small mean free pathlength in water before it annihilated on a free electron ($e^-e^+ \rightarrow 2\gamma$) within about 1 ns of creation to produce two 511 keV γ rays which were subsequently detected in coincidence by the surrounding liquid scintillator. The neutron product of the inverse β^+decay thermalized through elastic collisions with the protons in the water molecules so as to be eventually captured by a cadmium nucleus some 10 μs later. This "radiative capture" by the cadmium resulted in an excited cadmium nucleus which, during de-excitation, emitted γ rays also detected by the surrounding liquid scintillator. The time signature of the two separate γ ray detections signaled an antineutrino detection.

The history of β decay, and the weak interaction it demonstrates is concluded by considering briefly the complexity of the lepton family beyond the electron and neutrino that resulted from the discovery of the muon in cosmic rays in 1937 by Neddermeyer and Anderson (1937)[13] and the determination that it was not subject to the strong nuclear force and was, hence, a lepton by Conversi et al. (1947). This was the first indication of the existence of the Generations of matter shown in Fig. 3.1 in Chap. 3 and of lepton flavor. Due to the leptonic similarities of the muon with an electron, it was of interest to determine if it also had an associate neutrino. That the muon neutrino existed was demonstrated by Lederman, Schwartz and Steinberger (Danby et al. 1962) in an experiment at Brookhaven National Laboratory in which protons bombarded a beryllium target to produce pions following which each decayed in flight to a muon and a neutrino (e.g., $\pi^+ \rightarrow \mu^+ + \nu_\mu$; the μ subscript indicates that the neutrino is associated with a muon and, in analogy to the electron and positron, the positively-charged muon is regarded as the antiparticle). The combined beam of muons and neutrinos then passed through a 13.5-m thick steel absorber so that only the neutrinos were able to pass through to be detected by a spark chamber on the exit side. Whereas the electron is a stable particle,[14] the muon is not. It decays, with a half-life of 2.197 μs, via $\mu^- \rightarrow e^- + \nu_e + \bar{\nu}_e$. However, the simpler decay process of $\mu^- \rightarrow e^- + \gamma$ has not been observed which empirically indicates the existence of the lepton quantum number. The existence of a charged lepton of the third flavor[15] was shown by Perl et al. (1975) through the topology of the trajectories of the products resulting from collisions between high-energy electron and positron beams leading to $e^-e^+ \rightarrow \tau^-\tau^+ \rightarrow e^\pm + e^\mp + 4$ neutrinos. The mean τ-lepton life is 290.6 fs and the existence of a neutrino associated with the τ-lepton was finally

[12] As the total cross-section for this reaction had been estimated from the measured half-life of free neutron decay to be about 6×10^{-44} cm^{-2}, an intense antineutrino flux such as that from a fission reactor was required in order for a detectable number of events to be obtained.

[13] The muon was initially called the mu -mesotron and incorrectly thought to have been the intermediary of the strong force postulated by Yukawa. That particle is the pion which is subject to the strong nuclear force which the muon is not.

[14] The electron has a measured lifetime in excess of 4.6×10^{26} yrs (90% confidence level) (Particle Data Group 2004).

[15] This heavy lepton is referred to as the τ-lepton referring it to being the third lepton discovered.

Table 4.1 Lepton flavors

Electron flavor	
Lepton	Mass (MeV)[a]
e	0.510999
ν_e	$<4.6 \times 10^{-4}$ (68% c.l.)
Muon flavor	
Lepton	Lepton
μ	105.658369
ν_μ	<0.19 (90% c.l.)
Tau-lepton flavor	
Lepton	Mass (MeV)[a]
τ	1776.99
ν_τ	<18.2 (95% c.l.)

[a]Masses are averages taken from the Review of Particle Physics (Particle Data Group 2004); neutrino masses are provided with specified confidence levels

confirmed experimentally in 2000 (Kodama et al. 2001). The family of leptons is summarized in Table 4.1.

Within a modern viewpoint, β decay and electron capture can be considered at three different scales of dimension. At the lowest spatial resolution, they can be regarded as transitions between nuclear isobars which change the atomic number of the parent nucleus by unity:

$$(Z, A) \rightarrow (Z + 1, A) + e^- + \bar{\nu}_e$$

$$(Z, A) \rightarrow (Z - 1, A) + e^+ + \nu_e$$

$$(Z, A) + e^- \rightarrow (Z - 1, A) + \nu_e$$

Going beyond the nuclear picture by increasing the spatial resolution to nucleon dimensions, these processes are seen as isospin-projection changing transitions between nucleons:

$$n \rightarrow p + e^- + \bar{\nu}_e$$

$$p \rightarrow n + e^+ + \nu_e$$

$$p + e^- \rightarrow n + \nu_e$$

Finally, at the spatial resolution of sub-nucleon dimensions, the transitions are now seen as a quark flavor change with the emission of a $W^{\pm}$ intermediate vector boson (so called as it has spin 1) which subsequently decays into a lepton pair,

$$d \rightarrow u + W^- \rightarrow u + e^- + \bar{\nu}_e$$

$$u \rightarrow d + W^+ \rightarrow d + e^+ + \nu_e$$

$$u + e^- \rightarrow d + W^+ + e^- \rightarrow d + \nu_e$$

as shown in Fig. 4.10.

As described in the introduction, the small interaction cross-section of the neutrino, the long physical half-lives of nuclei subject to β decay compared to γ decay and the change in nuclear isospin (through the isospin flips of n → p and p → n and the underlying quark flavor changes) led to the postulate that β decay was indeed a manifestation of a new force, termed the weak force. The electron and neutrino are leptons with the electron interacting through both electromagnetic and weak forces and the electrically-neutral neutrino interacting through the weak force alone. Both particles have antiparticles, the positron and antineutrino, the positron having been predicted by Dirac and experimentally detected in cosmic rays by Anderson (1933). Isospin and flavor, which are manifestations of the strong nuclear force, are not conserved by this weak force.

β decay is the most commonly observed weak interaction and is of significance to internal radiation dosimetry for several reasons:

- The daughter nucleus resulting from β decay or EC is often in an excited state which subsequently de-excites by γ ray emission or other radioactive processes. The γ ray emission can be directly useful for nuclear medicine imaging (e.g., ^{99}Mo undergoing β decay to ^{99m}Tc which makes an isomeric transition (IT) to ^{99}Tc through the emission of a 140.5 keV γ ray). For heavy nuclei, these other processes include fission and delayed nucleon emission as shown in Fig. 4.11.
- While the electron resulting from β^- decay does not contribute to the nuclear medicine imaging process,[16] it does deposit energy in tissue while decelerating, creating an absorbed dose.
- The positron created in β^+ decay will also deposit energy as it traverses tissue to annihilate with an electron to produce two collinear 511 keV γ rays

[16]Excluding imaging of the *bremsstrahlung* radiation produced by the decelerating electron.

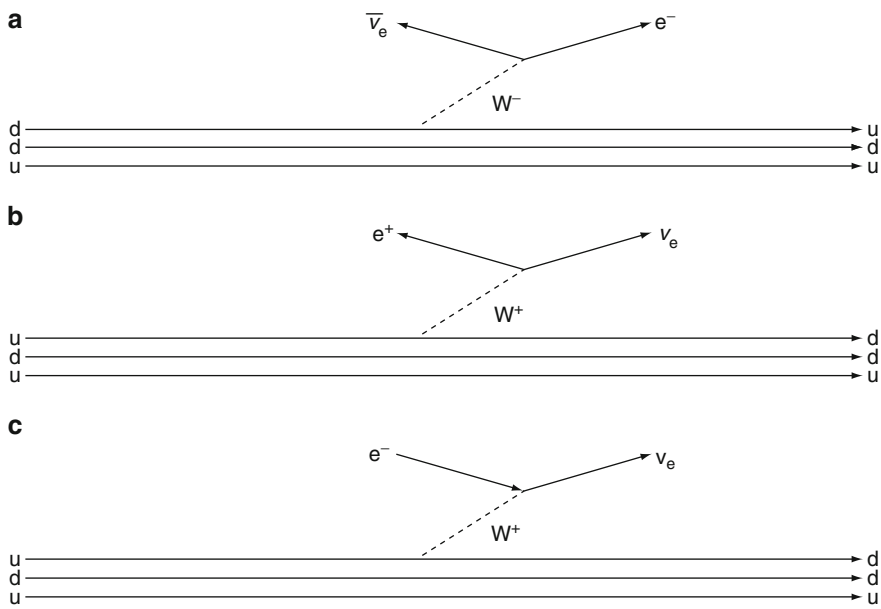

Fig. 4.10 Quark-boson-lepton diagrams for (**a**) β^- decay of a neutron; (**b**) β^+ decay of a proton; and (**c**) electron capture by a proton

which can be detected externally to form a tomographic image.

- Electron capture leaves an atomic electron vacancy inducing fluorescence X-ray production (which can also be detected to form an image) or Auger/Coster–Kronig electron cascades.

4.3.2 Kinematics of β Decay and Electron Capture

4.3.2.1 Neutron β Decay

The study here of β decay kinematics begins by considering free neutron decay, $n \rightarrow p + e^- + \bar{\nu}_e$. The mass-energy balance of a free neutron undergoing β^- decay is,

$$m_n = m_p + m_e + Q_- \tag{4.62}$$

Where the "−" subscript on Q signifies this as the energy released in β^- decay. Throughout this discussion, the masses of the (anti)neutrinos are neglected and, upon substituting the appropriate rest masses, it is found that free neutron decay is exoergic with $Q_- = 0.782$ MeV. Thus, a free neutron is unstable to β^- decay to a proton with a half-life of 885.7 s and the 0.782 MeV of energy available will be distributed amongst the kinetic energies of the three decay products. By contrast, the mass-energy balance for a proposed β^+ decay of a free proton is,

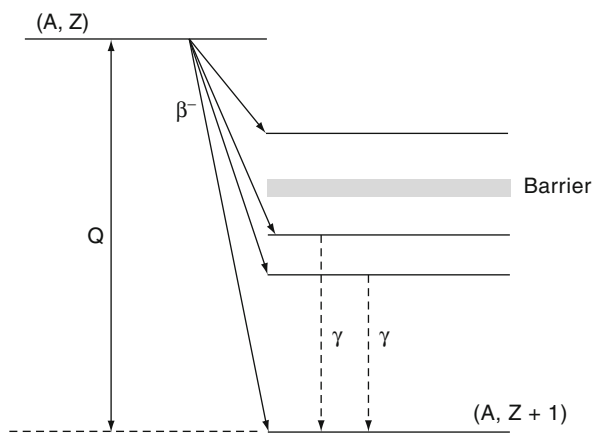

Fig. 4.11 Representative decay scheme for β^- decay with transitions to the ground state and various excited states of the daughter nucleus. The barrier signifies the minimum energy required in order for processes such as delayed nucleon emission and nuclear fission to occur

$$m_p = m_n + m_e + Q_+ \tag{4.63}$$

Again, substituting the rest-mass values will show that this reaction is endoergic since $Q_+ = -1.765$ MeV

and, hence, $p \rightarrow n + e^+ + \nu_e$ cannot occur for a free proton. It can occur only if the proton is bound within the nucleus such that the additional energy required for the transition arises from the nuclear binding energy.

4.3.2.2 Nuclear β Decay

Introduction

Now consider nuclear β decay between isobars (Grotz and Klapdor 1990). Such β decays can only occur if there is an adjacent isobar with a smaller mass (i.e., greater binding energy). Figure 4.12 presents a summary of the kinematics of nuclear β decay and electron capture. Recall from the discussion of the Segrè plot that, with increasing atomic mass number A in stable nuclei, the number of neutrons N increases relative to the number of protons, Z. An unstable nucleus (i.e., one which is displaced from the locus of stable nuclei in the Segrè plot) can be created either through the bombardment of a stable nucleus with charged particles or neutrons or through the fission of a heavy nucleus. Such an unstable nucleus will lie on either side of the stable nuclei locus. The type of β decay available to the displaced nucleus will be dictated by the magnitudes of the Coulomb and symmetry terms of the Weizsäcker formula and these will follow the mass parabolae.

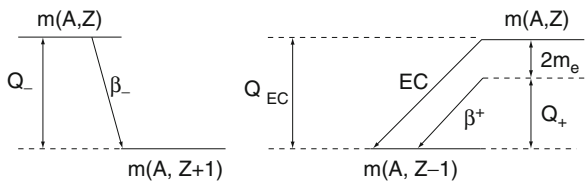

Fig. 4.12 Kinematics of β decay and electron capture

The Coulomb term reduces the net binding energy with increasing Z whereas the symmetry term increases the binding energy with increasing Z. As seen, the result is a maximum in the binding energy indicating the stable nucleus in the mass parabola (which would lie along the isobar line of Fig. 4.13). If the artificially produced nucleus were to be to the left of the locus of stable nuclei (i.e., it has an excess of neutrons or is "neutron-rich"), it has a deficit of electric charge for its mass. Hence, the Coulomb term is reduced and the symmetry term increased. A maximum in the binding energy is then achieved by an increase in the former and a decrease in the latter which results from β^- decay. Should the nucleus instead be to the right of the locus of stable nuclei (i.e., it has an excess of protons or is "proton-rich"), the relative magnitudes of the Coulomb and symmetry terms are reversed and a maximum in the binding energy is achieved by decreasing the magnitude of the Coulomb term and increasing that of the symmetry term through β^+ decay or electron capture.

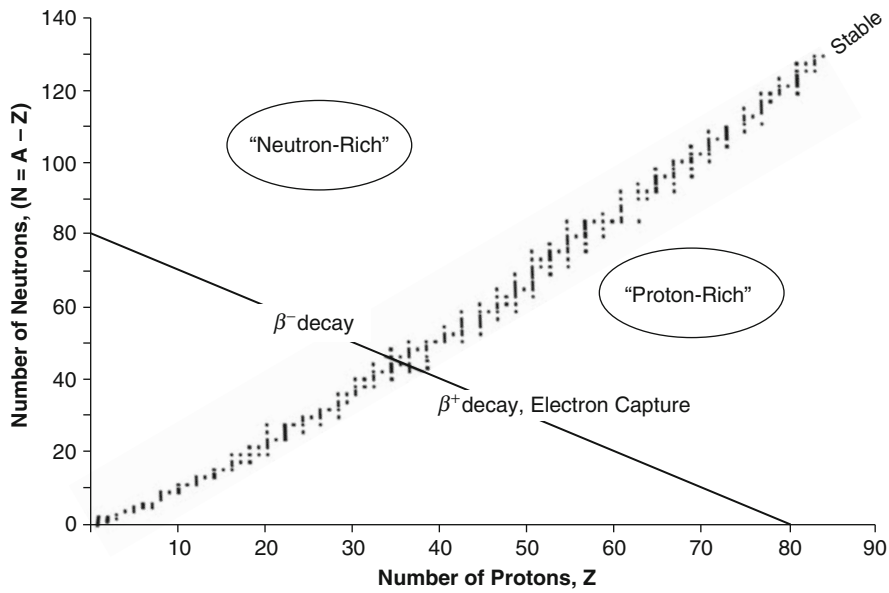

Fig. 4.13 Segrè plot showing the "neutron-rich" region, where β^- decay can occur, and the "proton-rich" region, where β^+ decay or electron capture can occur, are shown. The isobar line of A = 80 is provided as an example to show the directions of these transitions towards the locus of stable nuclei

The mass difference required between parent and daughter nuclei is next calculated in order to determine whether or not nuclear β decay or electron capture is energetically possible.

Nuclear β^- Decay

Nuclear β^- decay between the isobar pair ${}^{A}_{Z}X$ and ${}^{A}_{Z+1}Y$ is,

$$ {}^{A}_{Z}X \rightarrow {}^{A}_{Z+1}Y + e^- + \bar{\nu}_e \tag{4.64} $$

and which has the nuclear mass-energy balance,[17]

$$ m(A,Z) = m(A,Z+1) + m_e + Q_-. \tag{4.65} $$

As the nuclear mass is $m(A,Z) = Zm_p + (A-Z)m_n - B(A,Z)$, (4.65) gives the Q_- value for nuclear β^- decay as,

$$ \begin{aligned} Q_- = &\left(m_n - m_p - m_e\right) \\ &+ \left(B(A,Z+1) - B(A,Z)\right) \end{aligned} \tag{4.66} $$

where the first term in parentheses in (4.66) is the Q_- for free neutron decay and the second term is the difference in nuclear binding energies. A simpler expression for Q_- can be extracted from (4.66) by recalling that the nuclear binding energy can be written in terms of atomic masses, $B(A,Z) = ZM_H + (A-Z)m_n - M(A,Z)$, or,

$$ Q_- = M(A,Z) - M(A,Z+1). \tag{4.67} $$

As Q_- must be positive, nuclear β^- decay is energetically permissible should the parent's atomic mass exceeds that of the daughter. An example of β^- decay shown in Fig. 4.14 is that of the radionuclide ^{32}P, which is produced through neutron bombardment of stable ^{31}P, and undergoes β^- decay to ^{32}S with a half-life of 14.263 days and a Q_- of 1.71 MeV.

[17]Note that any excitation energy conferred to the daughter nucleus is ignored.

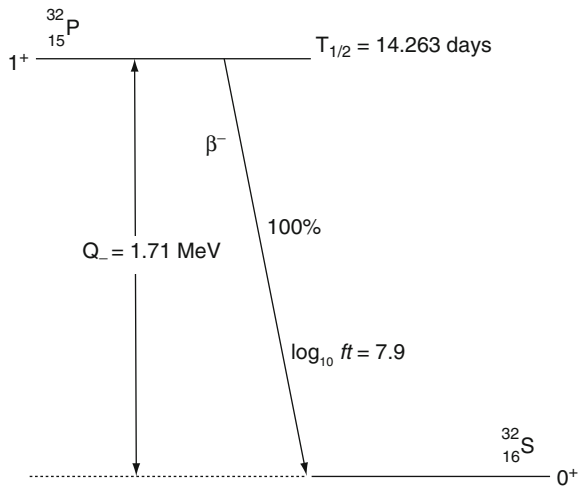

Fig. 4.14 $^{32}P \rightarrow {}^{32}S + e^- + \bar{\nu}_e$. The $\log_{10} ft$ value is a measure of the transition rate and is discussed in the text

Nuclear β^+ Decay

β^+ decay is inherently nuclear as the β^+ decay of a free proton is energetically impossible. A nucleus in the proton-rich region of Fig. 4.13 will have excessive electric charge for its mass and will seek to reduce this charge by either positron emission or electron capture. The β^+ decay between the isobar pair ${}^{A}_{Z}X$ and ${}^{Y}_{Z+1}Y$ is,

$$ {}^{A}_{Z}X \rightarrow {}^{A}_{Z-1}Y + e^+ + \nu_e \tag{4.68} $$

with a nuclear mass-energy balance,

$$ m(A,Z) = m(A,Z-1) + m_e + Q_+. \tag{4.69} $$

Substituting the expression for nuclear mass gives,

$$ \begin{aligned} Q_+ = &-\left(m_n - m_p - m_e\right) - 2m_e \\ &- \left(B(A,Z-1) - B(A,Z)\right) \end{aligned} \tag{4.70} $$

which, in terms of parent and daughter nuclear masses, is,

$$ Q_+ = \left(M(A,Z) - M(A,Z-1)\right) - 2m_e. \tag{4.71} $$

Thus, in order for β^+ decay to occur, the parent atom must be heavier than the daughter nucleus by an amount of at least double the electron/positron rest-mass of $2m_e$ (1.022 MeV). An example is shown in

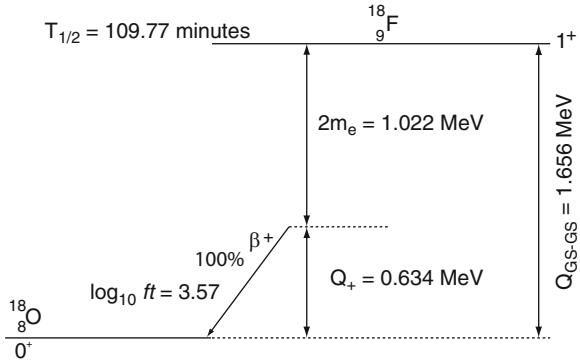

Fig. 4.15 $^{18}\mathrm{F} \rightarrow {}^{18}\mathrm{O} + \mathrm{e}^{+} + \nu_{\mathrm{e}}$

Fig. 4.15 of ^{18}F which undergoes β^{+}-decay with a 109.77 min half-life to produce ^{18}O.

Electron Capture

The process of electron capture can compete with β^{+} decay as the wavefunction of an orbital electron, especially that of the K-orbital, will have a finite extension into the nuclear volume.[18] As a consequence, it is possible for a nucleus to capture an orbital electron through $\mathrm{e}^{-} + \mathrm{Z} \rightarrow (\mathrm{Z}-1) + \nu_{\mathrm{e}}$, a reaction which occurs preferentially for high-A nuclei which, with their large nuclear radii, will have greater overlaps with the orbital electrons' wavefunctions. The EC process is,

$$ {}^{\mathrm{A}}_{\mathrm{Z}}\mathrm{X} + \mathrm{e}^{-} \rightarrow {}^{\mathrm{A}}_{\mathrm{Z}-1}\mathrm{Y} + \nu_{\mathrm{e}} \tag{4.72} $$

with the nuclear mass-energy balance,

$$ \mathrm{m}(\mathrm{A},\mathrm{Z}) + \mathrm{m}_{\mathrm{e}} - \mathrm{B}_{\mathrm{K}} = \mathrm{m}(\mathrm{A},\mathrm{Z}-1) + \mathrm{Q}_{\mathrm{EC}}. \tag{4.73} $$

The capture of a K-shell electron with B_{K} binding energy has been assumed. Solving for Q_{EC} in terms of nuclear binding energies,

$$ \begin{aligned} \mathrm{Q}_{\mathrm{EC}} = &-\left(\mathrm{m}_{\mathrm{n}} - \mathrm{m}_{\mathrm{p}} - \mathrm{m}_{\mathrm{e}}\right) - \mathrm{B}_{\mathrm{K}} \\ &+ \left(\mathrm{B}(\mathrm{A},\mathrm{Z}-1) - \mathrm{B}(\mathrm{A},\mathrm{Z})\right) \end{aligned} \tag{4.74} $$

and of atomic masses,

$$ \mathrm{Q}_{\mathrm{EC}} = \left(\mathrm{M}(\mathrm{A},\mathrm{Z}) - \mathrm{M}(\mathrm{A},\mathrm{Z}-1)\right) - \mathrm{B}_{\mathrm{K}} \tag{4.75} $$

Hence, EC is energetically feasible if the parent's atomic mass exceeds the sum of that of the daughter and the electron binding energy (which, in practice, can be neglected). Comparing Q_{EC} and Q_{+},

$$ \mathrm{Q}_{+} = \mathrm{Q}_{\mathrm{EC}} - 2\mathrm{m}_{\mathrm{e}} \tag{4.76} $$

Because EC does not produce a positron and the neutrino cannot be readily detected, experimental evidence for EC is obtained indirectly via the emission of a characteristic X-ray daughter nucleus (Alvarez 1937). EC creates a hole in the atomic energy orbital which is subsequently filled by an electron from a higher-order orbital to produce an X-ray with energy equal to the difference between the binding energies of the two orbitals. Although β^{+} decay of a proton-rich nucleus yields the same daughter nucleus as that of electron capture, the former cannot occur unless there is a mass-energy differential of 1.022 MeV between the parent and daughter atoms, whereas the threshold for the latter simply requires that the parent atom be heavier than the daughter (if the magnitude of the orbital electron binding energy is neglected). Hence, if the mass-energy difference between the parent and daughter atoms for which EC occurs exceeds 1.022 MeV, β^{+} decay can become possible, in which the total transition probability is the sum of the two individual probabilities for each transition type.

Summary of β Decay and Electron Capture Kinematics

The thresholds for β decay and electron capture in terms of the parent (X) and daughter (Y) atomic masses are,

$$ \mathrm{M}_{\mathrm{X}} > \mathrm{M}_{\mathrm{Y}} \qquad \beta^{-},\ \mathrm{EC} $$

$$ \mathrm{M}_{\mathrm{X}} > \mathrm{M}_{\mathrm{Y}} + 2\mathrm{m}_{\mathrm{e}} \qquad \beta^{+} $$

Table 4.2 presents Q values for a variety of β decays of particular interest to diagnostic nuclear medicine and PET imaging.

[18] The probabilities of L and higher orbital wavefunctions extending into the nucleus are much smaller and are not considered here.

Table 4.2 Q values for various β decays of nuclear medicine interest

Parent	Daughter	Decay mode (% of all decays)	Q (MeV)	Applications
^{11}C	^{11}B	β^+ (99.7%)	0.961	PET imaging
		EC (0.3%)	1.983	
^{14}C	^{14}N	β^-	0.156	^{14}C-labelled urea for *Helicobacter pyloris* diagnosis
^{15}O	^{15}N	β^+ (99.9%)	1.732	PET imaging
		EC (0.1%)	2.754	
^{18}F	^{18}O	β^+ (96.9%)	0.634	PET imaging
		EC (3.1%)	1.656	
^{51}Cr	^{51}V	EC	0.752	$Na_2{}^{51}CrO_4$ used to label red blood cells (RBC) for measurement of RBC volume or RBC sequestration
^{59}Fe	^{59}Co	β^-	1.565	^{59}Fe ferrous citrate used to assess gastrointestinal iron absorption by oral administration or of iron metabolism by intravenous injection
^{64}Cu	^{64}Ni	β^+ (18%)	0.653	PET imaging
	^{64}Ni	EC (44.9%)	1.675	
	^{64}Zn	β^- (37.1%)	0.578	
^{67}Ga	^{67}Zn	EC (100%)	1.000	^{67}Ga citrate used for imaging tumors and inflammation with γ-ray scintigraphy
^{68}Ga	^{68}Zn	β^+ (89.1%)	1.899	PET Imaging
		EC (10.9%)	2.921	
^{90}Y	^{90}Zr	β^- (100%)	2.280	^{90}Y-labelled *ibritumomab tiuxetan* for treatment of non-Hodgkin'slymphoma

4.3.3 Fermi Theory of β Decay: Part I

4.3.3.1 Introduction

Having established the kinematic requirements to be fulfilled in order for β decay and electron capture to occur, we now progress to calculating the transition probabilities and decay rates of these processes. Although dating from the 1930s, Fermi's theory (1934a, b) remains an inspired and pragmatic approach to understanding β decay and electron capture, evaluating their transition probabilities and calculating the electron and positron energy spectra. The insight of Fermi's theory was its being an analogy to that describing the interaction between charges in quantum electrodynamics.[19] Even though it has been supplanted by the modern Glashow–Salam–Weinberg electroweak theory, the Fermi theory provides the low-energy limit of that theory which is appropriate and useful for our study of β decay.

4.3.3.2 Nuclear β Decay

Introduction

In this subsection, the transition rates for β decay and electron capture are derived from perturbation theory using Fermi's Golden Rule No 2,[20]

$$\lambda_{fi} = \frac{2\pi}{\hbar}\left|\int d^3\mathbf{r}\,\psi_f^* U \psi_i\right|^2 \rho_f \qquad (4.77)$$

Matrix Element

The matrix element, $\int d^3\mathbf{r}\,\psi_f^* U\psi_i$, is calculated by first noting that the initial wavefunction is that of the parent

[19]Fermi's paper on his β decay theory was, famously, rejected by *Nature* in 1933 but was subsequently published in Italian in *Nuovo Cimento* and in German in *Zeitschrift für Physik*. Fermi never again published on this subject (Segrè 1970).

[20]For simplicity in this discussion, "electron" will refer to either an electron or a positron and "neutrino" will refer to either a neutrino or antineutrino. An exact assignment will be apparent from the context of the discussion.

nucleus' wavefunction $\psi_i \equiv \psi_{nuc,i}$, and the final wavefunction ψ_f is the product of the three wavefunctions corresponding to the daughter nucleus, electron and neutrino, $\psi_f \equiv \psi_{nuc,f}\psi_e\psi_{\nu_e}$. The lepton wavefunctions are represented by plane waves,

$$\psi_e^*\psi_{\nu_e} = \frac{1}{L^3}e^{i\frac{\mathbf{q}\bullet\mathbf{r}}{\hbar c}} \tag{4.78}$$

where L^3 is the volume containing the system and $\mathbf{q} = \mathbf{p}_{\nu_e} - \mathbf{p}_e$. Because of the distortion induced by the nuclear Coulomb field, a plane wave expansion for the electron is not entirely valid, but its use will corrected for later. Expanding the exponential,

$$e^{i\frac{\mathbf{q}\bullet\mathbf{r}}{\hbar c}} = \sqrt{4\pi}\sum_{l=0}^{\infty}\sqrt{2l+1}\; j_l\left(\frac{qr}{\hbar c}\right)Y_{l0}(\theta,0) \tag{4.79}$$

where θ is the angle between $\mathbf{q}$ and $\mathbf{r}$. As the lepton momenta are of the order of 1–2 MeV/c and the nuclear dimension is of the order of 5 fm, then the argument of the spherical Bessel function is $qr/\hbar c \approx 0.05$ or less. In this case, the small-argument form of the spherical Bessel function, $j_l(x) \approx x^l/(2l+1)!!$, can be used where the double factorial is defined by $(2l+1)!! = 1\times 3\times 5\ldots(2l+1)$. Hence, the low-argument approximation to the spherical Bessel function diminishes rapidly with l for $x \ll 1$ and the expansion of (4.79) can be restricted to $l = 0$ to give $\psi_e^*\,\psi_{\nu_e} \approx 1/L^3$. Hence, a simplified result for the matrix element is obtained,

$$\int d^3\mathbf{r}\,\psi_f^* U\psi_i \approx \frac{1}{L^3}\int d^3\mathbf{r}\,\psi_{nuc,f}^* U\psi_{nuc,i}. \tag{4.80}$$

The perturbation potential inducing the β decay is taken to be weak and to have an infinitely small range[21] allowing the perturbation to be approximated by a scalar constant and removed from the integral,

$$\begin{aligned}\int d^3\mathbf{r}\,\psi_f^* U\psi_i &\approx \frac{g}{L^3}\int d^3\mathbf{r}\,\psi_{nuc,f}^*\psi_{nuc,i}\\ &= \frac{g}{L^3}M_{fi}\end{aligned} \tag{4.81}$$

where M_{fi} is the nuclear matrix element. The β decay transition rate from initial state i to final state f can now be written as,

$$\lambda_{fi} = \frac{2\pi}{\hbar}\frac{g^2}{L^6}|M_{fi}|^2\rho_f \tag{4.82}$$

Phase Space Factor

From the previous derivation of β decay kinematics, the total kinetic energy available to the electron and neutrino is equal to the Q of the appropriate decay. Neglecting a neutrino rest mass, the total energy made available is the sum of the kinetic and rest-mass energies, $E_0 = Q_\pm + m_e$, which is also equal to the electron and neutrino total energies,

$$E_0 = E_e + E_{\nu_e} \tag{4.83}$$

Equation (4.82) can be generalized into the differential form,

$$d\lambda_{fi}(E_e) = \frac{2\pi}{\hbar}\frac{g^2}{L^6}|M_{fi}|^2\frac{d\rho_f(E_0,E_e)}{dE_e}dE_e \tag{4.84}$$

which is the differential probability that the electron will be emitted with a total energy between E_e and $E_e + dE_e$. As the volume of a unit cell in phase space is $(2\pi\hbar c)^3$ and the electron-antineutrino final state will have a 12-dimensional phase space (three-dimensions each for the electron and antineutrino momenta and position), the phase space differential volume element in electron and neutrino momentum is,

$$\begin{aligned}d^2\rho_f &= \left(\frac{L}{2\pi\hbar c}\right)^3 4\pi\,p_e^2\;dp_e \bullet \left(\frac{L}{2\pi\hbar c}\right)^3\\ &\quad\times 4\pi p_{\nu_e}^2 dp_{\nu_e}\delta(Q - T_e - T_{\nu_e})\\ &= \frac{1}{4\pi^4}\left(\frac{L}{\hbar c}\right)^6 p_e^2\,dp_e\,p_{\nu_e}^2\,dp_{\nu_e}\delta(Q - T_e - T_{\nu_e})\end{aligned} \tag{4.85}$$

where the δ-function specifies the required energy conservation. It is convenient to solve for this expression by using the particles' total energies as the variables instead. As the total energy is $E = \sqrt{p^2 + m^2}$,

[21] In the modern-day picture of the W intermediate vector boson-mediated β decay, the range of the force is of the order of 10^{-3} fm. Hence, Fermi's approximation of a zero-range force was insightful.

then $dE/dp = p/E$ and $p^2dp = E\sqrt{E^2 - m^2}dE$, then (4.85) can be written in the form,

$$d^2\rho_f = \frac{1}{4\pi^4}\left(\frac{L}{\hbar c}\right)^6 \times E_e\sqrt{E_e^2 - m_e^2}\, dE_e\, E_{\nu_e}^2\, dE_{\nu_e}\delta(E_0 - E_e - E_{\nu_e}). \tag{4.86}$$

The arguments of the δ functions of (4.85) and (4.86) are equivalent. As the neutrino is not detected, this result is subsequently integrated over the neutrino energy,

$$\begin{aligned} d\rho_f &= \frac{1}{4\pi^4}\left(\frac{L}{\hbar c}\right)^6 E_e\sqrt{E_e^2 - m_e^2}\, E_e\, dE_e \\ &\quad \times \int dE_{\nu_e}\, E_{\nu_e}^2\, \delta(E_0 - E_e - E_{\nu_e}) \\ &= \frac{1}{4\pi^4}\left(\frac{L}{\hbar c}\right)^6 E_e\sqrt{E_e^2 - m_e^2}(E_0 - E_e)^2 dE_e. \end{aligned} \tag{4.87}$$

So far, this calculation has neglected the interaction between the product electron and the daughter nucleus. As noted earlier, this will distort the electron's wavefunction, thus invalidating the original assumption of describing its wavefunction as a plane. For β^- emission, the attractive Coulomb interaction slows down the electron and increases the low-energy portion of the spectrum. Thus, the electron is emitted with a higher energy than that detected or, in other words, the phase space is larger than $4\pi p_e^2 dp_e$. On the other hand, for β^+ emission, the Coulomb force between the positron and the nucleus is repulsive, thus suppressing the low-energy portion of the spectrum and correspondingly decreasing the available phase space. In order to account for these Coulomb effects, but still retain the overall form of the result obtained from a plane-wave approximation, a correction to the phase space is inserted into the phase space factor. This correction term is the Fermi factor, $F(Z_Y, E_e)$,

$$\frac{d\rho_f}{dE_e} = \frac{1}{4\pi^4}\left(\frac{L}{\hbar c}\right)^6 E_e\sqrt{E_e^2 - m_e^2}\,(E_0 - E_e)^2 \times F(Z_Y, E_e) \tag{4.88}$$

where Z_Y is the atomic number of the recoil daughter nucleus. The Fermi factor is the ratio of the electron/positron wavefunctions at the centre of the nucleus with the Coulomb interaction to that without,

$$F(Z_Y, E_e) = \frac{|\psi_{e,with}(0)|^2}{|\psi_{e,without}(0)|^2}. \tag{4.89}$$

A suitable nonrelativistic approximation of the Fermi factor is,

$$F(Z_Y, E_e) = \frac{2\pi\eta}{1 - e^{-2\pi\eta}} \tag{4.90}$$

where

$$\eta = \pm\alpha Z_Y \frac{E_0}{\sqrt{E_e^2 - m_e^2}} \tag{4.91}$$

and where the ± sign corresponds to electron/positron emission. The nonrelativistic Fermi factor is plotted in Fig. 4.16 as a function of the ratio $\frac{E_e}{E_0} = \frac{T_e + m_e}{Q + m_e}$ for four different β decays. By expanding the exponential term in (4.90) to second order, the features of Fig. 4.16 become more apparent,

$$\begin{aligned} F(Z_Y, E_e) &= \frac{1}{1 - \pi\eta} \\ &= \frac{p_e}{p_e \mp \mu\pi\alpha Z E_0} \\ &= \frac{\sqrt{\left(\frac{E_e}{E_0}\right)^2 - \left(\frac{m_e}{E_0}\right)^2}}{\sqrt{\left(\frac{E_e}{E_0}\right)^2 - \left(\frac{m_e}{E_0}\right)^2} \mp \pi\alpha Z} \end{aligned} \tag{4.92}$$

This result shows that $F(Z_Y, E_e) > 1$ for electrons and $F(Z_Y, E_e) < 1$ for positrons and that both factors approach unity with increasing energy. However, the nonrelativistic approximation fails for high-Z nuclei and the Fermi factor must then be calculated from the Dirac equation and an extended Coulomb potential. Tabulated values for $F(Z_Y, E_e)$ can be found in Behrens and Jähnecke (1969).

Energy Spectra

The transition rate can now be written as,

$$\frac{d\lambda_{fi}(E_e)}{dE_e}dE_e = \left(\frac{g^2}{2\pi^3\hbar(\hbar c)^6}\right)|M_{fi}|^2 E_e\sqrt{E_e^2 - m_e^2} \times (E_0 - E_e)^2 \times F(Z_Y, E_e)dE_e \tag{4.93}$$

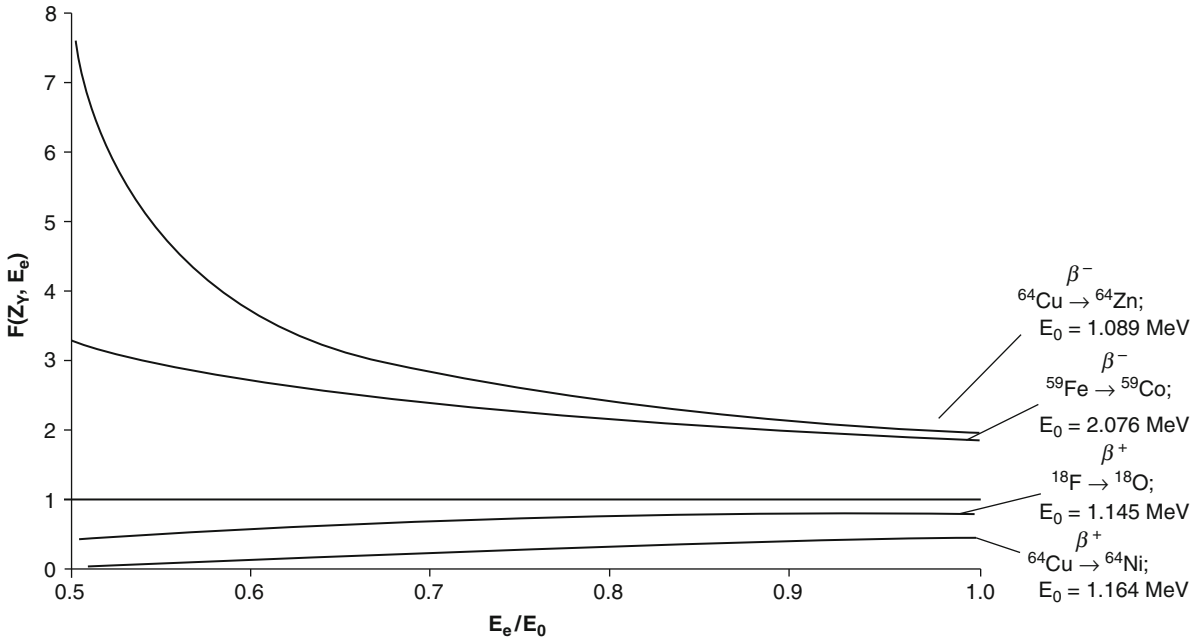

Fig. 4.16 Nuclear Coulomb correction factor used in the phase space factor for Fermi β decay theory to correct for electron/positron plane-wave assumption for two different types each of β^- and β^+ decays as a function of the total electron/positron energy (sum of kinetic and rest mass energies) normalized to the maximum total energy available from the decay kinematics. $F(Z_Y, E_e) = 1$ is shown as a *horizontal line*

As a result of the zeroth-order truncation of the lepton wavefunction expansions, the nuclear matrix element M_{fi} will be independent of the electron and neutrino momenta (those cases of when the expansion of the wavefunctions going beyond first-order and the nuclear matrix element no longer independent of the electron and neutrino momenta are considered later). The shape of the electron/positron energy spectrum is thus defined by the combination of the phase space of the emitted electron/positron and the Fermi factor. Now consider the example of ^{64}Cu, an interesting radionuclide used in a number of nuclear medicine applications and which undergoes all three types of β decay: β^- decay to ^{64}Zn and both β^+ decay and electron capture to ^{64}Ni, as shown in Fig. 4.17.

The ^{64}Cu electron and positron energy spectra are shown in Fig. 4.18 and the differences in the shapes of the spectra at low energies due to the differing electron-nuclear and positron-nuclear Coulomb interactions are readily apparent. The proportion of low-energy electrons exceeds that of low-energy positrons due to the nuclear Coulomb attraction and repulsion, respectively.

Kurie Plot

Additional information about β decay can be had by analyzing the algebraic rearrangement of (4.93),

$$\left(\frac{g^2}{2\pi^3\hbar(\hbar c)^6}\right)|M_{fi}|^2(E_0 - E_e)^2 = \left[\frac{\left(\frac{d\lambda_{fi}}{dE_e}\right)}{F(Z_Y, E_e)E_e\sqrt{E_e^2 - m_e^2}}\right]. \tag{4.94}$$

By taking the square-root of both sides, one can form the linearized equation,

$$K(E_e) \equiv C(E_0 - E_e) \tag{4.95}$$

where,

$$K(E_e) \equiv \sqrt{\frac{\left(\frac{d\lambda_{fi}}{dE_e}\right)}{F(Z_Y, E_e)E_e\sqrt{E_e^2 - m_e^2}}}. \tag{4.96}$$

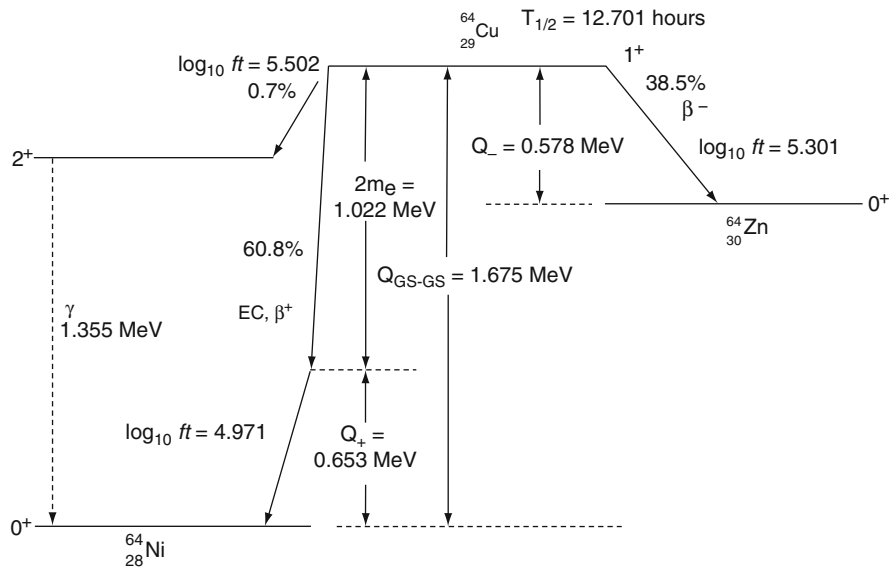

Fig. 4.17 $\beta^{\pm}$ and EC decay schema for ^{64}Cu

The constant is,

$$C = \sqrt{\left(\frac{g^2}{2\pi^3\hbar(\hbar c)^6}\right)|M_{fi}|^2}. \tag{4.97}$$

A plot of (4.96) vs. electron energy, known as the Kurie plot, can yield considerable information concerning a β decay, as shown schematically in Fig. 4.19. Linear extrapolation to $K(E_e) = 0$ yields $E_e = E_0$ or the Q of the decay for a zero neutrino mass. For a non-zero neutrino mass, the Kurie curve would become nonlinear at high electron energies. This is, in fact, one method used for determining the neutrino mass. Another cause for deviation from linearity arises from C being a constant as a result of, for example, the nuclear matrix element being dependent upon the electron energy. Recall that the independence of M_{fi} from E_e was due to the truncation of the electron wavefunction at zeroth-order due to the assumption of a point nucleus. When nuclear size is not neglected, higher orders of the plane wave expansion are required and the matrix element becomes dependent upon the electron momentum/energy. Such nonlinearities occur for forbidden transitions, so-called for their reduced transition rates.

Decay Constant

In order to calculate the decay constant, λ, it should be recognized that it will be for all final states and is thus obtained by integrating (4.93) over all possible β particle total energies,

$$\begin{aligned}\lambda &= \int_{m_e}^{E_0} dE_e \frac{d\lambda_{fi}(E_e)}{dE_e} \\ &= \left(\frac{g^2}{2\pi^3\hbar(\hbar c)^6}\right)|M_{fi}|^2 \int_{m_e}^{E_0} dE_e E_e\sqrt{E_e^2 - m_e^2} \\ &\quad \times (E_0 - E_e)^2 F(Z_Y, E_e) \\ &= \left(\frac{g^2}{2\pi^3\hbar(\hbar c)^6}\right)|M_{fi}|^2 \int_{m_e}^{E_0} dE_e E_e\sqrt{E_e^2 - m_e^2} \\ &\quad \times (E_0 - E_e)^2 F(Z_Y, E_e).\end{aligned} \tag{4.98}$$

Using the change of variable $x = E_e/m_e$, the transition rate can be rewritten as,

$$\begin{aligned}\lambda &= \left(\frac{g^2 m_e^5}{2\pi^3\hbar(\hbar c)^6}\right)|M_{fi}|^2 \\ &\quad \times \int_1^{x_0} dx\, x\sqrt{x^2 - 1}(x_0 - x)^2 F(Z_Y, x) \\ &= \left(\frac{g^2 m_e^5}{2\pi^3\hbar(\hbar c)^6}\right)|M_{fi}|^2 f(Z_Y, x_0)\end{aligned} \tag{4.99}$$

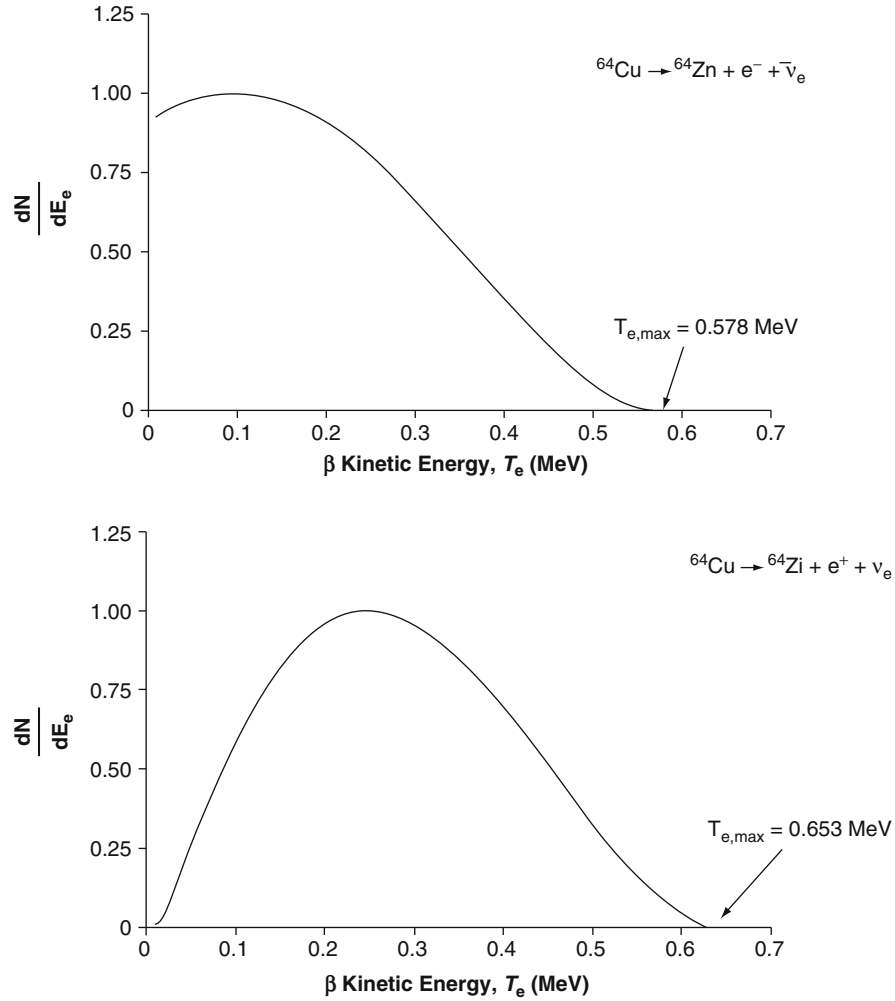

Fig. 4.18 Calculated electron and positron energy spectra for the β^- and β^+ decays of ^{64}Cu. Curves are not normalized

where

$$x_0 = \frac{E_0}{m_e} = 1 + \frac{Q}{m_e} \tag{4.100}$$

and where the Fermi integral is,

$$f(Z_Y, x_0) = \int_1^{x_0} dx\, x\sqrt{x^2 - 1}(x_0 - x)^2 F(Z_Y, x). \tag{4.101}$$

While this integral itself does not have an analytical solution, an approximation to it can be readily solved

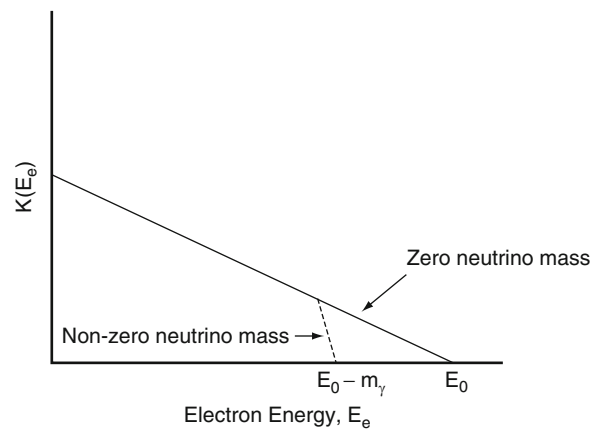

Fig. 4.19 Plot of Kurie function vs. electron energy for zero and non-zero neutrino masses

should the daughter nucleus have a sufficiently small Z_Y such that the Fermi factor is $F(Z_Y, x) \approx 1$,

$$\begin{aligned} f(Z_Y, x_0) &\approx \int_1^{x_0} dx\, x\sqrt{x^2-1}(x_0 - x)^2 \\ &\approx x_0^2 \int_1^{x_0} dx\, x\sqrt{x^2-1} + \int_1^{x_0} dx\, x^3\sqrt{x^2-1} \\ &\quad - 2x_0 \int_1^{x_0} dx\, x^2\sqrt{x^2-1} \\ &\approx \frac{x_0^2}{3}\left(x_0^2-1\right)^{\frac{3}{2}} + \frac{1}{15}\left(x_0^2-1\right)^{\frac{3}{2}}\left(3x_0^2+2\right) \\ &\quad - \frac{x_0^2}{4}\sqrt{x_0^2-1}\,2\left(x_0^2-1\right) \\ &\approx \frac{\sqrt{x_0^2-1}}{60}\left(2x_0^4 - 9x_0^2 - 8\right). \end{aligned} \tag{4.102}$$

From this result, it can be see that an approximate proportionality arises for the transition rate,

$$\lambda \propto \frac{E_0^5}{30} \tag{4.103}$$

which predicts a strong dependence of the transition rate upon the magnitude of the energy released by the decay and that the transition rate will increase markedly with released energy. Equation (4.103) is Sargent's rule (1933). This strong dependence of the transition rate upon the decay kinematics must be addressed if one wishes to compare different β-decays with varying kinematics. This dependence upon Q can be removed by defining the comparative half-life as the product of the physical half-life and the integral of (4.101),

$$\begin{aligned} ft &\equiv f(Z_Y, x_0) T_{1/2} \\ &= \frac{\ln 2}{\left(\frac{g^2 m_e^5}{2\pi^3 \hbar (\hbar c)^6}\right)|M_{fi}|^2} \propto \frac{1}{|M_{fi}|^2}. \end{aligned} \tag{4.104}$$

As values of ft range considerably in magnitude, it is conventional to work with the logarithm of the comparative half-life, $\log_{10}$ ft (where t is in units of seconds). This large variation of the comparative half-life is indicative of the dependence upon the nuclear wavefunctions, as shown by (4.104). The simplest β decays (generally involving low-Z nuclei) involve the greatest overlap of the initial- and final-state nuclear wavefunctions and, from (4.102), the smallest comparative half-life values. $\log_{10}$ ft values are provided in the β decay schema and in Table 4.3.

4.3.3.3 Electron Capture

While the decay constant for EC will be calculated in the same manner as that for β decay, two distinct differences between EC and β decay should be noted in the calculation of the matrix element and the phase space factor. First, the neutrino is the only lepton in the final state. Second, the electron is present in the initial state but, because it is an orbital atomic electron, it cannot be approximated by a plane-wave wavefunction. The EC transition rate is,

$$\lambda_{fi,EC} \approx \frac{2\pi}{\hbar}\frac{1}{L^3}\left|\int d^3\mathbf{r}\,\psi^*_{nuc,f}\, U \psi_{nuc,i}\psi_e\right|^2 \rho_f \tag{4.105}$$

where the plane-wave approximation has been applied to the neutrino only with, again, truncation to zeroth-order. As before, the potential is set equal to a coupling constant g within the nucleus and zero beyond, giving,

$$\lambda_{fi,EC} \approx \frac{2\pi}{\hbar}\frac{g^2}{L^3}\left|\int d^3\mathbf{r}\,\psi^*_{nuc,f}\,\psi_{nuc,i}\,\psi_e\right|^2 \rho_f. \tag{4.106}$$

As lower orbitals predominate in electron capture due to their closer proximity to the nucleus and the resultant greater degree of overlap between the nuclear and electronic wavefunctions, we calculate $\lambda_{fi,EC,K}$ for a K-shell electron. The wavefunction for a 1s-orbital electron in a hydrogen-like atom with atomic number, Z_X, is,

$$\psi_{e,K}(r) = \sqrt{\frac{Z_X^3}{\pi r_\infty^3}} e^{-\left(\frac{Z_X r}{r_\infty}\right)} \tag{4.107}$$

where r_∞ is the Bohr radius and Z_x is the atomic number for the parent nucleus. As r is of the order of 5 fm, the ratio $r/r_\infty \approx 10^{-4}$ allowing the exponential term to be neglected and the electron wavefunction treated as being spatially invariant within the nucleus,

$$\psi_{e,K} \approx \sqrt{\frac{Z_X^3}{\pi r_\infty^3}}. \tag{4.108}$$

This simplifies the expression of the EC transition rate to,

$$\lambda_{fi,EC,K} \approx \left(\frac{2g^2}{\hbar r_\infty^3}\right) Z_X^3 \frac{1}{L^3} |M_{fi}|^2 \rho_f \tag{4.109}$$

where the subscript K for the decay constant indicates that the calculation is explicitly for the capture of a K-orbital electron. The differential phase space term for this 2-body decay is,

$$d\rho_f = \frac{1}{(2\pi\hbar c)^3} (4\pi L^3) p_{\nu_e}^2 dp_{\nu_e} \delta(Q - T_{\nu_e})$$

which, for the massless neutrino, reduces to,

$$\frac{d\rho_f}{dE_{\nu_e}} = \frac{L^3}{2\pi^2(\hbar c)^3} E_{\nu_e}^2 \delta(E_0 - E_{\nu_e}).$$

Integrating over the neutrino energy gives the complete phase space factor (as this is a 2-body decay with a negligible recoil kinetic energy, the neutrino will take all of the available energy),

$$\rho_f(E_0) = \frac{L^3}{2\pi^2(\hbar c)^3} E_0^2 \tag{4.110}$$

which yields the electron capture transition rate,

$$\lambda_{fi,EC,K} = \left(\frac{g^2}{\pi^2\hbar(\hbar c)^3 r_\infty^3}\right) Z_X^3 |M_{fi}|^2 E_0^2.$$

As $r_\infty = \hbar c/\alpha m_e$,

$$\lambda_{fi,EC,K} = \left(\frac{g^2 m_e^3 \alpha^3}{\pi^2\hbar(\hbar c)^6}\right) Z_X^3 |M_{fi}|^2 E_0^2. \tag{4.111}$$

By defining the dimensionless quantity

$$f_{EC,K}(Z_X, E_0) = (\alpha Z_X)^3 \left(\frac{E_0}{m_e}\right)^2 \tag{4.112}$$

the electron capture decay constant can be written in the form,

$$\lambda_{fi,EC,K} \equiv \left(\frac{g^2 m_e^5}{\pi^2\hbar(\hbar c)^6}\right) |M_{fi}|^2 f_{EC,K}(Z_X, E_0). \tag{4.113}$$

Note that electron capture decay rate has a Z^3-dependence contained within the $f_{EC,K}(Z_X, E_0)$ term.

4.3.4 Selection Rules for β Decay

4.3.4.1 Introduction

Having established the kinematic requirements for β decay to occur and the probability with which it will occur, it is now necessary to include the two so far neglected two important and linked features: first, the constituents of a β decay have angular momentum and, second, the decaying nucleus has a finite size. These have significant effects upon the probability of a given β decay (Lipkin 1962).

Conservation of the total angular momentum in β decay requires that the difference between the angular momenta of the parent and daughter states equals the total angular momentum carried away by the lepton pair. This investigation of the deep role angular momentum plays in β decay is begun by considering the simplest case of β^- decay, free neutron decay, $n \rightarrow p + e^- + \bar{\nu}_e$, as shown in Fig. 4.20. As the neutron is considered to be a point entity, no orbital angular momentum is involved.

There are two possible final states resulting from free neutron decay which correspond to the emitted lepton pair having either antiparallel or parallel spins. The transition leading to the final state in which the lepton pair forms a spin singlet (i.e., coupled spin of 0) is referred to as a Fermi transition, for a reason to be shown later. As a consequence of the lepton spin coupling, the spin state of the proton must be the same as that of the neutron. The other final state, that in which the lepton pair form a triplet (coupled spin of 1) and the spin states of the neutron and proton are consequently opposed, is the result of a Gamow–Teller transition (Gamow and Teller 1936). In a

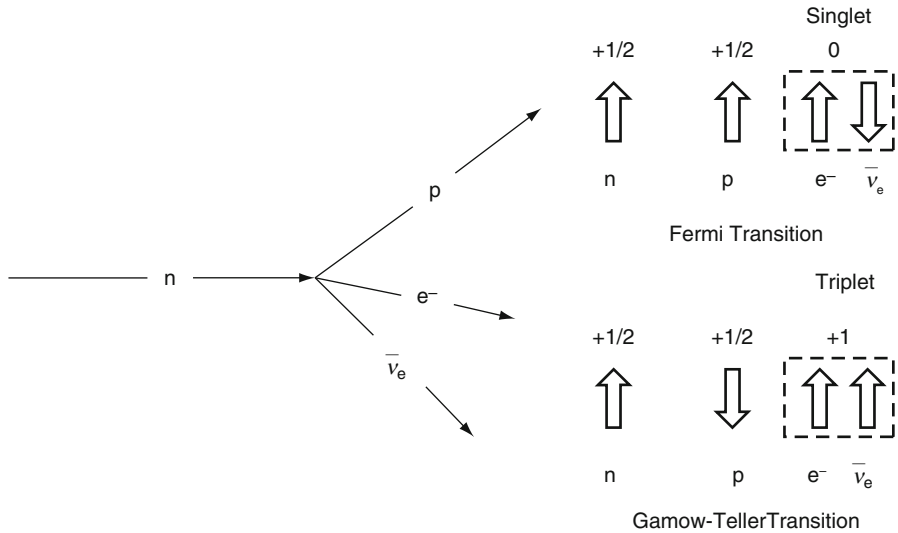

Fig. 4.20 β decay in the four-point vertex approximation of a free neutron and the combinations of final spin states for Fermi and Gamow–Teller transitions

Fermi transition for neutron decay, the operator transforming the neutron spin state to that of a proton is the unit operator. On the other hand, in the Gamow–Teller transition the transformation of the neutron spin to the proton spin is linked through the Pauli spin matrices. Purely on the basis of this result, one would expect the probability of a Gamow–Teller transition for neutron decay to be three times greater than that of the Fermi transition. This is not quite the case and the ratio of the Gamow–Teller to Fermi transitions is actually equal to $3c_A^2$, where $c_A = 1.26$, a consequence of the quark structure of the nucleon.

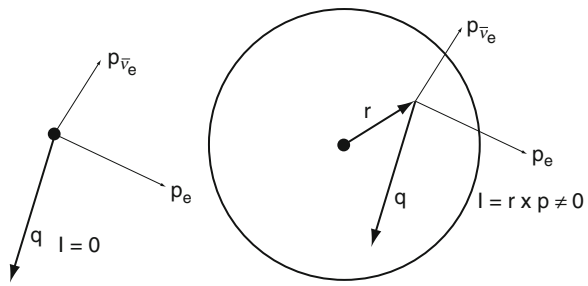

Fig. 4.21 Effects of angular momentum in β decay. In the first case, the nucleus is considered as a point and the matrix element as being independent of electron and antineutrino momenta. The orbital angular momentum of the exiting leptons is zero. In the second case, the nucleus has a finite size and the lepton pair leaves with a non-zero angular momentum

4.3.4.2 Selection Rules in Nuclear β decay

Introduction

Next consider the role of angular momentum in nuclear β decay. Throughout this study of nuclear β decay so far, it has been noted several times that the finite size of the nucleus has been ignored. This allows the lepton wavefunction expansions to be truncated to zeroth-order and, implicitly, for the lepton pair to be taken to have been emitted from the nucleus with zero angular momentum. As, classically, $\mathbf{l} = \mathbf{r} \times \mathbf{p} = \mathbf{0}$, this latter condition is equivalent to saying that the leptons are emitted radially (i.e., s wave) from the nucleus as shown in Fig. 4.21. Thus, as in free neutron decay, the change in nuclear angular momentum will equal the coupling of the leptons into either a singlet or triplet state.

When nuclear size is not neglected, there are two significant consequences to the description of nuclear β decay. First, non-zero orbital angular momentum is now made available to the lepton pair and the change in nuclear angular momentum can be greater than one. Second, these non-zero orbital angular momentum β decays contribute to the transition rate through the higher-order terms of the lepton wavefunctions' expansions. As these additional contributions are of the order of $(qR_N)^l$, the non-zero orbital angular momentum transition will be highly suppressed relative to the s-wave transitions. Consequently, β decays

associated with $l = 0$ are referred to as being "allowed" whereas those with $l > 0$ are labeled as being "forbidden."

Of the allowed transitions, the Fermi requirement of a singlet lepton pair obviously dictates that there be no change in the nuclear angular momentum between parent and daughter nuclei, $\Delta J = 0$. As the lepton pair is in the triplet state following a Gamow–Teller decay, the vector difference between the parent's and daughter's nuclear angular momenta must equal unity and the change in nuclear angular momentum will be $\Delta J = 0,\ 1$ but with no $0 \rightarrow 0$ transition. In either allowed transition, there will be no change in nuclear parity due to $l = 0$.

Allowed Nuclear β decays

As β decay results in the change of isospin-projection, isospin operators are required in describing these transitions. Recalling the isospin ladder operators of Chap. 3, $\tau_{\pm} = \frac{\tau_1 \pm i\tau_2}{2}$, one can write operators for Fermi and Gamow–Teller transitions for the nucleus as summations of the isospin ladder operators over all nucleons (i.e., the operators act over the entire nuclear wavefunction),

$$\mathbf{T}_{\pm} = \sum_{i=1}^{A} \boldsymbol{\tau}_{\pm}(i) \quad \text{Fermi transition} \tag{4.114}$$

$$\mathbf{Y}_{\pm} = \sum_{i=1}^{A} \boldsymbol{\sigma}(i)\boldsymbol{\tau}_{\pm}(i) \quad \text{Gamow} - \text{Teller transition.} \tag{4.115}$$

As the Gamow–Teller transition results in a change in angular momentum, the Pauli spin matrix operator, $\boldsymbol{\sigma}(i)$, must be included. Table 4.3 summarizes the selection rules for Fermi and Gamow–Teller transitions.

Fermi's β decay theory, to which this discussion shall return, predicted only $\Delta J = 0$ transitions and the characteristics of the first row of Table 4.3. However, there was experimental evidence of the β^- decay $^6\text{He} \rightarrow {}^6\text{Li} + e^- + \bar{\nu}_e$, in which the J^π of the parent and daughter nuclei are 0^+ and 1^+ and the change in nuclear isospin was $|\Delta T| = 1$. Such a transition would

Table 4.3 Selection rules for Fermi and Gamow–Teller allowed β decays

Transition	Change in Angular momentum, ΔJ	Parity ΔΠ	Isospin ΔT
Fermi	0	0	0
Gamow–Teller	$\lvert\Delta J\rvert = 0,1$ No $0 \rightarrow 0$	0	$\lvert\Delta T\rvert = 0,1$ No $0 \rightarrow 0$

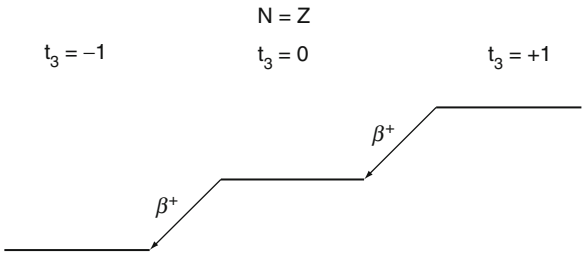

Fig. 4.22 Fermi transitions for β^+ decay between isobaric analogue states. Due to the Coulomb interaction between protons, corresponding energy levels in an isobar multiplet are higher for an isobar with a greater number of protons

be forbidden by the Fermi selection rules but obey the Gamow–Teller selection rule. As there are β decays that satisfy the Fermi selection rule (e.g., the $^{14}\text{O} \rightarrow {}^{14}\text{N}^* + e^+ + \nu_e$ for which the J^π of the parent and daughter nuclei are both 0^+), both transitions existed in nature. Moreover, the summary of the transition rules of Table 4.3 shows that some β decays are permitted by both Fermi and Gamow–Teller selection rules, an obvious example being that of free neutron decay. In other words, every Fermi transition contains an admixture of a Gamow–Teller transition, except for a $0 \rightarrow 0$ transition.

From (4.114), one sees that the Fermi transition occurs through the isospin ladder operator and, hence, can only occur between isospin multiplets. This sets a severe restriction upon this transition type. As these transitions can only occur between isobaric analogue states, it is necessary to reflect upon the energy differences between the nuclear levels of the parent and daughter nuclei. The energies of matching levels will increase with atomic number due to the Coulomb repulsion between protons. Hence, Fermi transitions cannot occur in β^- decays, as shown by Fig. 4.22. But even within the permitted β^+ decays, Fermi transitions can occur only for nuclei with more protons than neutrons since, in the case of $N > Z$, the isospin of the daughter nucleus exceeds

that of the parent. In practice, Fermi transitions are relegated to β^+ decays in light nuclei.

The β-decay transition matrix element can be split up into Fermi and Gamow–Teller components,

$$|M_{fi}|^2 = |C_F|^2|M_F|^2 + |C_{GT}|^2|M_{GT}|^2 \qquad (4.116)$$

where one averages over the initial spin states and sums over the final spin states,

$$|M_F|^2 = \frac{1}{2J_i+1}\sum_{i,f}|\langle\psi_f|\mathbf{T}_\pm|\psi_i\rangle|^2 \qquad (4.117)$$

$$|M_{GT}|^2 = \frac{1}{2J_i+1}\sum_{i,f}|\langle\psi_f|\mathbf{Y}_\pm|\psi_i\rangle|^2. \qquad (4.118)$$

The reduced transition probabilities are defined as,

$$B_F^\pm = \frac{|\langle\psi_f|\mathbf{T}_\pm|\psi_i\rangle|^2}{2J_i+1} \qquad (4.119)$$

$$B_{GT}^\pm = \frac{c_A^2|\langle\psi_f|\mathbf{Y}_\pm|\psi_i\rangle|^2}{2J_i+1}. \qquad (4.120)$$

The effects of the nuclear structure upon the allowed transition are contained within $B_F^\pm$ and $B_{GT}^\pm$. The transition rate of (4.99) can thus be rewritten as,

$$\lambda = \left(\frac{g^2 m_e^5}{2\pi^3\hbar(\hbar c)^6}\right)(B_F + B_{GT})f(Z_Y, x_0) \qquad (4.121)$$

Forbidden Nuclear β decays

Forbidden transitions are those with large log ft values, involve parity change and an angular momentum change of greater than one (Marshak 1942). The total angular momentum taken by the lepton pair is $\mathbf{J} = \mathbf{L} \oplus \mathbf{S}$, which, for a lepton pair, assumes values of $(l-1), l, (l+1)$. A first-forbidden transition is one for $l = 1$, a second-forbidden transition is one for $l = 2$, etc. Parity can change in forbidden transitions as $\Delta\Pi = \Pi_f\Pi_i = (-1)^l$ and $l > 0$. Table 4.4 presents the categories of allowed and forbidden β-decay transitions and the corresponding observed ranges of $\log_{10} ft$ values, and Table 4.5 gives transition data for a variety of β decays.

Table 4.4 Categories of β decay transitions

Decay type	ΔJ	ΔΠ	Typical range of $\log_{10} ft$
Superallowed (Fermi and GT)	0	No	3
Allowed	0, 1; not $0 \to 0$	No	4–6
First forbidden	0, 1, 2	Yes	5–10
Second forbidden	2, 3	No	11–16
Third forbidden	3, 4	Yes	17–22
Fourth forbidden	4, 5	No	22–24

4.3.5 Fermi Theory of β Decay: Part II

4.3.5.1 Four-Fermion Interaction Vertex

Modern weak interaction theory underlying β decay is based upon the exchange of the massive intermediate vector bosons, $W^\pm$ and Z^0, between fermions. Fermi's theory did not include these exchanges but instead described the weak interaction in analogy to the electromagnetic interaction (Fig. 4.23) but as occurring at a vertex at which four fermions meet. Because the intermediate vector bosons are massive (the $W^\pm$ has a rest mass of over 80 GeV), the corresponding interaction distance is small (of the order of 10^{-3} fm) and, hence, Fermi's use of a point interaction is valid for β decay. In fact, the Fermi theory represents the low-energy limit of the modern Glashow–Weinberg–Salam theory. Here, we look at Fermi's relativistic theory applied to the simple case of neutron decay and the weak interaction.

To work through the Fermi theory, one can begin by considering it, as did Fermi, as an analogue to the electromagnetic interaction. Electrons produce an electromagnetic four-current density of the form, $J_\mu^{EM}(X) = -\overline{\psi}_e(X)\gamma_\mu\psi_e(X)$ which couples to the electromagnetic field $A^\mu(X)$ to form the electromagnetic Hamiltonian density, $H_{EM}(X) = -e\overline{\psi}_e(X)\gamma_\mu\psi_e(X)A^\mu(X)$. Before deriving the Fermi theory, recall that the matrix

Table 4.5 Transition data for β decays (in order of increasing log *ft*)

Parent	Decay mode	Daughter	$J_i^\pi \rightarrow J_f^\pi$	Transition	Half-life	$\log_{10} ft$
^{6}He	β^-	^{6}Li	$0^+ \rightarrow 1^+$	GT	797 ms	2.77
^{3}H	β^-	^{3}He	$\frac{1}{2}^+ \rightarrow \frac{1}{2}^+$	F/GT	12.33 years	3.05
^{14}O	β^-	^{14}N[a]	$0^+ \rightarrow 0^+$	F	71.36 s	3.495
^{18}F	96.86% β^+, 3.14% EC	^{18}O	$1^+ \rightarrow 0^+$	GT	1.8295 h	3.57
^{11}C	99.7% β^+, 0.3% EC	^{11}B	$\frac{3}{2}^- \rightarrow \frac{3}{2}^-$	F/GT	20.39 min	3.592
^{15}O	99.9% β^+, 0.1% EC	^{15}N	$\frac{1}{2}^- \rightarrow \frac{1}{2}^-$	F/GT	2.037 min	3.6
^{13}N	99.8% β^+, 0.2% EC	^{13}C	$\frac{1}{2}^- \rightarrow \frac{1}{2}^-$	F/GT	9.965 min	3.654
^{64}Cu	18% β^+, 44.9% EC	^{64}Ni	$1^+ \rightarrow 0^+$	GT	12.701 h	4.97
	37.1% β^-	^{64}Zn				5.29
^{14}C	β^-	^{14}N	$0^+ \rightarrow 1^+$	GT	5,730 years	9.04[a]
^{39}Ar	β^-	^{39}K	$\frac{7}{2}^- \rightarrow \frac{3}{2}^+$	Forbidden	269 years	9.03
^{10}Be	β^-	^{10}B	$0^+ \rightarrow 3^+$		1.6×10^6 years	12.08
^{40}K	β^-	^{40}Ca	$4^- \rightarrow 0^+$		1.26×10^9 years	15.6
^{115}In	β^-	^{115}Sn	$\frac{9}{2}^+ \rightarrow \frac{1}{2}^+$		6×10^{14} years	23.0

[a]Although $^{14}\mathrm{C} \xrightarrow{\beta^-} {}^{14}\mathrm{N}$ is an allowed transition, the high $\log_{10}$ ft value is due to a small matrix element

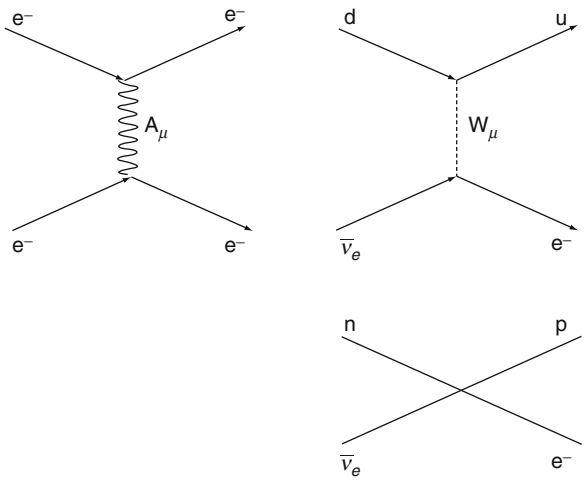

Fig. 4.23 The electromagnetic and weak interactions shown as the exchange of bosons; the Fermi four-fermion vertex approximates the short distance flavor-changing exchange of the intermediate vector $W^{\pm}$ boson as a single interaction point

element for β decay contains the wavefunctions of four spin-½ particles corresponding to,

$$\mathrm{n} \rightarrow \mathrm{p} + \mathrm{e}^- + \bar{\nu}_\mathrm{e}$$

$$\mathrm{p} \rightarrow \mathrm{n} + \mathrm{e}^+ + \nu_\mathrm{e}$$

$$\mathrm{p} + \mathrm{e}^- \rightarrow \mathrm{n} + \nu_\mathrm{e}.$$

In each case, there are hadronic and leptonic components[22] and, hence, weak hadronic and weak leptonic current densities must be constructed. The weak hadronic current density applied to free neutron decay is,

$$\mathrm{V}_\mu^{\mathrm{C}\,\dagger}(\boldsymbol{X}) = \overline{\psi}_\mathrm{p}(\boldsymbol{X})\gamma_\mu\,\psi_\mathrm{n}(\boldsymbol{X}) \tag{4.122}$$

and a leptonic current density is,

$$\mathrm{l}_\mu^\mathrm{C}(\boldsymbol{X}) = \overline{\psi}_\mathrm{e}(\boldsymbol{X})\gamma_\mu\,\psi_{\nu_\mathrm{e}}(\boldsymbol{X}). \tag{4.123}$$

Recall that the Dirac 4×4 matrices are,

$$\gamma_0 = \begin{pmatrix} \mathbf{1} & 0 \\ 0 & -\mathbf{1} \end{pmatrix}$$

$$\gamma_\mathrm{i} = \begin{pmatrix} 0 & \boldsymbol{\sigma}_\mathrm{i} \\ -\boldsymbol{\sigma}_\mathrm{i} & 0 \end{pmatrix} \quad \mathrm{i} = 1, 2, 3$$

and where the C superscript indicates that the electric charge of the hadron is being changed. For a point-like

[22]A full examination of the weak interaction would consider the pure leptonic currents of, say, $\mu^- \rightarrow \mathrm{e}^- + \nu_\mathrm{e} + \bar{\nu}_\mathrm{e}$ or the pure hadronic currents of $\mathrm{K}^+ \rightarrow \pi^+ + \pi^+ + \pi^-$.

interaction between these two currents, a Hermitian Hamiltonian density can be constructed as,

$$\begin{aligned} H(\boldsymbol{X}) &= g\left(V^{C\mu}(\boldsymbol{X})I_{\mu}^{C\dagger}(\boldsymbol{X}) + I^{C\mu}(\boldsymbol{X})V_{\mu}^{C\dagger}(\boldsymbol{X})\right) \\ &= g\left(\overline{\psi}_n(\boldsymbol{X})\gamma^{\mu}\psi_p(\boldsymbol{X})\overline{\psi}_{\nu_e}(\boldsymbol{X})\gamma_{\mu}\psi_e(\boldsymbol{X})\right. \\ &\quad \left. + \overline{\psi}_e(\boldsymbol{X})\gamma^{\mu}\psi_{\nu_e}(\boldsymbol{X})\overline{\psi}_p(\boldsymbol{X})\gamma_{\mu}\psi_n(\boldsymbol{X})\right) \\ &= gV. \end{aligned} \tag{4.124}$$

The V denotes this to be a vector interaction as $\bar{\psi}\,\gamma_{\mu}\,\psi$ transforms like a polar vector when undergoing a Lorentz transformation. The first term of this Hamiltonian describes β^+ decay and electron capture and the second term describes β^- decay. Importantly, the vector Hamiltonian describes a Fermi transition. To demonstrate this, consider the nonrelativistic case for which the nucleon wavefunction is $\psi = \begin{pmatrix} \phi \\ 0 \end{pmatrix}$. Then, the $\mu = 0$ component of the nucleon current is,

$$\begin{aligned} \overline{\psi}_p\gamma_0\psi_n &= \psi_p^+\gamma_0\gamma_0\psi_n \\ &= \begin{pmatrix} \phi_p^+ & 0 \end{pmatrix}\begin{pmatrix} \mathbf{1} & 0 \\ 0 & \mathbf{1} \end{pmatrix}\begin{pmatrix} \phi_n \\ 0 \end{pmatrix} \\ &= \phi_p^+\phi_n \end{aligned} \tag{4.125}$$

and the $\mu = 1, 2, 3$ space component is,

$$\begin{aligned} \overline{\psi}_p\gamma_{\mu}\psi_n &= \psi_p^+\gamma_0\gamma_{\mu}\psi_n \\ &= \begin{pmatrix} \phi_p^+ & 0 \end{pmatrix}\begin{pmatrix} \mathbf{1} & 0 \\ 0 & -\mathbf{1} \end{pmatrix}\begin{pmatrix} 0 & \boldsymbol{\sigma}_{\mu} \\ -\boldsymbol{\sigma}_{\mu} & 0 \end{pmatrix}\begin{pmatrix} \phi_n \\ 0 \end{pmatrix} \\ &= \begin{pmatrix} \phi_p^+ & 0 \end{pmatrix}\begin{pmatrix} \mathbf{1} & 0 \\ 0 & -\mathbf{1} \end{pmatrix}\begin{pmatrix} 0 \\ -\boldsymbol{\sigma}_{\mu}\phi_n \end{pmatrix} \\ &= \begin{pmatrix} \phi_p^+ & 0 \end{pmatrix}\begin{pmatrix} 0 \\ \boldsymbol{\sigma}_{\mu}\phi_n \end{pmatrix} \\ &= 0. \end{aligned} \tag{4.126}$$

Hence, $\Delta J = 0$. However, as Gamow–Teller transitions exist in nature, it is clear that this vector–vector (VV) coupling cannot be the only interaction involved in weak decays. Gamow and Teller noted that other Lorentz-invariant current densities beyond the VV coupling of $\gamma^{\mu}\gamma_{\mu}$ can be made. From these constructs, there are five types of current density structure,

Scalar (S)	$\overline{\psi}_p\psi_n$
Pseudoscalar (P)	$\overline{\psi}_p\gamma_5\psi_n$
(Polar) vector (V)	$\overline{\psi}_p\gamma_{\mu}\psi_n$
(Axial) vector (A)	$\overline{\psi}_p\gamma_5\gamma_{\mu}\psi_n$
Tensor (T)	$\overline{\psi}_p\gamma_{\mu}\gamma^{\nu}\psi_n$

As has been done for the VV current coupling, Hamiltonians can be constructed from these structures. However, a real Hamiltonian must reduce to a single component and, hence, can only be a scalar or pseudoscalar quantity. The only resulting possible couplings yielding such quantities are SS, VV, TT, AA, PS and VA. A pseudoscalar weak Hamiltonian was not considered acceptable as it violated parity conservation (recall Table 3.2 in Chap. 3) and, as the PS and VA couplings yielded such a parity-nonconserving Hamiltonian, they were rejected until the 1950s. It was not considered possible that parity would not be conserved in weak interactions as it was in the strong and electromagnetic interactions. Up until that time, the weak interaction was assumed to be made up of SS and TT components which permitted a Gamow–Teller transition with a scalar Hamiltonian. But before this is demonstrated to not be the case, the experimental evidence of parity violation by the weak interaction during the 1950s and which led to the appropriate current coupling is reviewed.

4.3.5.2 Evidence for Parity Nonconservation in Weak Interactions

The θ-τ Dilemma

θ and τ mesons were discovered in cosmic rays (they are now known as K mesons, or kaons). Experiment demonstrated that while they had the same mass, spin, and half-life, they differed in their decay processes,

$$\tau^+ \rightarrow \pi^+ + \pi^0$$

$$\theta^+ \rightarrow \pi^+ + \pi^0 + \pi^0 \text{ or } \theta^+ \rightarrow \pi^+ + \pi^+ + \pi^-.$$

These are weak decays (with mean lifetimes of the order of 10^{-8} s) and it was within this difference between decay products that a fundamental dilemma arose. The pion has zero spin and a negative intrinsic parity as shown experimentally by pion absorption in deuterium. Hence the dipion final state of τ meson decay has a parity of $+1$ whereas the tripion final

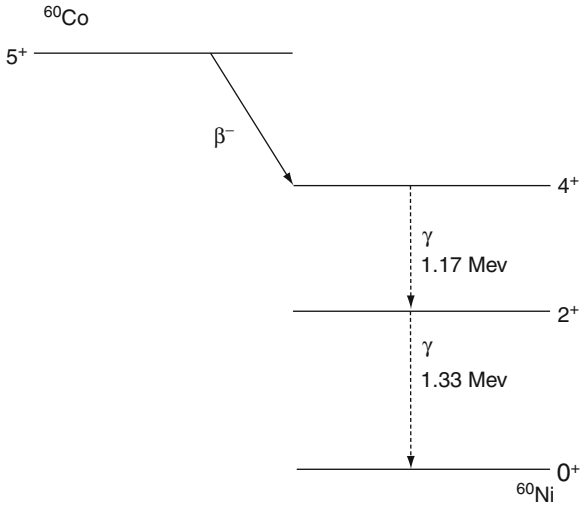

Fig. 4.24 ^{60}Co β^- decay to ^{60}Ni

state of θ meson decay has a parity of −1. The only evident difference between the θ and τ mesons was their parity, and this indicated the nonconservation of parity. This result was problematic as parity selection rules had worked well in nuclear and atomic physics (i.e., parity was conserved in strong and electromagnetic interactions). Triggered by this dilemma, Lee and Yang (1956) postulated the possibility that parity was in fact not conserved in weak interactions. They reviewed the results of all known experiments of the weak interaction performed to that time to detect evidence for parity nonconservation. Their review concluded that all prior experiments had in fact measured scalar quantities and, thus, unable to detect parity violation.[23] They recommended a number of tests to determine if parity is conserved in weak interactions. The critical one was performed by Wu et al. (1957) and is discussed next.

Parity Nonconservation in β Decay

On the basis of Lee's and Yang's suggestions, Wu et al. (1957) designed and performed a fundamental

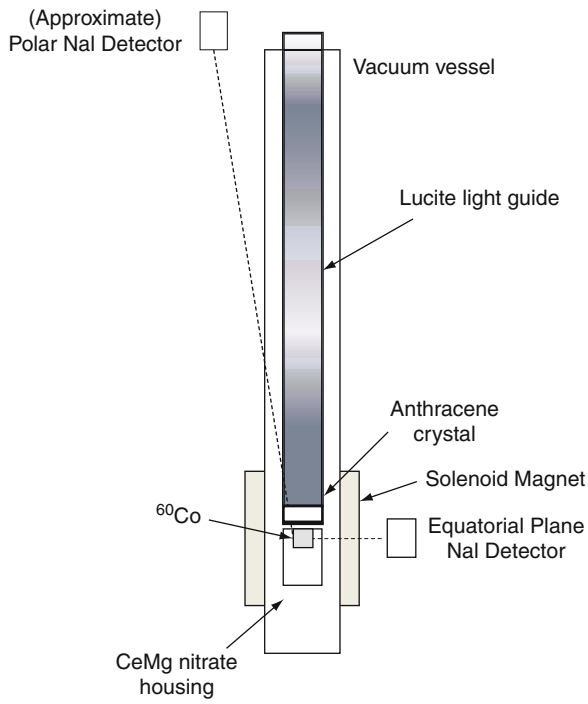

Fig. 4.25 Schematic diagram of experimental apparatus used by Wu et al. (1957) to detect parity nonconservation in β decay

experiment to prove the nonconservation of parity by measuring a pseudoscalar quantity in the Gamow–Teller β^- decay of ^{60}Co to ^{60}Ni of Fig. 4.24. It will be noted that photon emissions are associated with this decay.[24] The experiment was designed to measure the expectation value of the scalar product of the nuclear spin and the electron momentum, which is a pseudoscalar variable.

The experiment is shown schematically in Fig. 4.25. The apparatus was designed to measure the mean value of the pseudoscalar quantity given by the scalar product of the velocity of the electron emitted in the β^- decay of ^{60}Co and the orientation of the nuclear spin, $\overline{\mathbf{v} \bullet \mathbf{J}}$. Should parity be conserved, this mean value would be zero, indicating that β decay is symmetric in space. In order to orient the spin of the ^{60}Co nucleus, a ^{60}Co sample in the form of a 50 μm thick layer coated on the top of a paramagnetic crystal cerium magnesium nitrate was cooled to 0.003°K using adiabatic demagnetization. The entire structure was encased within a vacuum vessel and surrounded

[23]However, Cox et al. (1928) had unknowingly provided evidence for parity conservation in their measurements of the longitudinal polarization of electrons from β decay. This result was disbelieved at the time due to, for example, the failure of attempts to reproduce the measurements but by using unpolarized electrons arising from thermionic emission.

[24]The 1.17 and 1.33 MeV γ rays are used in radiotherapy.

by a solenoid coil that oriented the spin of the ^{60}Co nuclei.

An anthracene crystal set immediately above the source detected the β particles and a lucite light guide carried the scintillation light from the crystal resulting from electrons bombarding the crystal to an external photomultiplier tube. Two sodium iodide scintillators external to the vacuum vessel were used to detect the degree of ^{60}Co polarization. Regardless of the orientation of the polarized ^{60}Co spin being parallel or antiparallel to the magnetic field, the count-rate from the equatorial sodium iodide (NaI) scintillator counter exceeds that of the polar counter and, hence, provides a measure of the polarization of the nucleus. The measurement was of the change in β particle counting rate during the time following when the nuclei were oriented and then allowed to warm. As the sample warmed, the polarization of the ^{60}Co nuclei was lost, as can be seen in the schematic results of Fig. 4.26. This loss of photon anisotropy was a direct measure of nuclear polarization. As also shown in the figure, the detected β particle rate was greater in one orientation of the ^{60}Co nuclei than in the other: i.e., the emission of β particles is more favored in the direction opposite to that of the nuclear spin. Hence, $\overline{\mathbf{v} \bullet \mathbf{J}} \neq 0$ and the nonconservation of parity in β decay was demonstrated.

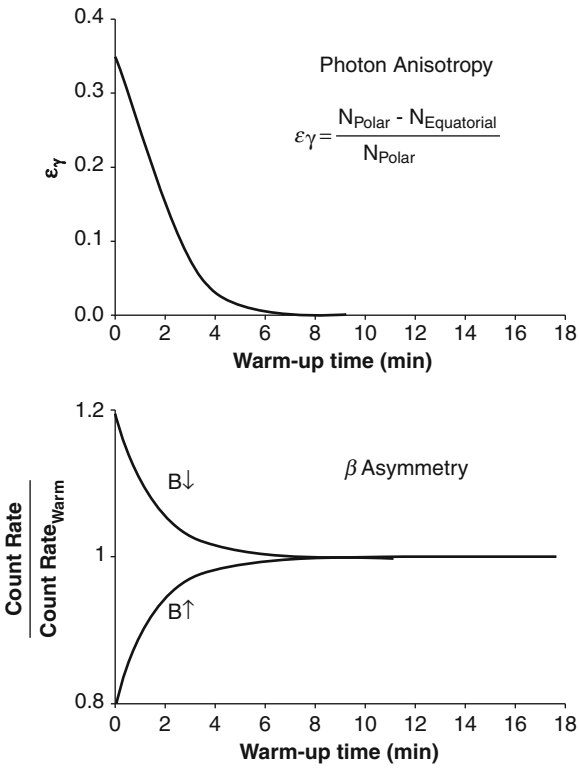

Fig. 4.26 Schematic representation of the results of Wu et al. (1957)

Neutrino Helicity

Here, what is properly regarded as one of the most elegant and cleverest physics experiments ever performed is described. This experiment demonstrated that the orientation of the spin of a neutrino is antiparallel to the neutrino's direction of motion. As the spin is an axial vector and the momentum is a polar vector, a non-zero longitudinal polarization of the neutrino is indicative of parity violation. The helicity operator for a fermion is defined as,

$$\aleph = \frac{\mathbf{p} \bullet \boldsymbol{\sigma}}{|\mathbf{p} \bullet \boldsymbol{\sigma}|} = 2\hat{\mathbf{p}} \bullet \boldsymbol{\sigma} \tag{4.127}$$

where $\boldsymbol{\sigma}$ is the spin operator and $\mathbf{p}$ is the momentum operator. $\aleph$ has the eigenvectors $|\psi_\pm\rangle$, which are states in which the spin is parallel or antiparallel to the particle's direction of motion with eigenvalues ± 1,

$$\aleph|\psi_\pm\rangle = \pm|\psi_\pm\rangle. \tag{4.128}$$

Parity invariance would require that neutrinos with positive or negative helicities be equally probable and any type of measured neutrino helicity asymmetry would thus reflect parity violation. The Goldhaber–Grodzins–Sunyar experiment (Goldhaber et al. 1958) demonstrated this helicity asymmetry for ν_e. Their method was to begin with a nucleus with angular momentum 0 which decays through allowed EC (i.e., $l = 0$) to an excited state of a daughter nucleus with angular momentum 1. As the decay is through electron capture, only the daughter nucleus and neutrino are present in the final state and, hence, the neutrino will have a fixed energy due to the at-rest initial state and the two-body final state. The combined angular momenta of the daughter nucleus (angular momentum of 1) and neutrino must equal that of the K-shell electron prior to capture, so one need only measure the polarization of the daughter nucleus in order to determine that of the neutrino. The initial nucleus was

the metastable isomer ^{152m}Eu, produced through neutron bombardment of europium, which undergoes $\beta^{\pm}$ decay and electron capture and Fig. 4.27 shows that part of the decay chain from ^{152m}Eu to ^{152}Sm.

The EC from the 0^- state of ^{152}Eu to the excited 1^- state of ^{152}Sm (which is denoted as ^{152}Sm*) requires the following angular momentum balance. The initial state angular momentum of ½ (that of the K-shell electron) must equal the final state angular momentum made up of the angular momentum of 1 from the ^{152}Sm nucleus and the ½ – spin of the neutrino. This is shown schematically in Fig. 4.28. As the final state of EC is a two-body state with the initial state being at rest, the conservation of momentum requires that the momenta of the ^{152}Sm* nucleus and of the neutrino oppose each other. Further, as the conservation of angular momentum requires that the angular momentum of ^{152}Sm* and the spin of the neutrino oppose each other, the polarizations of the neutrino and the ^{152}Sm* nucleus must be the same. Hence, it is only needed to measure the polarization of the ^{152}Sm* nucleus in order to determine the neutrino polarization. The measurement of the ^{152}Sm* polarization is enabled by the fact that ^{152}Sm* decays electromagnetically through the emission of a γ ray to the ground state of ^{152}Sm, which has zero angular momentum. As the photon is spin-1, the photon spin must be parallel to the angular momentum of ^{152}Sm*, as shown in Fig. 4.29. Hence, photons emitted in the same direction as the ^{152}Sm* nucleus will have the same polarization, to within a factor of ½) as the neutrino. As a result, the measurement of the neutrino polarization/helicity reduces to measurements of the polarization of the photon and its direction relative to that of the ^{152}Sm* nucleus. How this was achieved is shown schematically in Fig. 4.30.

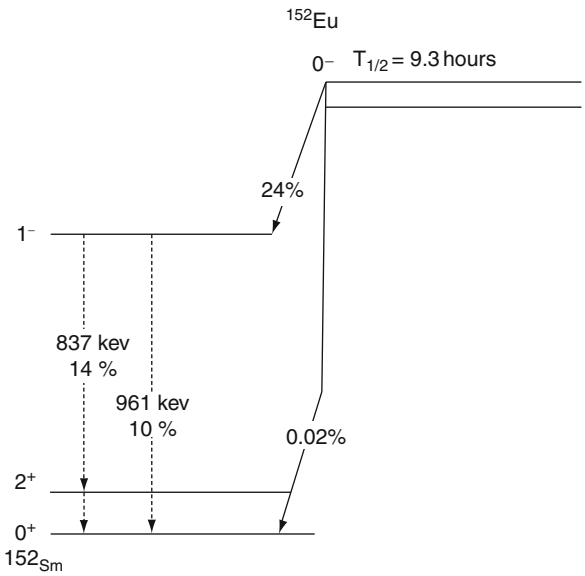

Fig. 4.27 Partial decay schema of ^{152}Eu to ^{152}Sm

The basic structure of the apparatus was of a source of ^{152m}Eu placed within an iron analyzing magnet and a detector consisting of a sodium iodide scintillator coupled to a photomultiplier tube. Surrounding the scintillator was the annular conical frustum made of Sm_2O_3 and the scintillator was shielded from the direct γ rays from the ^{152m}Eu source by lead. The γ rays from the ^{152}Sm* de-excitation that were transmitted through the analyzing magnet were scattered by the Sm_2O_3 annulus through nuclear resonant scattering to be detected by the scintillator. Recall that the

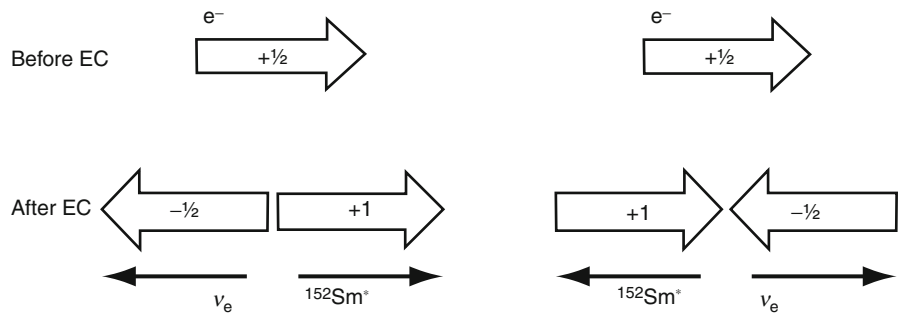

Fig. 4.28 This shows schematically the possible arrangement of the z-components of the spins/angular momenta (*full arrows*) and the momenta (*thin arrows*) of the excited 1^- state of the ^{152}Sm* nucleus and neutrino following electron capture by the 0^- state of ^{152m}Eu. Those on the left correspond to a right-handed neutrino in which the neutrino spin orientation is parallel to the neutrino's direction of motion. Those on the right correspond to a left-handed neutrino in which the neutrino spin orientation is antiparallel to the neutrino's direction of motion

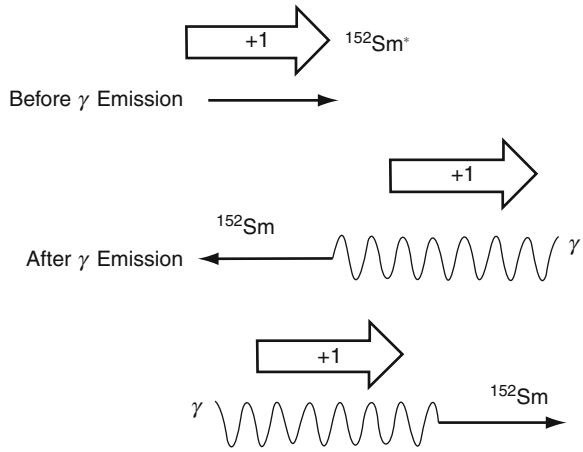

Fig. 4.29 This shows schematically the possible arrangement of the z-components of the spins/angular momenta (*full arrows*) and the momenta (*thin arrows*) of the excited 1^- state of the $^{152}Sm^*$ nucleus and neutrino following electron capture by the 0^- state of ^{152m}Eu. The photon spin is always in the same direction as the angular momentum of $^{152}Sm^*$

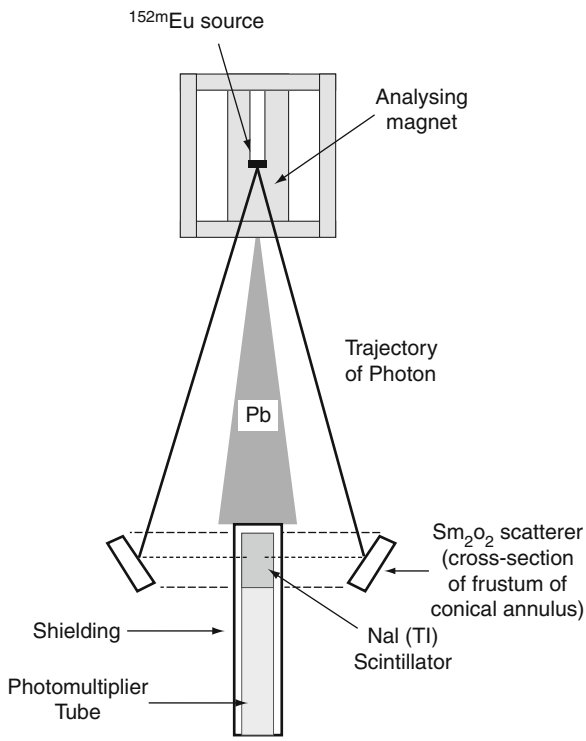

Fig. 4.30 Schematic representation of the Goldhaber–Grodzins–Sunyar experiment to measure the neutrino helicity. See text for description

experiment is to measure the polarization of the photons and their direction relative to the recoil ^{152}Sm nucleus. Depending upon the orientations of the directions of the photon polarization and the spin of the electrons in the magnetized iron, the γ rays resulting from the $^{152}Sm^*$ de-excitation interact with the electrons in the magnetic material differently. If the photon and electron spins are parallel, the incident photon cannot affect the electron spin and does not interact with the electron. If the electron spin is anti-parallel to that of the γ ray, then the photon induces a spin-flip in the electron and is consequently absorbed. Hence, those γ rays with spins parallel to those of the atomic electrons in the magnetic will penetrate the magnet and exit to impinge on the Sm_2O_3 scatterer. By selecting the direction of the field of the analyzing magnet, it was then possible to select the polarization of the transmitted γ rays.

Next, in order to measure the direction of the γ ray relative to the $^{152}Sm^*$ nucleus recoiling from the emission of the neutrino as a result of the EC, advantage was taken over the phenomenon of nuclear resonant scattering. Consider the case in which a nucleus in an excited state of energy E_i decays to a state of energy E_f with the emission of a photon with an energy equal to $\Delta E = E_i - E_f$ in the reference frame of the nucleus. Should another nucleus in the state of energy E_f and of the same species be present in that same reference frame, it can absorb this photon (to within a natural transition width, equal to 23 meV for $^{153}Sm^*$) to yield an excited nucleus with a state of energy E_i . This is the phenomenon of resonant absorption fundamental to the Mössbauer effect. However, an absorbing nucleus

in the ground state will not be found in the same reference frame as the emitting nucleus and, in the laboratory reference frame, the emitted photon will not have an energy equal toΔE but, rather an energy reduced by $(\Delta E)^2/2m_f$, where m_f is the rest mass of the daughter nucleus (this result is derived in the following section). This energy reduction is that due to the recoil energy of the daughter nucleus which, in the case of ^{152}Sm, is equal to about 3.2 eV. This recoil energy is more than enough to shift the photon energy to ensure that resonant scattering cannot occur. However, if the $^{152}Sm^*$ nucleus is already in motion prior to the γ ray de-excitation, it can compensate for this reduction in photon energy by transferring some of the recoil energy resulting from the EC and neutrino emission to the photon (i.e., a Doppler shift). Such a transfer will be a maximum if the photon is emitted in the direction of the $^{152}Sm^*$ motion, thus enabling a reabsorption of the photon by ^{152}Sm in the scatterer and a reemission (nuclear resonant scatter). Thus, those photons detected by the NaI scintillator were generated by those directed in the direction of the $^{152}Sm^*$ motion, the polarization of which were given by the orientation of the magnetic field in the analyzer. The analyzing power, equal to the difference in photon detection rate with the magnetic field directed upwards and that with the field directed downwards normalized to the average, was

$$P = 2\frac{N_+ - N_-}{N_+ + N_-} = 0.017 \pm 0.003$$

This was a non-zero result; in fact, Goldhaber, Grodzins and Sunyar determined, from the estimated three mean free paths for photons through the magnetic material, that 68% of the photons were polarized with negative helicity. Hence, it was demonstrated that neutrinos had negative helicity (i.e., were left-handed). This asymmetry, as noted at the beginning of this discussion, demonstrated the lack of parity conservation in weak interactions.

4.3.5.3 V-A Interaction

The experimental results clearly demonstrated the nonconservation of parity in β decay. The helicity operator ℵ of (4.127) is not relativistically invariant for massive fermions; for such fermions, it is always possible to have a Lorentz boost from one reference frame in which the helicity is positive/negative to another reference frame in which the helicity is, correspondingly, negative/positive. However, this discussion concerns a massless fermion, the neutrino. For massless fermions, the operator γ_5 is equivalent to the helicity operator ℵ, as shall now be demonstrated Recall that the Dirac spinor for a particle of mass m is,

$$u(\boldsymbol{p},s) = \sqrt{E+m}\begin{pmatrix} \chi_s \\ \frac{\boldsymbol{\sigma}\bullet\mathbf{p}}{\sqrt{E+m}}\chi_s \end{pmatrix}.$$

Thus, the Dirac spinor of a massless particle is,

$$u = \sqrt{p}\begin{pmatrix} \chi \\ \left(\frac{\boldsymbol{\sigma}\bullet\mathbf{p}}{p}\right)\chi \end{pmatrix}. \tag{4.129}$$

Applying the helicity operator to this spinor,

$$\begin{aligned} \aleph u &= -\frac{\boldsymbol{\sigma}\bullet\mathbf{p}}{|\mathbf{p}|}\sqrt{p}\begin{pmatrix} \chi \\ \left(\frac{\boldsymbol{\sigma}\bullet\mathbf{p}}{p}\right)\chi \end{pmatrix} \\ &= \sqrt{p}\begin{pmatrix} \left(\frac{\boldsymbol{\sigma}\bullet\mathbf{p}}{|\mathbf{p}|}\right)\chi \\ \left(\frac{\boldsymbol{\sigma}\bullet\mathbf{p}}{p}\right)^2\chi \end{pmatrix} \\ &= \sqrt{p}\begin{pmatrix} \left(\frac{\boldsymbol{\sigma}\bullet\mathbf{p}}{|\mathbf{p}|}\right)\chi \\ \chi \end{pmatrix}. \end{aligned} \tag{4.130}$$

It is also noted that

$$\begin{aligned} \gamma_5 u &= \sqrt{p}\begin{pmatrix} 0 & \mathbf{1} \\ \mathbf{1} & 0 \end{pmatrix}\begin{pmatrix} \chi \\ \left(\frac{\boldsymbol{\sigma}\bullet\mathbf{p}}{p}\right)\chi \end{pmatrix} \\ &= \sqrt{p}\begin{pmatrix} \left(\frac{\boldsymbol{\sigma}\bullet\mathbf{p}}{p}\right)\chi \\ \chi \end{pmatrix}. \end{aligned} \tag{4.131}$$

The chirality operator $(1-\gamma_5)/2$ projects out the left-handed components of any spinor for massless particles with negative helicity, i.e., neutrinos. This can be shown using the Pauli two-component spinors $\chi_\pm$ which are described by,

$$\frac{\boldsymbol{\sigma}\bullet\mathbf{p}}{p}\chi_\pm = \pm\chi_\pm \tag{4.132}$$

where $\pm$ describes the spin orientation of a spin-½ particle. Thus, from (4.129) the corresponding Dirac spinors are,

$$u_{\pm} = \sqrt{p}\begin{pmatrix} \chi_{\pm} \\ \pm\chi \end{pmatrix} \tag{4.133}$$

from which is obtained,

$$\left(\frac{1-\gamma_5}{2}\right)u_{-} = -u_{-} \tag{4.134}$$

and

$$\left(\frac{1-\gamma_5}{2}\right)u_{+} = 0. \tag{4.135}$$

Returning to the hadronic and leptonic current densities of β decay given by (4.122) and (4.123) and using the chirality operator, one can now construct a leptonic current density which produces left-handed neutrinos,

$$l_{\mu}^{C}(\boldsymbol{X}) = \bar{\psi}_{e}(\boldsymbol{X})\gamma_{\mu}(1-\gamma_5)\psi_{\bar{\nu}_e}(\boldsymbol{X}) \tag{4.136}$$

and a similar form of the hadronic current density,

$$V_{\mu}^{C\,\dagger}(\boldsymbol{X}) = \bar{\psi}_{p}(\boldsymbol{X})\gamma_{\mu}(1-c_A\gamma_5)\psi_{n}(\boldsymbol{X}). \tag{4.137}$$

Both weak currents contain the Fermi polar vector component and an axial vector component which is the V-A (pronounced V minus A) structure of the weak interaction.

4.4 γ Transitions and Internal Conversion

4.4.1 Introduction

The daughter nucleus resulting from α or β decay will be left in one of three states. It may be stable to further radioactive decay: the maximum nuclear binding energy for the isobar series (i.e., the mass parabola's minimum) will have been attained. The nucleus may still yet undergo further α or β decay. Finally, the nucleus may be such that while further α or β decay is not energetically feasible, it is in an excited state in which one or more nucleons are placed in higher orbitals above the ground state. The nucleus can de-excite through the release of electromagnetic energy as the nucleon cascades to the ground state. There are two energy-transfer channels available. In the first, energy is released in the form of γ rays with energies, in the reference frame of the nucleus, equal to the energy differences between the orbitals that the nucleon transits between. This γ transition is a nuclear process. On the other hand, the second channel is an atomic process and is one in which the excess nuclear energy is transferred directly to an atomic electron (through the exchange of a virtual photon) but without the emission of electromagnetic energy. Should this transferred energy exceed the electron binding energy, the electron is ejected from the atom, inducing a variety of atomic relaxation processes as discussed in Chap. 6. This second channel is known as IC.

While a full description of nuclear electromagnetic processes is inherently quantum-mechanical, considerable understanding can be achieved through the use of classical and semiclassical theories. As a result, these will be the foundation of the derivations of the transition probabilities of γ rays and the selection rules that arise through the conservation of angular momentum and parity. Links to quantum theory will be forged where appropriate and necessary. This section begins with a review of the kinematics of γ decay and, using classical multi-pole expansions of the electromagnetic field, derives transition selection rules (similar to those of β decay) based upon the angular momentum carried away by the emitted photon (equal to the difference between those of the initial and final nuclear states) and parity. These expansions also allow a derivation of the transition rate (the reciprocal of the mean lifetime) of a given nuclear state and this is examined as a function of photon energy and photon multi-pole type. Following this study of γ decay, IC is reviewed.

4.4.2 γ Decay

4.4.2.1 Kinematics

Consider an excited nucleus with energy E_i making a transition to a state with energy E_f through the

emission of a γ ray. While it is frequently stated that the γ ray is emitted with an energy equal to the energy difference between the two states, $k = \Delta E = E_i - E_f$, this is only true in the reference frame of the nucleus. In the laboratory reference frame, however, consideration of the simultaneous conservations of energy and linear momentum shows the nucleus takes some of this energy difference as a recoil kinetic energy. The conservation of energy in the laboratory is,

$$m_i = m_f + k + T_f. \tag{4.138}$$

where $m_{i,f}$ are the rest masses of the nucleus before and after the transition such that $\Delta E = m_i - m_f$ and T_f is the nuclear recoil kinetic energy. The conservation of momentum is,

$$p_f = k. \tag{4.139}$$

As the nucleus is sufficiently massive to assume that its recoil is nonrelativistic, then,

$$\Delta E = k + \frac{k^2}{2m_f}. \tag{4.140}$$

Solving the resulting quadratic equation $k^2 + 2m_f k - 2m_f \Delta E = 0$ for the photon energy gives the full result for the photon energy,

$$k = \frac{m_f}{2}\left(\sqrt{1 + 2\frac{\Delta E}{m_f}} - 1\right). \tag{4.141}$$

Expanding the square-root to second order,

$$k = \Delta E\left(1 - \frac{\Delta E}{2m_f}\right) \tag{4.142}$$

Hence, the photon energy will be reduced by, to second order, an amount of $\Delta E^2/2m_f$ due to the recoil of the nucleus. But, as $\Delta E \ll m_f$, $k = \Delta E$ can be assumed in practice.

4.4.2.2 Multi-Pole Radiation

Introduction

The nucleus with excitation energy ΔE prior to γ decay can be thought of as distributions of electric charge, current and (as the nucleons have intrinsic spin) magnetization moving with periodic motion at a frequency $\omega = \Delta E/\hbar$ and confined to a region of the order of nuclear dimensions. As there is a marked range in measured γ decay lifetimes, selection rules based upon the conservations of angular momentum and parity are suggested. Hence, nuclear radiation emission can be investigated in terms of classical theory of electric and magnetic multi-poles.

The multi-pole expansion in free space is initially applied to nuclear γ emission in order to first establish these selection rules and then to calculate energy, angular momentum and spatial distribution of multi-pole radiation. This derivation shows, inter alia, that $0 \rightarrow 0$ γ transitions are impossible in γ emission, although they are permissible in IC. These results are extended to the case of where the source is present and used to estimate the rate at which γ emission occurs as a function of photon energy, atomic mass number, and multi-pole order.

Multi-Pole Expansion in Free Space

Modelling the excited nucleus as a conglomeration of periodically moving electric charges with frequency ω leads to induction and radiation zones based upon the inequalities of $r \ll c/\omega$ and $r \gg c/\omega$, respectively. One can use analogous inequalities of $r \ll \hbar c/k$ and $r \gg \hbar c/k$ where $\hbar c/k \approx 200\,\text{fm}$ and $\hbar c/k \approx 20\,\text{fm}$ for 1 and 10 MeV photons, respectively. Within the induction zone, the electric and magnetic fields are calculated directly from Maxwell's equations knowing the positions and velocities of the moving charges. Extending into the radiation zone, retardation (i.e., the time delay between when an electromagnetic wave is "emitted" and when it is "detected" at a distance) must be accounted for. The multi-pole expansion in the radiation zone in vacuo and with no source present in the region is evaluated first. In this case, Maxwell's equations are,

$$\nabla \bullet \mathbf{E} = 0 \tag{4.143}$$

$$\nabla \bullet \mathbf{H} = 0 \tag{4.144}$$

$$\nabla \times \mathbf{E} = -\mu_0 \frac{\partial \mathbf{H}}{\partial t} \tag{4.145}$$

$$\nabla \times \mathbf{H} = \varepsilon_0 \frac{\partial \mathbf{E}}{\partial t} \tag{4.146}$$

The fields harmonically vary as $e^{-i\omega t}$ (where it is understood that the real part of the complex quantity is taken) so that the time derivatives are,

$$\frac{\partial \mathbf{E}}{\partial t} = -i\omega \mathbf{E} \tag{4.147}$$

$$\frac{\partial \mathbf{H}}{\partial t} = -i\omega \mathbf{H}. \tag{4.148}$$

The curls of the fields can be written as,

$$\nabla \times \mathbf{E} = i\kappa \sqrt{\frac{\mu_0}{\varepsilon_0}} \mathbf{H} \tag{4.149}$$

$$\nabla \times \mathbf{H} = -i\kappa \sqrt{\frac{\varepsilon_0}{\mu_0}} \mathbf{E}. \tag{4.150}$$

Note that the wave-number $\kappa = \omega/c$ and the relationship $c = 1/\sqrt{\varepsilon_0 \mu_0}$ have been used. In order to develop the multi-pole expansion of the electromagnetic field, the Helmholtz equation is derived for the individual vector components of the fields by taking the curl of (4.149) and substituting (4.150)

$$\begin{aligned} \nabla \times (\nabla \times \mathbf{E}) &= i\kappa \sqrt{\frac{\mu_0}{\varepsilon_0}} \nabla \times \mathbf{H} \\ &= \kappa^2 \mathbf{E}. \end{aligned} \tag{4.151}$$

As the vector triple product is,

$$\begin{aligned} \nabla \times (\nabla \times \mathbf{E}) &= (\nabla \bullet \mathrm{E}) \nabla - \nabla^2 \mathbf{E} \\ &= -\nabla^2 \mathbf{E} \end{aligned} \tag{4.152}$$

then,

$$\left(\nabla^2 + \kappa^2\right) \mathbf{E} = \mathbf{0} \tag{4.153}$$

and, similarly,

$$\left(\nabla^2 + \kappa^2\right) \mathbf{H} = \mathbf{0}. \tag{4.154}$$

As these are vector equations, it is the Cartesian coordinates of the electric and magnetic fields that will satisfy the Helmholtz equation,

$$\left(\nabla^2 + \kappa^2\right) \mathrm{f} = 0 \tag{4.155}$$

where f is a scalar function. The Helmholtz equation is solved via a separation of variables and by writing the scalar function as an expansion in spherical harmonics,

$$\mathrm{f}(\mathbf{r}) = \sum_{l=1}^{\infty} \sum_{\mathrm{m}=-l}^{l} \mathrm{f}_l(\mathrm{r}) \mathrm{Y}_{l\mathrm{m}}(\theta, \phi). \tag{4.156}$$

The radial term is solved through a form of (2.104),

$$\left(\mathrm{r}^2 \frac{\mathrm{d}^2}{\mathrm{dr}^2} + 2\mathrm{r} \frac{\mathrm{d}}{\mathrm{dr}} + \mathrm{r}^2 \kappa^2 - l(l+1)\right) \mathrm{f}_l(\mathrm{r}) = 0 \tag{4.157}$$

which is rearranged and, following the substitution $\mathrm{u}_l(\mathrm{r}) = \sqrt{\mathrm{r}}\mathrm{f}_l(\mathrm{r})$, arrives at Bessel's equation for half-integer order (l+1/2),

$$\left(\frac{\mathrm{d}^2}{\mathrm{dr}^2} + \frac{1}{\mathrm{r}} \frac{\mathrm{d}}{\mathrm{dr}} + \kappa^2 - \frac{(l+1/2)^2}{\mathrm{r}^2}\right) \mathrm{u}_l(\mathrm{r}) = 0. \tag{4.158}$$

From (2.109) to (2.111), one can then write a general solution to the Helmholtz equation of the form,

$$\begin{aligned} \mathrm{f}(\mathbf{r}; \mathrm{k}) = \frac{1}{\sqrt{\mathrm{r}}} \sum_{l=1}^{\infty} \sum_{\mathrm{m}=-l}^{l} \Big(& \mathrm{A}_l \mathrm{J}_{l+1/2}(\kappa \mathrm{r}) \\ & + \mathrm{B}_l \mathrm{N}_{l+1/2}(\kappa \mathrm{r}) \Big) \mathrm{Y}_{l\mathrm{m}}(\theta, \phi) \end{aligned} \tag{4.159}$$

where the coefficients A_l and B_l are defined by the boundary conditions. This solution can be simplified by using the Hankel functions which are defined by,

$$\mathrm{h}_l^{(1)}(\mathrm{kr}) = \sqrt{\frac{\pi}{2\kappa \mathrm{r}}} \left(\mathrm{J}_{l+1/2}(\kappa \mathrm{r}) + i\mathrm{N}_{l+1/2}(\kappa \mathrm{r})\right) \tag{4.160}$$

$$h_l^{(2)}(\kappa r) = \sqrt{\frac{\pi}{2\kappa r}}(J_{l+1/2}(\kappa r) - iN_{l+1/2}(\kappa r)). \quad (4.161)$$

The general solution to the Helmholtz equation is,

$$f(\mathbf{r};\kappa) = \sum_{l=1}^{\infty}\sum_{m=-l}^{l}\left(A_l h_l^{(1)}(\kappa r) + B_l h_l^{(2)}(\kappa r)\right)Y_{lm}(\theta,\phi). \quad (4.162)$$

Rather than calculate for the field vector Cartesian components from the above, a simpler approach originally devised by Bowkamp and Casimir (1954) is followed in which the scalar products $\mathbf{r} \bullet \mathbf{E}$ and $\mathbf{r} \bullet \mathbf{H}$ are instead solved for and the electric and magnetic fields of the electric and magnetic multi-poles subsequently extracted.[25] To show the suitability of these substitutions, consider the Laplacian acting upon the scalar product $\mathbf{r} \bullet \mathbf{H}$,

$$\nabla^2(\mathbf{r} \bullet \mathbf{E}) = \mathbf{r} \bullet \nabla^2\mathbf{E} + 2\nabla \bullet \mathbf{E} \quad (4.163)$$

so that,

$$\left(\nabla^2 + \kappa^2\right)(\mathbf{r} \bullet \mathbf{E}) = \mathbf{r} \bullet \nabla^2\mathbf{E} + 2\nabla \bullet \mathbf{E} + \kappa^2(\mathbf{r} \bullet \mathbf{E}). \quad (4.164)$$

As the second term is equal to zero for the source-less case and the sum of the first and third terms is equal to zero, then $\mathbf{r} \bullet \mathbf{E}$ satisfies the Helmhotz equation as does $\mathbf{r} \bullet \mathbf{H}$.

The multi-pole expansions of the electromagnetic fields are determined by first calculating for the magnetic multi-pole field of order (l, m). The conditions,

$$\mathbf{r} \bullet \mathbf{H}_{lm}^{(M)} = \frac{l(l+1)}{\kappa} \times \left(A_l h_l^{(1)}(\kappa r) + B_l h_l^{(2)}(\kappa r)\right)Y_{lm}(\theta,\phi) \quad (4.165)$$

$$\mathbf{r} \bullet \mathbf{E}_{lm}^{(M)} = 0 \quad (4.166)$$

are specified.

[25] Jackson (1999) provides a detailed derivation.

The rationale for the inclusion of the $l(l+1)/\kappa$ factor in (4.165) will soon be demonstrated.[26] One can then write a relationship between the scalar product $\mathbf{r} \bullet \mathbf{H}$ and the electric field from (4.149),

$$i\kappa\sqrt{\frac{\mu_0}{\varepsilon_0}}\mathbf{r} \bullet \mathbf{H} = \mathbf{r} \bullet (\nabla \times \mathbf{E})$$

or

$$\kappa\sqrt{\frac{\mu_0}{\varepsilon_0}}\mathbf{r} \bullet \mathbf{H} = \mathbf{L} \bullet \mathbf{E} \quad (4.167)$$

where the operator $\mathbf{L} = -i(\mathbf{r} \times \nabla)$ has been defined. It will be noted that this operator is $\hbar^{-1}$ times the quantum-mechanical angular momentum operator and its properties are briefly reviewed here. From Chap. 2, one has, for the spherical harmonic,

$$-\left(\frac{\partial^2}{\partial\theta^2} + \cot\theta\frac{\partial}{\partial\theta} + \frac{1}{\sin^2\theta}\frac{\partial^2}{\partial\phi^2}\right) \times Y_{lm}(\theta,\phi) = l(l+1)Y_{lm}(\theta,\phi) = L^2\,Y_{lm}(\theta,\phi). \quad (4.168)$$

It is apparent that the $\mathbf{L}$ operator acts only upon the angular variables. Raising and lowering operators can be created from the components of $\mathbf{L}$,

$$L_\pm = L_x \pm iL_y = e^{\pm i\phi}\left(\pm\frac{\partial}{\partial\theta} + i\cot\theta\frac{\partial}{\partial\phi}\right) \quad (4.169)$$

$$L_z = -i\frac{\partial}{\partial\phi}. \quad (4.170)$$

Applying these to the spherical harmonics,

$$L_\pm Y_{lm}(\theta,\phi) = \sqrt{(l \mp m)(l \pm m + 1)}Y_{lm\pm1}(\theta,\phi) \quad (4.171)$$

[26] As the electric field is transverse to the radius vector, the magnetic multipole field is sometimes referred to, especially in engineering textbooks, as a transverse electric (TE) field. Similarly, the electric multi-pole field is also referred to as a transverse magnetic (TM) field.

$$\mathrm{L_z Y}_{l\mathrm{m}}(\theta,\phi) = \mathrm{m\, Y}_{l\mathrm{m}}(\theta,\phi). \tag{4.172}$$

L acts upon the spherical harmonic to transform the m value leaving the l value unaffected. Consequently, the electric field of the magnetic multi-pole must satisfy,

$$\mathbf{L} \bullet \mathbf{E}^{(\mathrm{M})}_{\mathrm{lm}} = l(l+1)\sqrt{\frac{\mu_0}{\varepsilon_0}} \times \left(\mathrm{A}_l \mathrm{h}^{(1)}_l(\kappa r) + \mathrm{B}_l \mathrm{h}^{(2)}_l(\kappa r)\right) \mathrm{Y}_{l\mathrm{m}}(\theta,\phi) \tag{4.173}$$

which demonstrates the convenience of the $l(l+1)/\kappa$ factor introduced in (4.165). Recalling the properties of the **L** operator, the electric field of the magnetic multi-pole can be extracted from this result. First, as the **L** operator acts only upon the angular variables,

$$\mathbf{L}\left(\mathbf{L} \bullet \mathbf{E}^{(\mathrm{M})}_{l\mathrm{m}}\right) = l(l+1)\sqrt{\frac{\mu_0}{\varepsilon_0}} \times \left(\mathrm{A}_l \mathrm{h}^{(1)}_l(\kappa r) + \mathrm{B}_l \mathrm{h}^{(2)}_l(\kappa r)\right) \mathbf{L}\mathrm{Y}_{l\mathrm{m}}(\theta,\phi). \tag{4.174}$$

As $\mathbf{L}\left(\mathbf{L} \bullet \mathbf{E}^{(\mathrm{M})}_{l\mathrm{m}}\right) = \mathrm{L}^2 \mathbf{E}^{(\mathrm{M})}_{l\mathrm{m}} = l(l+1)\mathbf{E}^{(\mathrm{M})}_{l\mathrm{m}}$, this result then gives the electric field of the magnetic multi-pole as,

$$\mathbf{E}^{(\mathrm{M})}_{l\mathrm{m}} = \sqrt{\frac{\mu_0}{\varepsilon_0}}\left(\mathrm{A}_l \mathrm{h}^{(1)}_l(\kappa r) + \mathrm{B}_l \mathrm{h}^{(2)}_l(\kappa r)\right) \times \mathbf{L}\mathrm{Y}_{l\mathrm{m}}(\theta,\phi) = \sqrt{\frac{\mu_0}{\varepsilon_0}}\sqrt{l(l+1)} \times \left(\mathrm{A}_l \mathrm{h}^{(1)}_l(\kappa r) + \mathrm{B}_l \mathrm{h}^{(2)}_l(\kappa r)\right) \mathbf{X}_{l\mathrm{m}}(\mathrm{r},\phi) \tag{4.175}$$

where the normalized vector spherical harmonic is defined as,

$$\mathbf{X}_{l\mathrm{m}}(\mathrm{r},\phi) = \frac{1}{\sqrt{l(l+1)}}\mathbf{L}\mathrm{Y}_{l\mathrm{m}}(\mathrm{r},\phi). \tag{4.176}$$

The normalized vector spherical harmonic has the orthonormality,

$$\int \mathrm{d}\Omega\, \mathbf{X}^*_{l'\mathrm{m}'}(\theta,\phi) \bullet \mathbf{X}_{l\mathrm{m}}(\theta,\phi) = \delta_{ll'}\delta_{\mathrm{mm}'} \tag{4.177}$$

and

$$\int \mathrm{d}\Omega\, \mathbf{X}^*_{l'\mathrm{m}'}(\theta,\phi) \bullet (\mathbf{r} \times \mathbf{X}_{l\mathrm{m}}(\theta,\phi)) = 0. \tag{4.178}$$

The magnetic field of the magnetic multi-pole is then defined from (4.149),

$$\mathbf{H}^{(\mathrm{M})}_{l\mathrm{m}} = -\frac{\mathrm{i}}{\kappa}\sqrt{\frac{\varepsilon_0}{\mu_0}}\nabla \times \mathbf{E}^{(\mathrm{M})}_{l\mathrm{m}}. \tag{4.179}$$

Repeating the above derivation for the electric and magnetic fields of the electric multi-pole gives,

$$\mathbf{H}^{(\mathrm{E})}_{l\mathrm{m}} = \sqrt{l(l+1)} \times \left(\mathrm{C}_l \mathrm{h}^{(1)}_l(\kappa r) + \mathrm{D}_l \mathrm{h}^{(2)}_l(\kappa r)\right) \mathbf{X}_{l\mathrm{m}}(\theta,\phi) \tag{4.180}$$

$$\mathbf{E}^{(\mathrm{M})}_{l\mathrm{m}} = \frac{\mathrm{i}}{\kappa}\sqrt{\frac{\mu_0}{\varepsilon_0}}\nabla \times \mathbf{H}^{(\mathrm{E})}_{l\mathrm{m}}. \tag{4.181}$$

These allow the electric and magnetic fields to be written as the sums of the multi-pole fields,

$$\mathbf{E}(\mathbf{r}) = \sum_{l=1}^{\infty}\sum_{\mathrm{m}=-l}^{l}\left[\frac{\mathrm{i}}{\kappa}\mathrm{a}^{(\mathrm{E})}_{l\mathrm{m}}(\nabla \times \mathrm{f}_l(\kappa r)\mathbf{X}_{l\mathrm{m}}(\theta,\phi)) + \mathrm{a}^{(\mathrm{M})}_{l\mathrm{m}}\mathrm{g}_l(\kappa r)\mathbf{X}_{l\mathrm{m}}(\theta,\phi)\right] \tag{4.182}$$

$$\mathbf{H}(\mathbf{r}) = \sum_{l=1}^{\infty}\sum_{\mathrm{m}=-l}^{l}\left[\mathrm{a}^{(\mathrm{E})}_{l\mathrm{m}}\mathrm{f}_l(\kappa r)\mathbf{X}_{l\mathrm{m}}(\theta,\phi) - \frac{\mathrm{i}}{\kappa}\mathrm{a}^{(\mathrm{M})}_{l\mathrm{m}}(\nabla \times \mathrm{g}_l(\kappa r)\mathbf{X}_{l\mathrm{m}}(\theta,\phi))\right] \tag{4.183}$$

where

$$\mathrm{f}_l(\mathrm{k}r) = \left(\mathrm{A}_l \mathrm{h}^{(1)}_l(\kappa r) + \mathrm{B}_l \mathrm{h}^{(2)}_l(\kappa r)\right) \tag{4.184}$$

and

$$g_l(\kappa r) = \left(C_l h_l^{(1)}(\kappa r) + D_l h_l^{(2)}(\kappa r)\right). \tag{4.185}$$

The coefficients $a_{lm}^{(E)}$ and $a_{lm}^{(M)}$ indicate the contributing amounts of electric and magnetic multi-poles, respectively, to the fields and are specified by the boundary conditions and sources as determined through,

$$a_{lm}^{(E)} f_l(r) = -\frac{\kappa}{\sqrt{l(l+1)}}\sqrt{\frac{\varepsilon_0}{\mu_0}} \times \int d\Omega\, Y_{lm}^*(\theta,\phi)\mathbf{r}\bullet\mathbf{E}(\mathbf{r}) \tag{4.186}$$

$$a_{lm}^{(M)} g_l(r) = \frac{\kappa}{\sqrt{l(l+1)}} \times \int d\Omega\, Y_{lm}^*(\theta,\phi)\mathbf{r}\bullet\mathbf{H}(\mathbf{r}). \tag{4.187}$$

Equations (4.182) and (4.183) demonstrate the dual transformation relationship between the fields of an electric multi-pole and those of a magnetic multi-pole through which one can transfer from one multi-pole to another by interchanging the electric and magnetic fields and changing the sign of the electric field.

Before concluding this introduction to multi-pole radiation, consider one characteristic of the vector spherical harmonic which will be of importance. This is, that for $l = 0$,

$$-i(\mathbf{r}\times\nabla)Y_{00}(\theta,\phi) = 0 \tag{4.188}$$

with the result that there is no multi-pole radiation for $l = 0$. In other words, there is no transition between nuclear states both with $l = 0$ that can result in γ-ray emission

Energy and Angular Momentum of Multi-Pole Radiation

The energy and angular momentum of multi-pole radiation are derived through calculating the electric and magnetic fields of the electric and magnetic multi-poles in the radiation zone. This result will then be used to demonstrate that the radiation emitted by a multi-pole of order (l, m) carries away m$\hbar$ of the z-component of angular momentum for each emitted photon of energy $\hbar\omega$ (in the reference frame of the nucleus). Begin by calculating the multi-pole fields in the radiation zone, within which the asymptotic forms of the spherical Bessel functions are, from Chap. 2,

$$j_l(\kappa r) \to \frac{\sin(\kappa r - l\pi/2)}{\kappa r} \quad \kappa r \to \infty \tag{4.189}$$

$$y_l(\kappa r) \to -\frac{\cos(\kappa r - l\pi/2)}{\kappa r} \quad \kappa r \to \infty \tag{4.190}$$

and the Hankel functions become,

$$\begin{aligned} h_l^{(1)}(\kappa r) &\approx \frac{\sin(\kappa r - l\pi/2)}{\kappa r} - i\frac{\cos(\kappa r - l\pi/2)}{\kappa r} \\ &\approx -ie^{i\kappa r} \\ &\approx -i^{(l+1)}\frac{e^{i\kappa r}}{\kappa r} \quad \kappa r \gg 1 \end{aligned} \tag{4.191}$$

$$\begin{aligned} h_l^{(2)}(\kappa r) &\approx \frac{\sin(\kappa r - l\pi/2)}{\kappa r} + i\frac{\cos(\kappa r - l\pi/2)}{\kappa r} \\ &\approx -i^{l}\frac{e^{-i\kappa r}}{\kappa r} \quad \kappa r \gg 1. \end{aligned} \tag{4.192}$$

These far-field approximations are then applied to the previously-derived expressions for the electric and magnetic fields of multi-pole radiation. From (4.175), the electric field of the magnetic multi-pole in the radiation zone is,

$$\begin{aligned} \mathbf{E}_{lm}^{(M)} &= -i^l\sqrt{\frac{\mu_0}{\varepsilon_0}} \\ &\quad\times \frac{\left(B_1 e^{-i\kappa r} + iA_1 e^{i\kappa r}\right)}{\kappa r}\mathbf{X}_{lm}(r,\phi) \\ &\kappa r \gg 1 \end{aligned} \tag{4.193}$$

and, for an outgoing wave,

$$\begin{aligned} \mathbf{E}_{lm}^{(M)} &= -i^{(l+1)}\sqrt{\frac{\mu_0}{\varepsilon_0}}\sqrt{l(l+1)}\frac{e^{i\kappa r}}{\kappa r}\mathbf{X}_{lm}(\theta,\phi) \\ &\kappa r \gg 1 \end{aligned} \tag{4.194}$$

and the magnetic field of the magnetic multi-pole will be given by,

$$\mathbf{H}_{lm}^{(M)} = \sqrt{\frac{\varepsilon_0}{\mu_0}}\mathbf{E}_{lm}^{(M)} \times \hat{\mathbf{r}}. \tag{4.195}$$

From (4.180), the magnetic field of the electric multi-pole in the radiation zone is,

$$\mathbf{H}_{lm}^{(E)} = -i^l\sqrt{l(l+1)}\frac{\left(D_l e^{-i\kappa r} + iC_l e^{i\kappa r}\right)}{\kappa r} \times \mathbf{X}_{lm}(\theta,\phi) \quad \kappa r \gg 1 \tag{4.196}$$

and, for an outgoing wave,

$$\mathbf{H}_{lm}^{(E)} = -i^{(l+1)}\sqrt{l(l+1)}\frac{e^{i\kappa r}}{\kappa r}\mathbf{X}_{lm}(\theta,\phi) \quad kr \gg 1 \tag{4.197}$$

and the electric field of the electric multi-pole is,

$$\mathbf{E}_{lm}^{(E)} = \frac{i^l}{\kappa^2}\sqrt{\frac{\mu_0}{\varepsilon_0}}\sqrt{l(l+1)}\nabla \times \left(\frac{e^{i\kappa r}}{r}\mathbf{X}_{lm}(\theta,\phi)\right) \tag{4.198}$$

As these are in the far-field region, the curl is calculated to powers no greater than $1/r$ and the identity $\nabla \times \mathbf{L} = -i\mathbf{r}\nabla^2 - \nabla\left(1 + r\frac{\partial}{\partial r}\right)$ used to give, for the electric field of the electric multi-pole,

$$\mathbf{E}_{lm}^{(E)} = -i^{(l+1)}\sqrt{\frac{\mu_0}{\varepsilon_0}}\frac{e^{i\kappa r}}{\kappa r}\left(\sqrt{l(l+1)}\hat{\mathbf{r}} \times \mathbf{X}_{lm}(\theta,\phi) - \frac{1}{\kappa}\left(\mathbf{r}\nabla^2 - \nabla\right)Y_{lm}\left(\theta,\phi\right)\right) \tag{4.199}$$

where $\hat{\mathbf{r}}$ is the unit radial vector. The second term can be neglected,

$$\mathbf{E}_{lm}^{(E)} = -i^{(l+1)}\sqrt{\frac{\mu_0}{\varepsilon_0}}\frac{e^{i\kappa r}}{\kappa r} \times \left(\sqrt{l(l+1)}\hat{\mathbf{r}} \times \mathbf{X}_{lm}(\theta,\phi)\right). \tag{4.200}$$

Using (4.198),

$$\mathbf{E}_{lm}^{(E)} = \sqrt{\frac{\mu_0}{\varepsilon_0}}\mathbf{H}_{lm}^{(E)} \times \hat{\mathbf{r}}. \tag{4.201}$$

It is now demonstrated that the radiation emitted by a multi-pole of order (l,m) carries away m$\hbar$ of the z-component of angular momentum for each photon of energy $\hbar\omega$, doing so for a pure multi-pole field (in this case, the electric). Following the example of Jackson (1999), consider the electromagnetic field to be a linear superposition of electric multi-poles of order (l,m) but with the requirement that l be the same for the multi-poles but each have a different value of m. The magnetic field of a pure electric multi-pole (i.e., $a_{lm}^{(M)} = 0$) is, assuming a harmonic time dependence,

$$\mathbf{H}(\mathbf{r}) = \sum_{m=-l}^{l} a_{lm}^{(E)} h_{lm}^{(1)}(\kappa r)\mathbf{X}_{lm}(\theta,\phi)e^{-i\omega t} \tag{4.202}$$

which, in the radiation zone is,

$$\mathbf{H}(\mathbf{r}) = \sum_{m=-l}^{l} a_{lm}^{(E)} h_{lm}^{(1)}(\kappa r)\mathbf{X}_{lm}(\theta,\phi)e^{-i\omega t} \approx -i^{(l+1)}\frac{e^{i\kappa r}}{\kappa r} \quad \kappa r \gg 1 \tag{4.203}$$

and the corresponding electric field is,

$$\mathbf{E}(\mathbf{r}) = \frac{i}{\kappa}\sqrt{\frac{\mu_0}{\varepsilon_0}}\nabla \times \mathbf{H}(\mathbf{r}). \tag{4.204}$$

The time-averaged energy density is,

$$u = \frac{1}{4}\left[\varepsilon_0\mathbf{E}(\mathbf{r}) \bullet \mathbf{E}^*(\mathbf{r}) + \mu_0\mathbf{H}(\mathbf{r}) \bullet \mathbf{H}^*(\mathbf{r})\right] \tag{4.205}$$

and the change in energy with radius is,

$$\frac{dE}{dr} = \frac{\mu_0}{2\kappa^2}\sum_{m=-l}^{l}\left|a_{lm}^{(E)}\right|^2. \tag{4.206}$$

In the case of the field being made up of electric and magnetic multi-poles, this would be,

$$\frac{dE}{dr} = \frac{\mu_0}{2\kappa^2} \sum_{m=-l}^{l} \left(\left| a_{lm}^{(E)} \right|^2 + \left| a_{lm}^{(M)} \right|^2 \right). \tag{4.207}$$

Next consider the angular momentum density which one obtains from the electromagnetic field linear momentum. This follows from the Lorentz equation and Newton's second law for a spatially-distributed charge,

$$\frac{d\mathbf{P}}{dt} = \int d^3\mathbf{r}(\rho_e \mathbf{E} + \mathbf{J} \times \mathbf{B}) \tag{4.208}$$

where ρ_e and $\mathbf{J}$ are the electric charge and current densities. Using Maxwell's equations for the case of the fields in free space and with a source present,

$$\nabla \bullet \mathbf{E} = \frac{\rho_e}{\varepsilon_0} \tag{4.209}$$

$$\mathbf{J} = \nabla \times \mathbf{H} - \varepsilon_0 \frac{\partial \mathbf{E}}{\partial t} \tag{4.210}$$

the integrand can be rewritten, using $\varepsilon_0 \mu_0 = 1/c^2$, as,

$$\begin{aligned} &\rho_e \mathbf{E} + \mathbf{J} \times \mathbf{B} \\ &\quad = \varepsilon_0 \left[\mathbf{E}(\nabla \bullet \mathbf{E}) + \mathbf{B} \times \frac{\partial \mathbf{E}}{\partial t} - c^2 \mathbf{B} \times (\nabla \times \mathbf{B}) \right]. \end{aligned} \tag{4.211}$$

With some additional manipulations, the momentum of the electromagnetic field arises from the volume integral,

$$\begin{aligned} \mathbf{p} &= \varepsilon_0 \int d^3\mathbf{r}(\mathbf{E} \times \mathbf{B}) \\ &= \frac{1}{c^2} \int d^3\mathbf{r}(\mathbf{E} \times \mathbf{H}). \end{aligned} \tag{4.212}$$

The angular momentum then follows as,

$$\mathbf{m} = \frac{1}{c^2} \int d^3\mathbf{r}\, \mathbf{r} \times (\mathbf{E} \times \mathbf{H}) \tag{4.213}$$

from which one can obtain the time-averaged angular momentum density,

$$\mathbf{m} = \frac{1}{2c^2} \mathrm{Re}\left[\mathbf{r} \times (\mathbf{E} \times \mathbf{H}^*) \right]. \tag{4.214}$$

Expanding the vector triple cross product, $\mathbf{r} \times (\mathbf{E} \times \mathbf{H}^*) = (\mathbf{r} \bullet \mathbf{H}^*)\mathbf{E} - (\mathbf{r} \bullet \mathbf{E})\mathbf{H}^*$, leads to,

$$\mathbf{m} = \frac{\mu_0}{2\omega} \mathrm{Re}\left[\mathbf{H}^* (\mathbf{L} \bullet \mathbf{H}) \right]. \tag{4.215}$$

The change in the z-component of the angular momentum with radius is,

$$\frac{dm_z}{dr} = \frac{\mu_0}{2\omega\,\kappa^2} \sum_{m=-l}^{l} m \left| a_{lm}^{(E)} \right|^2. \tag{4.216}$$

Comparing this result with the derivative of (4.207) leads to,

$$\begin{aligned} \frac{dm_z}{dr} &= \frac{m}{\omega} \frac{dE}{dr} \\ &= \frac{\hbar m}{\hbar \omega} \frac{dE}{dr}. \end{aligned} \tag{4.217}$$

This result is interpreted as representing that, for multi-pole radiation of order (l, m), a photon emitted with an energy $\hbar\omega$ carries away $m\hbar$ units of the z-component of angular momentum.

Selection Rules for Multi-Pole Radiation

In a radiative transition, the state changes from ψ_i to ψ_f and the overall angular momentum is conserved. If the quantum carries away angular momentum l with z-component m (all in units of $\hbar$), then the conservation of angular momentum stipulates that,

$$\mathbf{J}_i = l \oplus \mathbf{J}_f \tag{4.218}$$

where $\mathbf{J}_i$ and $\mathbf{J}_f$ are the total angular momenta of the initial and final nuclear states leading to multi-pole radiation of order (l,m) being emitted only if,

$$|\mathbf{J}_i - \mathbf{J}_f| \le l \le |\mathbf{J}_i + \mathbf{J}_f| \tag{4.219}$$

and

$$m_{z,i} - m_{z,f} = m \tag{4.220}$$

As, from (4.188), there is no $l = 0$ multi-pole radiation, a radiative transition between nuclear states with $J_i = J_f = 0$ will be forbidden. In addition to this angular momentum selection rule, an additional selection rule arises as a result of the conservation of parity. The parity of the final state is equal to the product of the parity of the final nuclear state and that of the multi-pole radiation. That is, the matrix element of the transition will be non-zero when,

$$\Pi_i = \Pi_f \quad \text{for even} - \text{parity radiation} \tag{4.221}$$

$$\Pi_i = -\Pi_f \quad \text{for odd} - \text{parity radiation.} \tag{4.222}$$

The magnetic field can be used to specify the parity, the rationale for which becomes apparent by noting that the matrix element of the transition is proportional to $\int d^3\mathbf{r}\,\psi_f(\mathbf{J} \bullet \mathbf{A})\psi_i$ (where the $\mathbf{J}$ is the current operator and is the electromagnetic vector potential). $\mathbf{A}$ has the same parity as the electric field, $\mathbf{E}$. As $\mathbf{J}$ is a polar vector, it will have negative parity and the scalar product $\mathbf{J} \bullet \mathbf{A}$ will thus have the opposite parity of the electric field. Because the curl operation changes parity, we then have the result that $\mathbf{J} \bullet \mathbf{A}$ has the same parity as $\mathbf{H}$. Consider, first, the electric multi-pole field where the electric and magnetic fields of the multi-pole are

$$\mathbf{H}^{(E)}_{lm} = \sqrt{l(l+1)}\left(C_l h_l^{(1)}(\kappa r) + D_l h_l^{(2)}(\kappa r)\right)\mathbf{X}_{lm}(\theta, \phi)$$

and

$$\mathbf{E}^{(E)}_{lm} = \frac{i}{\kappa}\sqrt{\frac{\mu_0}{\varepsilon_0}}\nabla \times \mathbf{H}^{(E)}_{lm}.$$

As the spherical harmonic is $\mathbf{X}_{lm}(\theta, \phi) = \frac{i}{\sqrt{l(l+1)}}(\mathbf{r} \times \nabla)Y_{lm}(\theta, \phi)$ and $\mathbf{r} \times \nabla$ is invariant under inversion, the parity properties of $\mathbf{H}^{(E)}_{lm}$ are given by those of the spherical harmonic, $Y_{lm}(r, \phi)$, which has parity $(-1)^l$ and the parity of electric multi-pole radiation will be given by $(-1)^{l+1}$. Table 4.6 summarizes the selection rules for multi-pole electromagnetic radiation. Let us use a pragmatic example to describe these selection rules. Consider an excited nuclear state with $J_i = 1/2$ which de-excites to a state with $J_f = 3/2$ through the emission of a γ ray. From (4.219), $l = 1, 2$ so that the only allowed transitions are dipole ($l = 1$) and quadrupole ($l = 2$). If the parities of the initial and final nuclear states are the same ($\Pi_i = \Pi_f$), then only the magnetic dipole (M1) and electric quadrupole (E2) transitions can occur. Should, the parities of the initial and final nuclear states differ ($\Pi_i = -\Pi_f$), then only electric dipole (E1) and magnetic quadrupole (M2) transitions are allowed.

Table 4.6 Selection rules for electromagnetic multipole radiation

Rule	Dipole E1	Quadrupole E2	Sextupole E3	Octupole E4
	E1	E2	E3	E4
$\Delta\Pi$	1	0	1	0
$\lvert\Delta J\rvert$	1	2	3	4
	M1	M2	M3	M4
$\Delta\Pi$	0	1	0	1
$\lvert\Delta J\rvert$	1	2	3	4

Angular Distributions of Multi-Pole Radiation

From the above, it can be seen that the time-averaged power radiated will be proportional to $|\mathbf{X}_{lm}(\theta, \phi)|^2$. Table 4.7 presents the angular distributions of some dipole and quadrupole radiations and which are shown in Fig. 4.31. The sum of the squared magnitudes of the vector spherical harmonics for a set of multi-poles of order l is,

Table 4.7 Angular distributions of dipole and quadrupole radiations

Type	l	m 0	± 1	± 2
Dipole	1	$\left(\frac{3}{8\pi}\right)\sin^2\theta$	$\left(\frac{3}{16\pi}\right)(1 + \cos^2\theta)$	–
Quadrupole	2	$\left(\frac{15}{8\pi}\right)\sin^2\theta\cos^2\theta$	$\left(\frac{5}{16\pi}\right)(1 - 3\cos^2\theta + 4\cos^4\theta)$	$\left(\frac{5}{16\pi}\right)(1 - \cos^4\theta)$

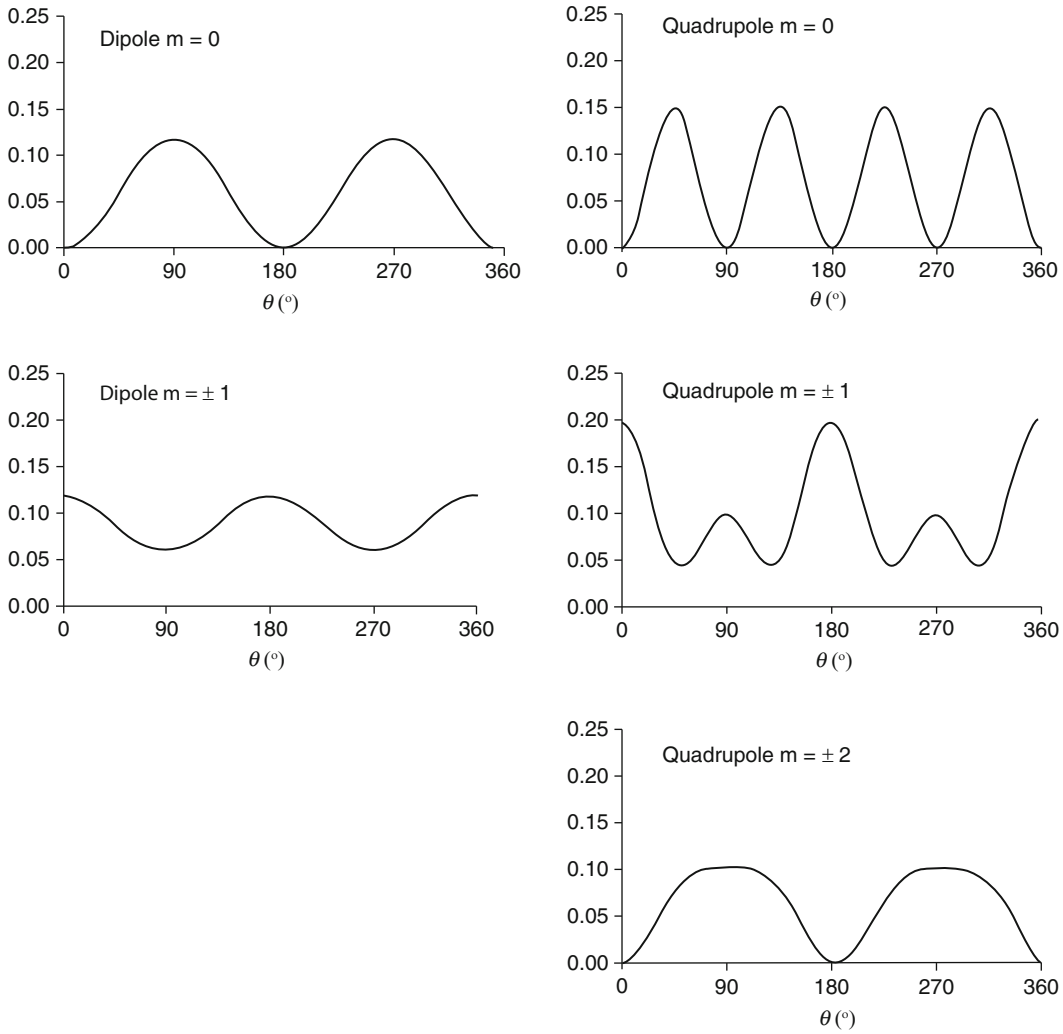

Fig. 4.31 Angular distributions of dipole and quadrupole radiations

$$\sum_{\mathrm{m}=-l}^{l} |\mathbf{X}_{l\mathrm{m}}(\theta,\phi)|^2 = \frac{2l+1}{4\pi} \tag{4.223}$$

which demonstrates that the radiation is isotropic from a radiating source consisting of this set of multi-poles with multi-poles added incoherently.

Multi-Pole Expansion With Source Present

It is necessary to connect the multi-pole fields with the sources that have generated them; i.e., the coefficients $a_{lm}^{(E)}$ and $a_{lm}^{(M)}$ are related to the source that has produced the multi-pole radiation. The source, which is the nucleus, is considered to be a harmonically-varying distribution of charge, current and magnetization,

$$\rho(\mathbf{r},\mathrm{t}) = \rho(\mathbf{r})\mathrm{e}^{-\mathrm{i}\omega\mathrm{t}} \tag{4.224}$$

$$\mathbf{J}(\mathbf{r},\mathrm{t}) = \mathbf{J}(\mathbf{r})\mathrm{e}^{-\mathrm{i}\omega\mathrm{t}} \tag{4.225}$$

$$\mathbf{M}(\mathbf{r},\mathrm{t}) = \mathbf{M}(\mathbf{r})\mathrm{e}^{-\mathrm{i}\omega\mathrm{t}} \tag{4.226}$$

where it is understood that the real part of the complex quantities are to be taken.[27] Maxwell's equations are now,

[27] It is also possible to simply write, for example, $\rho(\mathbf{r},\mathrm{t}) = 1/2\big(\rho(\mathbf{r})\mathrm{e}^{-\mathrm{i}\omega\mathrm{t}} + \rho^*(\mathbf{r})\mathrm{e}^{+\mathrm{i}\omega\mathrm{t}}\big)$ to achieve the same result.

$$\nabla \bullet \mathbf{E} = \frac{\rho}{\varepsilon_0} \tag{4.227}$$

$$\nabla \bullet \mathbf{B} = 0 \tag{4.228}$$

$$\nabla \times \mathbf{E} = \mathrm{i}\omega\mathbf{B} \tag{4.229}$$

$$\nabla \times \mathbf{B} = \mu_0(\mathbf{J} + \nabla \times \mathbf{M}) - \mathrm{i}\frac{\omega}{c^2}\mathbf{E}. \tag{4.230}$$

Some simplification is possible by defining $\mathbf{H}' = \mathbf{B}/\mu_0$ and $\mathbf{E}' = \mathbf{E} + \frac{\mathrm{i}}{\omega\varepsilon_0}\mathbf{J}$ to yield the set of equations,

$$\nabla \bullet \mathbf{E}' = 0 \tag{4.231}$$

$$\nabla \bullet \mathbf{H}' = 0 \tag{4.232}$$

$$\nabla \times \mathbf{E} = \frac{\mathrm{i}}{\omega\varepsilon_0}\nabla \times \mathbf{J} + \omega\mu_0\mathbf{H}' \tag{4.233}$$

$$\nabla \times \mathbf{H}' = \nabla \times \mathbf{M} - \mathrm{i}\kappa\sqrt{\frac{\varepsilon_0}{\mu_0}}\mathbf{E}'. \tag{4.234}$$

From the two curl equations,

$$\left(\nabla^2 + \kappa^2\right)\mathbf{E}' = -\mathrm{i}\kappa\sqrt{\frac{\mu_0}{\varepsilon_0}}\nabla \times \left(\mathbf{M} + \frac{\nabla \times \mathbf{J}}{\kappa^2}\right) \tag{4.235}$$

$$\left(\nabla^2 + \kappa^2\right)\mathbf{H}' = -\nabla \times (\mathbf{J} + \nabla \times \mathbf{M}). \tag{4.236}$$

As before, the scalars $\mathbf{r} \bullet \mathbf{E}'$ and $\mathbf{r} \bullet \mathbf{H}'$ are solved for. Using (4.163), (4.235) and (4.236), and the relationship for an arbitrary vector field $\mathbf{F}$,

$$\begin{aligned}\mathbf{r} \bullet (\nabla \times \mathbf{F}) &= (\mathrm{r} \times \nabla) \bullet \mathbf{F} \\ &= \mathrm{i}\mathbf{L} \bullet \mathbf{F}\end{aligned} \tag{4.237}$$

one obtains the inhomogeneous equations,

$$\left(\nabla^2 + \kappa^2\right)\mathbf{r} \bullet \mathbf{E}' = \omega\mu_0\mathbf{L} \bullet \left(\mathbf{M} + \frac{\nabla \times \mathbf{J}}{\kappa^2}\right) \tag{4.238}$$

$$\left(\nabla^2 + \kappa^2\right)\mathbf{r} \bullet \mathbf{H}' = -\mathrm{i}\mathbf{L} \bullet (\mathbf{J} + \nabla \times \mathbf{M}). \tag{4.239}$$

These can be solved using Green's functions (cf Chap. 2). However, as the solution is involved, it will not be repeated here for clarity; the interested reader is referred to Chap. 9 of Jackson (1999) or Chap. XII of Blatt and Weisskopf (1979). The result of the calculation is that exact results of the multipole coefficients are given by the expressions,

$$\begin{aligned}\mathrm{a}_{lm}^{(\mathrm{E})} = &-\mathrm{i}\frac{\kappa^2}{\sqrt{l(l+1)}}\int \mathrm{d}^3\mathbf{r}\, \mathrm{Y}_{lm}(\theta,\phi) \\ &\times \left\{ \begin{array}{c} \mathrm{c}\rho(\mathbf{r})\frac{\partial}{\partial \mathrm{r}}(\mathrm{r}\mathrm{j}_l(\kappa\mathrm{r})) + \mathrm{i}\kappa(\mathbf{r} \bullet \mathrm{J}(\mathbf{r}))\mathrm{j}_l(\kappa\mathrm{r}) \\ -\mathrm{i}\kappa\nabla \bullet (\mathbf{r} \times \mathbf{M})\mathrm{j}_l(\kappa\mathrm{r}) \end{array} \right\}\end{aligned} \tag{4.240}$$

$$\begin{aligned}\mathrm{a}_{lm}^{(\mathrm{M})} = &-\mathrm{i}\frac{\kappa^2}{\sqrt{l(l+1)}} \\ &\times \int \mathrm{d}^3\mathbf{r}\, \mathrm{Y}_{lm}(\theta,\phi)\left\{ \begin{array}{l} \nabla \bullet (\mathbf{r} \times \mathbf{J}(\mathbf{r}))\mathrm{j}_l(\kappa\mathrm{r}) + \\ \nabla \bullet \mathbf{M}(\mathbf{r})\frac{\partial}{\partial \mathrm{r}}(\mathrm{r}\mathrm{j}_l(\kappa\mathrm{r})) \\ -\mathrm{k}^2(\mathbf{r} \bullet \mathrm{M}(\mathbf{r}))\mathrm{j}_l(\kappa\mathrm{r}) \end{array} \right\}.\end{aligned} \tag{4.241}$$

Significant simplifications of these exact results are possible when it is recognized that the source dimensions (i.e., nuclear size) are much smaller than the photon wavelength. In this case, the small-argument limit of the spherical Bessel function,

$$\mathrm{j}_l(\mathrm{x}) \approx \frac{\mathrm{x}^l}{(2l+1)!!} \quad \mathrm{x} \ll 1 \tag{4.242}$$

can be used. Keeping the smallest powers in $\kappa\mathrm{r}$ in the integrals, simplified expressions for the multi-pole coefficients of the form are obtained,

$$\mathrm{a}_{\mathrm{lm}}^{(\mathrm{E})} \cong -\mathrm{i}\frac{\mathrm{c}\kappa^{l+2}}{(2l+1)!!}\sqrt{\frac{l+1}{l}}\left(\mathrm{Q}_{lm} + \mathrm{Q}'_{lm}\right) \tag{4.243}$$

$$\mathrm{a}_{\mathrm{lm}}^{(\mathrm{M})} \cong \mathrm{i}\frac{\mathrm{c}\kappa^{l+2}}{(2l+1)!!}\sqrt{\frac{l+1}{l}}\left(\mathrm{M}_{lm} + \mathrm{M}'_{lm}\right). \tag{4.244}$$

Q_{lm} and M_{lm} are the electric and magnetic multipole moments, respectively, given by,

$$\mathrm{Q}_{lm} = \int \mathrm{d}^3\mathbf{r}\, \mathrm{r}^l\, \mathrm{Y}^*_{lm}(\theta,\phi)\rho_{\mathrm{e}}(\mathrm{r}) \tag{4.245}$$

$$\mathrm{M}_{l\mathrm{m}} = \int \mathrm{d}^3\mathbf{r}\, \mathrm{r}^l\, \mathrm{Y}^*_{l\mathrm{m}}(\theta,\phi)\frac{\nabla \bullet (\mathbf{r}\times\mathbf{J}(\mathbf{r}))}{l+1}. \quad (4.246)$$

The integrations are over the nuclear volume. In addition to these radiation contributions, it is also necessary to consider those linked to the nucleons' intrinsic spins which, classically, produce a spatial distribution of magnetization **M** changing with time. The corresponding electric and magnetic multi-pole moments are,

$$\mathrm{Q}'_{l\mathrm{m}} = -\mathrm{i}\left(\frac{\kappa}{l+1}\right)\int \mathrm{d}^3\mathbf{r}\, \mathrm{r}^l\, \mathrm{Y}^*_{l\mathrm{m}}(\theta,\phi) \times \nabla \bullet (\mathbf{r}\times\mathbf{M}) \quad (4.247)$$

$$\mathrm{M}'_{l\mathrm{m}} = -\mathrm{i}\int \mathrm{d}^3\mathbf{r}\, \mathrm{r}^l\, \mathrm{Y}^*_{l\mathrm{m}}(\theta,\phi)\nabla \bullet \mathbf{M} \quad (4.248)$$

The multi-pole expansions of the electric and magnetic fields are,

$$\mathbf{E}(\mathbf{r}) = \sum_{l=1}^{\infty}\sum_{\mathrm{m}=-l}^{l}\left(\mathrm{a}^{(\mathrm{E})}_{l\mathrm{m}}\mathbf{E}^{(\mathrm{E})}_{l\mathrm{m}}(\mathbf{r}) + \mathrm{a}^{(\mathrm{M})}_{l\mathrm{m}}\mathbf{E}^{(\mathrm{M})}_{l\mathrm{m}}(\mathbf{r})\right) \quad (4.249)$$

$$\mathbf{H}(\mathbf{r}) = \sum_{l=1}^{\infty}\sum_{\mathrm{m}=-l}^{l}\left(\mathrm{a}^{(\mathrm{E})}_{l\mathrm{m}}\mathbf{H}^{(\mathrm{E})}_{l\mathrm{m}}(\mathbf{r}) + \mathrm{a}^{(\mathrm{M})}_{l\mathrm{m}}\mathbf{H}^{(\mathrm{M})}_{l\mathrm{m}}(\mathbf{r})\right) \quad (4.250)$$

Transition Rates for Multi-Pole Radiation

The above derivations of the multi-pole transitions can be used to estimate the rate at which a nucleus can decay through γ emission and what nuclear characteristics dictate this rate. The power radiated in multi-pole radiation is,

$$\mathrm{P}^{(\mathrm{E})}(l,\mathrm{m}) = \frac{1}{2\kappa^2}\sqrt{\frac{\mu_0}{\varepsilon_0}}\left|\mathrm{a}^{(\mathrm{E})}_{l,\mathrm{m}}\right|^2 \quad (4.251)$$

Electric radiation

$$\mathrm{P}^{(\mathrm{M})}(l,\mathrm{m}) = \frac{1}{2\kappa^2}\sqrt{\frac{\mu_0}{\varepsilon_0}}\left|\mathrm{a}^{(\mathrm{M})}_{l,\mathrm{m}}\right|^2 \quad (4.252)$$

Magnetic radiation.

As the transition rate will be this radiated power divided by the photon energy $\hbar\omega$, the transition rates for El and Ml radiation are, respectively,

$$\lambda^{(\mathrm{E})}(l,\mathrm{m}) = \frac{8\pi(l+1)}{\hbar l((2l+1)!!)^2}\left(\frac{\omega}{\mathrm{c}}\right)^{2l+1}\left|\mathrm{Q}_{l\mathrm{m}} + \mathrm{Q}'_{l\mathrm{m}}\right|^2 \quad (4.253)$$

$$\lambda^{(\mathrm{M})}(l,\mathrm{m}) = \frac{8\pi(l+1)}{\hbar l((2l+1)!!)^2}\left(\frac{\omega}{\mathrm{c}}\right)^{2l+1}\left|\mathrm{M}_{l\mathrm{m}} + \mathrm{M}'_{l\mathrm{m}}\right|^2 \quad (4.254)$$

The moments are calculated as follows (see, e.g., Segrè (1977)). From (4.245) to (4.248), for a nucleus of mass m with A nucleons and Z protons,

$$\mathrm{Q}_{l\mathrm{m}} = \mathrm{e}\sum_{\mathrm{n}=1}^{\mathrm{Z}}\int \mathrm{d}^3\mathbf{r}\, \mathrm{r}^l_{\mathrm{n}}\, \mathrm{Y}^*_{l\mathrm{m}}(\theta_{\mathrm{n}},\phi_{\mathrm{n}})\psi^*_{\mathrm{f}}(\mathbf{r})\psi_{\mathrm{i}}(\mathbf{r}) \quad (4.255)$$

$$\mathrm{M}_{l\mathrm{m}} = -\left(\frac{l}{l+1}\right)\left(\frac{\mathrm{e}\hbar}{\mathrm{m_n c}}\right) \times \sum_{\mathrm{n}=1}^{\mathrm{Z}}\int \mathrm{d}^3\mathbf{r}\, \mathrm{r}^l_{\mathrm{n}}\, \mathrm{Y}^*_{l\mathrm{m}}(\theta_{\mathrm{n}},\phi_{\mathrm{n}})\nabla\bullet\left(\psi^*_{\mathrm{f}}(\mathbf{r})\mathbf{L}_{\mathrm{n}}\psi_{\mathrm{i}}(\mathbf{r})\right) \quad (4.256)$$

$$\mathrm{Q}'_{l\mathrm{m}} = -\mathrm{i}\frac{(\omega/\mathrm{c})}{l+1}\left(\frac{\mathrm{e}\hbar}{2\mathrm{m_n c}}\right)\sum_{\mathrm{n}=1}^{\mathrm{A}}\int \mathrm{d}^3\mathbf{r}\, \mathrm{r}^l_{\mathrm{n}}\, \mathrm{Y}^*_{l\mathrm{m}}(\theta_{\mathrm{n}},\phi_{\mathrm{n}}) \times \nabla \bullet \left(\psi^*_{\mathrm{f}}(\mathbf{r})(\mathbf{r}_{\mathrm{n}}\times\boldsymbol{\sigma})_{\mathrm{n}}\psi_{\mathrm{i}}(\mathbf{r})\right) \quad (4.257)$$

$$\mathrm{M}'_{l\mathrm{m}} = -\left(\frac{\mathrm{e}\hbar}{2\mathrm{m_n c}}\right) \times \sum_{\mathrm{n}=1}^{\mathrm{A}}\int \mathrm{d}^3\mathbf{r}\, \mu_{\mathrm{n}}\, \mathrm{r}^l_{\mathrm{n}}\mathrm{Y}^*_{l\mathrm{m}}(\theta_{\mathrm{n}},\phi_{\mathrm{n}})\nabla\bullet\left(\psi^*_{\mathrm{f}}(\mathbf{r})\boldsymbol{\sigma}_{\mathrm{n}}\psi_{\mathrm{i}}(\mathbf{r})\right) \quad (4.258)$$

where μ_{n} is the magnetic moment of the nth nucleon in units of $\mathrm{e}\hbar/2\mathrm{m_n c}$. For the moments due to charge, the summations are over the protons only; for those due to spin, the summations are over all nucleons. The transition probabilities are obtained by averaging $\lambda^{(\mathrm{E})}(l,\mathrm{m})$ and $\lambda^{(\mathrm{M})}(l,\mathrm{m})$ over the initial $\mathrm{m_i}$ states and summed over the final $\mathrm{m_f}$ states,

$$\lambda^{(\mathrm{E})}(l) = \frac{1}{2\mathrm{J_i}+1}\sum_{\mathrm{m_i}}\sum_{\mathrm{m_f}}\lambda^{(\mathrm{E})}(l,\mathrm{m}) \tag{4.259}$$

and

$$\lambda^{(\mathrm{M})}(l) = \frac{1}{2\mathrm{J_i}+1}\sum_{\mathrm{m_i}}\sum_{\mathrm{m_f}}\lambda^{(\mathrm{M})}(l,\mathrm{m}). \tag{4.260}$$

A transition rate calculation based upon the above expressions for the multi-pole moments is clearly quite involved and requires detailed knowledge of the nucleus. However, calculations for simple scenarios are possible, e.g., that of a single nucleon outside closed shells making an electromagnetic transition. Following the approach of Weisskopf (1951), a number of simplifications can be employed in order to solve for the moments so as to obtain expressions for electric and magnetic transition rates. The results are, while not accurate, elucidating and useful. One begins by invoking the independent-particle model of Chap. 3 in which there is a single nucleon outside a closed shell. Consider the case of the single proton being in an initial state with orbital angular momentum l making a transition to a final state with zero orbital angular momentum through the emission of electric multi-pole radiation of order l. Further, assume that the nucleon's spin is parallel to the orbital angular momentum (i.e., the transition is parity favored). Then the nucleon wavefunctions in the initial and final states are,

$$\psi_\mathrm{i} = \mathrm{g_i}(\mathrm{r})\mathrm{Y}_{l\mathrm{m}}(\theta,\phi)\mathrm{s} \tag{4.261}$$

$$\psi_\mathrm{f} = \frac{\mathrm{g_f}(\mathrm{r})}{\sqrt{4\pi}}\mathrm{s}. \tag{4.262}$$

where s is a spin function. If these are substituted into the expression for $\mathrm{Q}_{l\mathrm{m}}$ given by (4.255) (only the first term in the summation contributes), then,

$$\mathrm{Q}_{l\mathrm{m}} = \frac{\mathrm{e}}{\sqrt{4\pi}}\int_0^\infty \mathrm{d}\mathrm{r}\,\mathrm{r}^{l+2}\mathrm{g_i}(\mathrm{r})\mathrm{g_f}(\mathrm{r}). \tag{4.263}$$

A rough order-of-magnitude estimate of this integral is obtained by assuming that radial components of the nucleon wavefunctions are,

$$\begin{aligned}\mathrm{g_i}(\mathrm{r}) = \mathrm{g_f}(\mathrm{r}) &= \mathrm{C} \quad \mathrm{r} < \mathrm{R_N}\\ &= 0 \qquad \mathrm{r} > \mathrm{R_N}\end{aligned} \tag{4.264}$$

where $\mathrm{R_N}$ is the nuclear radius. From the normalization of the wavefunctions, $\mathrm{C} = \sqrt{3}/\mathrm{R_N^3}$ and we obtain an approximation to the electric multi-pole moment,

$$\mathrm{Q}_{l\mathrm{m}} \approx \frac{3\mathrm{e}}{\sqrt{4\pi}}\frac{\mathrm{R_N^{\,l}}}{l+3}. \tag{4.265}$$

The other moments are determined from ratios with this expression. Note that, in (4.256), the divergence operator can be approximated by $1/\mathrm{R_N}$ and that the operator $\mathbf{L}_\mathrm{n}$ will approximately cancel the $(l+1)$ factor in the denominator. These then provides the approximate ratio,

$$\frac{\mathrm{M}_{l\mathrm{m}}}{\mathrm{Q}_{l\mathrm{m}}} \approx \frac{\hbar\mathrm{c}}{\mathrm{m_n R_n}}. \tag{4.266}$$

The magnetic multi-pole moment $\mathrm{M}'_{l\mathrm{m}}$, which is due to the nucleons' spins, is roughly 2–3 times greater than that due to the nucleon orbits, $\mathrm{M}_{l\mathrm{m}}$, as can be surmised by comparing the ratio $\mathbf{L}/l+1$ with $\mu_\mathrm{n}\sigma$. Hence, it would not be unreasonable to approximate the ratio,

$$\frac{\left|\mathrm{M}_{l\mathrm{m}}+\mathrm{M}'_{l\mathrm{m}}\right|^2}{\left|\mathrm{Q}_{l\mathrm{m}}\right|^2} \approx 10\frac{\hbar\mathrm{c}}{\mathrm{m_n R_n}}. \tag{4.267}$$

The spin electric multi-pole moment $\mathrm{Q}'_{l\mathrm{m}}$ can be neglected in this approximation as can be shown by replacing the divergence operator in (4.257) with $l/\mathrm{R_N}$ to find that,

$$\frac{\mathrm{Q}'_{l\mathrm{m}}}{\mathrm{Q}_{l\mathrm{m}}} \approx \frac{\hbar\omega}{\mathrm{m_n}} \approx 10^{-3} \tag{4.268}$$

for photon energies typical in γ transitions. Using these approximations and (3.121), the transition probabilities for the Weisskopf single-proton model are, for photon energy k (replacing $\hbar\omega$) in MeV,

$$\begin{aligned}\lambda^{(\mathrm{E})}(l) = {}& \frac{4.4(l+1)}{l((2l+1)!!)^2}(1.2)^{2l}\left(\frac{\mathrm{k}}{197}\right)^{2l+1}\\ &\times \mathrm{A}^{2l/3}10^{2l}\mathrm{s}^{-1}\end{aligned} \tag{4.269}$$

$$\begin{aligned}\lambda^{(\mathrm{M})}(l) = {}& \frac{1.9(l+1)}{l((2l+1)!!)^2}(1.2)^{2l-2}\left(\frac{\mathrm{k}}{197}\right)^{2l+1}\\ &\times \mathrm{A}^{(2l-2)/3}10^{2l}\mathrm{s}^{-1}\\ = {}& \frac{0.3}{\mathrm{A}^{2/3}}\lambda^{(\mathrm{E})}(l)\end{aligned} \tag{4.270}$$

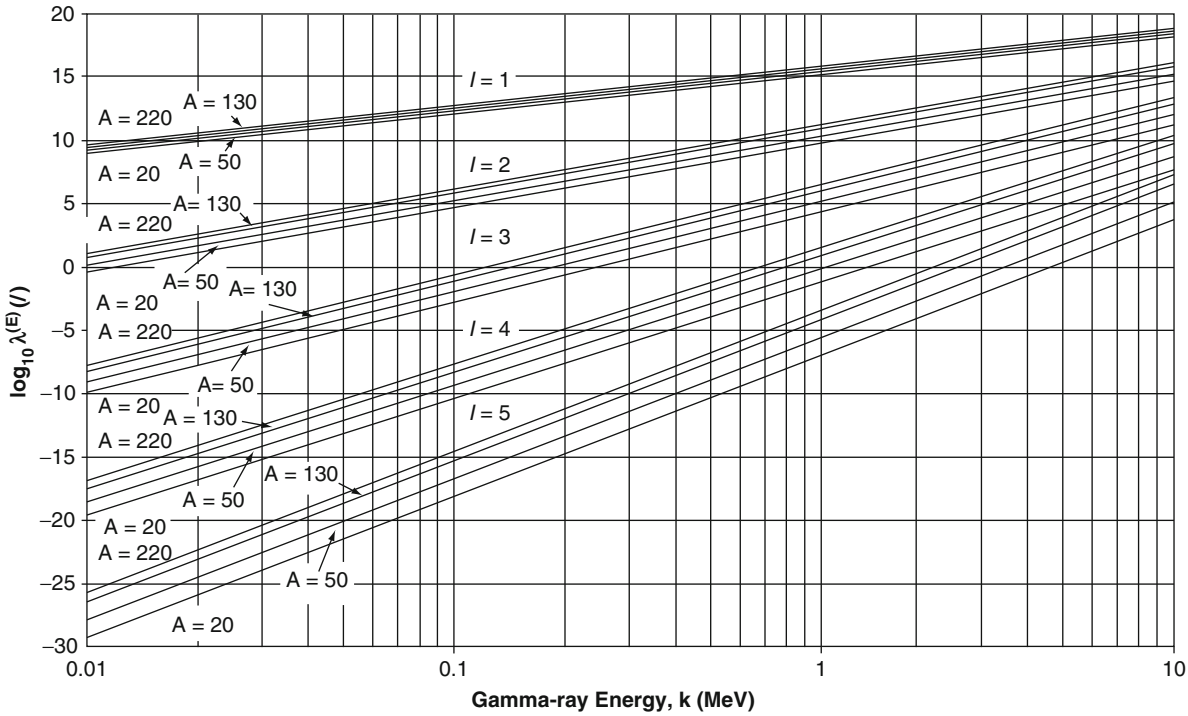

Fig. 4.32 Logarithm of the electric multi-pole transition probability (in s^{-1}) as a function of γ-ray energy for multi-pole orders of 1 through 5 and nuclei with atomic mass numbers of 20, 50, 130, and 220 calculated from the Weisskopf single-proton model. Internal conversion contributions are excluded

These transition probabilities are plotted in Figs. 4.32 and 4.33.

The general characteristics of these transition probabilities are as follows:

- The transition probabilities increase with γ-ray energy, with the rate of increase increasing with multi-pole order.
- For a given γ-ray energy, both transition probabilities decrease by up to about six orders-of-magnitude for each unit increase in l – hence, the dipole and quadrupole transitions will dominate.
- With the exception of the magnetic dipole radiation, the transition probability increases with atomic mass number.
- The magnetic multi-pole transition probability is at least an order-of-magnitude less than that of the electric multi-pole (for a given multi-pole order and photon energy) and decreases with increasing atomic number.

It is important to recall the approximations used to calculate the multi-pole moments, including the assumption of a single transiting nucleon, in the derivation of these multi-pole transition rates. Hence, one should not expect these results to be accurate in predicting γ-transition rates. In fact, Blatt and Weisskopf suggest that the above expressions overestimate the actual transition rates by factors of up to three orders-of-magnitude. Even despite the size of this error, the calculations are of some benefit, if not just for understanding the qualitative aspects of γ-transition rates, but when one recognizes that for γ-ray energies of less than about 1 MeV, there is a six orders-of-magnitude decrease in the multi-pole transition rates per unit increase in multi-pole order.

4.4.3 Internal Conversion

4.4.3.1 Introduction

In the discussion of γ decay, the excited nucleus was treated in isolation. One of the consequences of this

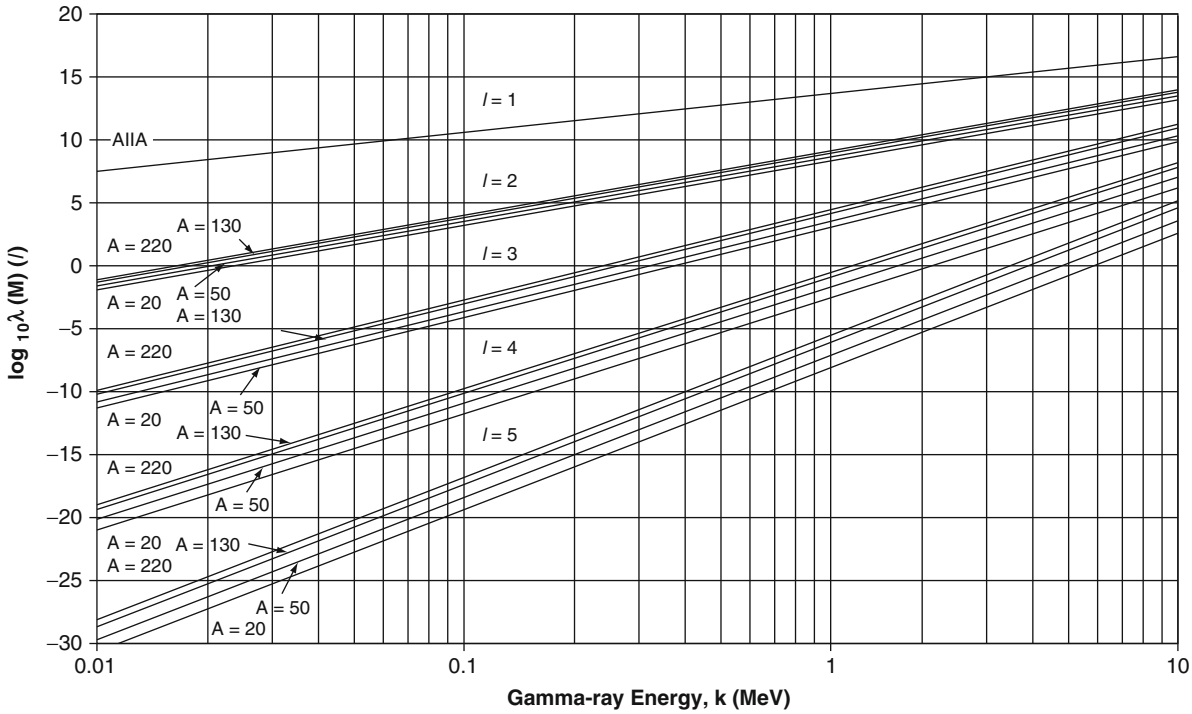

Fig. 4.33 Logarithm of the magnetic multi-pole transition probability (in s^{-1}) as a function of γ-ray energy for multipole orders of 1 through 5 and nuclei with atomic mass numbers of 20, 50, 130, and 220 calculated from the Weisskopf single-proton model. Contributions from internal conversion are excluded

consideration was that it was impossible for an excited nucleus to make a transition between states each with zero angular momentum through the emission of electromagnetic radiation. In reality, however, the nucleus is not isolated but is contained within the atom and interacts with the orbiting atomic electrons. This interaction provides two additional channels for the excited nucleus to lose energy: IC, in which there is direct energy-transfer to an atomic electron through a virtual photon (i.e., it is not an internal photoelectric process in which a photon is emitted from the nucleus and absorbed by the electron), and, should the energy of the transition exceed twice the electron rest mass, internal pair production. The latter process is infrequent and is not considered here.

As noted earlier, if the energy of the transition exceeds the atomic electron binding energy (which is usually the case), the electron is ejected. The IC coefficient is the ratio of the mean number of IC electrons ejected to the mean number of γ rays emitted,

$$\alpha^{(\mathrm{IC})} = \frac{\overline{\mathrm{N}}_{\mathrm{ICe}}}{\overline{\mathrm{N}}_{\gamma}}. \tag{4.271}$$

The coefficient is decomposed into those contributions from electrons in different orbitals,

$$\alpha^{(\mathrm{IC})} = \alpha_{\mathrm{K}}^{(\mathrm{IC})} + \alpha_{\mathrm{L}}^{(\mathrm{IC})} + \alpha_{\mathrm{M}}^{(\mathrm{IC})} + \cdots. \tag{4.272}$$

A full and proper evaluation of the transition probabilities of the previous section would include a multiplicative factor of $1 + \alpha^{(\mathrm{IC})}$ to include the contributions of IC.

The contributions of IC to internal radiation dosimetry are significant (Smith et al. 1965). The ejected IC electrons travel short distances in tissue transferring energy to tissue as they slow down and, hence, produce an absorbed dose. The immediate atomic consequence of the ejection of the IC electron is that a vacancy is produced amongst the atomic electron

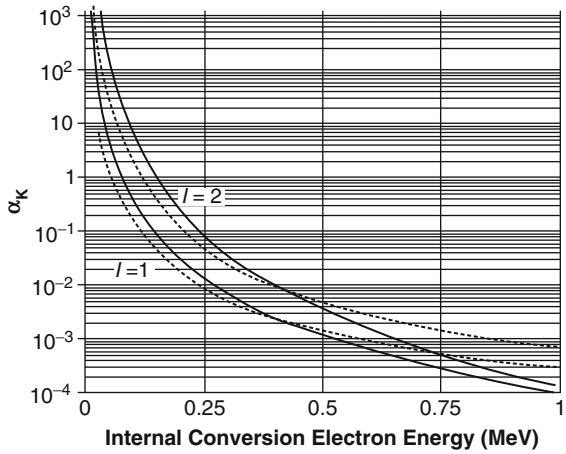

Fig. 4.34 K-orbital internal conversion coefficients for electric multi-poles $l = 1,2$ calculated from (4.289) (*solid lines*) and from the tabulated values of Widman and Powsner (1970) (*dashed line*) for $Z = 40$ (zirconium)

orbitals. This vacancy is filled by the transition of an electron from another orbital and the consequent emission of a characteristic (or fluorescent) X-ray or an Auger electron cascade. These also contribute to the absorbed dose to tissue and are the subjects of Chap. 6.

4.4.3.2 Calculation of the Internal Conversion Coefficient

Introduction

A full calculation of the IC coefficient will be quite involved, requiring detailed knowledge of the pre- and posttransition nuclear wavefunctions. Here, a simplified calculation of the conversion coefficient will be presented. However, it is one which is sufficient to demonstrate the gross dependence of the coefficient upon multi-pole order, excitation energy and atomic number. Tables of IC coefficients have been provided, for example, by Hager and Seltzer (1968) and current values are provided by the National Nuclear Data Center website http://www.nndc.bnl.gov/hsicc/; Widman and Powsner (1970) have provided tables of these coefficients for internal absorbed dose calculations. A critical evaluation of published IC coefficients has been provided recently by Kibédi et al. (2007).

The main contributor to the IC process is the static Coulomb interaction between the protons and the atomic electron. As IC will be more probable for K-shell electrons due to the greater overlap of nuclear and electronic wavefunctions, a calculation of $\alpha_K^{(IC)}$ is developed here using perturbation theory. The calculation is simplified by assuming that the ejected electron is nonrelativistic and, thus, can be modeled by a plane wave. The initial wavefunction is the product of the nuclear initial wavefunction and that of the K-shell electron and the final wavefunction is the product of the nuclear final wavefunction and the electron plane wave. Hence,

$$\psi_i = \psi_{nuc,i}\sqrt{\frac{Z^3}{\pi r_\infty^3}}\, e^{-(ZR/r_\infty)} \tag{4.273}$$

where r_∞ is the Bohr radius and,

$$\psi_f = \psi_{nuc,f}\left(\frac{1}{L^{3/2}}\right)e^{i\left(\frac{p_e \bullet R}{\hbar c}\right)} \tag{4.274}$$

where $\mathbf{R}$ is the position vector of the electron. The Coulomb interaction potential between the protons and the atomic electron is,

$$U = \alpha\hbar c \sum_{i=1}^{Z} \frac{1}{|\mathbf{R} - \mathbf{r}_i|} \tag{4.275}$$

where $\mathbf{r}_i$ is the position vector of the 1th proton.

Calculation of the Matrix Element

The matrix element is,

$$M_{if} = \alpha\hbar c\sqrt{\frac{Z^3}{\pi L^3 r_\infty^3}}\sum_{n=1}^{Z}\int d^3\mathbf{R}\int d^3\mathbf{r}_n \psi^*_{nuc,f}(\mathbf{r}_n) \times e^{-\left(\frac{p_e \bullet R}{\hbar c}\right)}\frac{1}{|\mathbf{R} - \mathbf{r}_n|} \times e^{-(ZR/r_\infty)}\psi_{nuc,i}(\mathbf{r}_n) \tag{4.276}$$

where the integration over $\mathbf{R}$ is over the electron position. The double integral is solved by first using the substitution of variable $\mathbf{R}' = \mathbf{R} - \mathbf{r}_n$ and noting that $Zr \gg r_\infty$ which allows the approximation $e^{-(ZR/r_\infty)} \approx 1$,

$$\begin{aligned}
&\int d^3\mathbf{R}\int d^3\mathbf{r}_n\psi^*_{nuc,f}(\mathbf{r}_n)e^{-\left(\frac{p_e\bullet\mathbf{R}}{\hbar c}\right)}\frac{1}{|\mathbf{R}-\mathbf{r}_n|}\\
&\quad\times e^{-\left(ZR/a\infty\right)}\psi_{nuc,i}(\mathbf{r}_n)\\
&\approx\int d^3\mathbf{r}_n\psi^*_{nuc,f}(\mathbf{r}_n)e^{-\frac{p_e\bullet\mathbf{r}_n}{\hbar c}}\psi_{nuc,i}(\mathbf{r}_n)\int d^3\mathbf{R}'\frac{e^{-\frac{p_e\bullet\mathbf{R}'}{\hbar c}}}{R'}\\
&=4\pi\left(\frac{\hbar c}{p_e}\right)^2\int d^3\mathbf{r}_n\psi^*_{nuc,f}(\mathbf{r}_n)e^{-\frac{p_e\bullet\mathbf{r}_n}{\hbar c}}\psi_{nuc,i}(\mathbf{r}_n)
\end{aligned}\tag{4.277}$$

to give,

$$\begin{aligned}
M_{if}&=4\pi\alpha\hbar c\sqrt{\frac{Z^3}{\pi L^3r_\infty^3}}\left(\frac{\hbar c}{p_e}\right)^2\\
&\quad\times\sum_{n=1}^{Z}\int d^3\mathbf{r}_n\psi^*_{nuc,f}(\mathbf{r}_n)e^{-\left(\frac{p_e\bullet\mathbf{r}_n}{\hbar c}\right)}\psi_{nuc,i}(\mathbf{r}_n).
\end{aligned}\tag{4.278}$$

The remaining integral is solved by, first expanding the plane wave into spherical waves,

$$e^{i\mathbf{b}\bullet\mathbf{r}}=4\pi\sum_{l=0}^{\infty}\sum_{m=-l}^{l}i^l j_l(br)Y^*_{lm}(\theta_b,\phi_b)Y_{lm}(\theta_r,\phi_r).\tag{4.279}$$

As $\left(p_e r/\hbar c\right)\ll 1$, the small-argument approximation to the spherical Bessel function can be used,

$$\begin{aligned}
e^{-\frac{p_e\bullet r_n}{\hbar c}}&=4\pi\sum_{l=0}^{\infty}\sum_{m=-l}^{l}\frac{(-i)^l}{(2l+1)!!}\left(\frac{p_e}{\hbar c}\right)^l r_n^l\\
&\quad\times Y_{lm}(\theta_e,\phi_e)Y^*_{lm}(\theta_n,\phi_n)
\end{aligned}\tag{4.280}$$

where the e and n subscripts of the angular variables refer to the electron and nucleon, respectively. Substituting (4.280) into (4.278) gives,

$$\begin{aligned}
M_{if}&=16\pi^2\alpha\hbar c\sqrt{\frac{Z^3}{\pi L^3r_\infty^3}}\sum_{n=1}^{Z}\sum_{l=0}^{\infty}\sum_{m=-l}^{l}\frac{(-i)^l}{(2l+1)!!}\left(\frac{p_e}{\hbar c}\right)^{l-2}\\
&\quad\times\int d^3\mathbf{r}_n\psi^*_{nuc,f}(\mathbf{r}_n)r_n^l\psi_{nuc,i}(\mathbf{r}_n)\\
&\quad\times Y_{lm}(\theta_e,\phi_e)Y^*_{lm}(\theta_n,\phi_n).
\end{aligned}\tag{4.281}$$

Recalling the definition of the electric multi-pole moment for electric charge given by (4.255), (4.281) can be reduced to,

$$\begin{aligned}
M_{if}&=16\pi^2\left(\frac{\alpha\hbar c}{e}\right)\sqrt{\frac{Z^3}{\pi L^3r_\infty^3}}\\
&\quad\times\sum_{l=0}^{\infty}\sum_{m=-l}^{l}\frac{(-i)^l}{(2l+1)!!}\left(\frac{p_e}{\hbar c}\right)^{l-2}Y_{lm}(\theta_e,\phi_e)Q_{lm}
\end{aligned}\tag{4.282}$$

with the squared amplitude,

$$\begin{aligned}
|M_{if}|^2&=256\pi^3\left(\frac{\alpha\hbar c}{e}\right)^2\frac{Z^3}{L^3r_\infty^3}\sum_{l=0}^{\infty}\sum_{m=-l}^{l}\sum_{l'=0}^{\infty}\\
&\quad\times\sum_{m=-l'}^{l'}\frac{(-i)^l i^{l'}}{((2l+1)!!)((2l+1)!!)}\\
&\quad\times\left(\frac{p_e}{\hbar c}\right)^{l+l'-4}Y_{lm}(\theta_e,\phi_e)Y^*_{l'm'}(\theta_e,\phi_e)Q_{lm}\,Q^*_{l'm'}.
\end{aligned}\tag{4.283}$$

Calculation of the Phase Space Factor

This is a straightforward calculation as only a single particle is ejected The number of states available in the differential element of momentum dp_e and differential solid angle $d\Omega_e$ is,

$$d^2N=\left(\frac{L}{2\pi\hbar c}\right)^3 p_e^2\,dp_e\,d\Omega_e.\tag{4.284}$$

As $p_e dp_e = m_e dT_e$ (the electron is considered non-relativistic), then,

$$\begin{aligned}
d\rho_f&=\frac{d^2N}{dT_e}\\
&=\left(\frac{L}{2\pi\hbar c}\right)^3 m_e\,p_e\,d\Omega_e.
\end{aligned}\tag{4.285}$$

Internal Conversion Transition Rate

The IC transition rate for a K-orbital electron is,

$$\lambda_K^{(IC)}=2\frac{2\pi}{\hbar}|M_{if}|^2\rho_f\tag{4.286}$$

where the additional factor of 2 is due to the two electrons in the K orbit. Inserting (4.283) and (4.285)

into (4.286), integrating $d\rho_f$ over Ω_e and noting the orthonormalization of the spherical harmonics, $\int d\Omega_e\, Y_{lm}(\theta_e, \phi_e) Y^*_{l'm'}(\theta_e, \phi_e) = \delta_{ll'}\delta_{mm'}$, an expression for the K-orbital transition rate is obtained,

$$\lambda_K^{(IC)} = \frac{128\,\pi\, m_e\, \alpha^2 Z^3}{\hbar\, e^2\, r_\infty^3} \times \sum_{lm} \frac{1}{((2l+1)!!)^2}\left(\frac{p_e}{\hbar c}\right)^{2l-3} |Q_{lm}|^2. \quad (4.287)$$

As only the static Coulomb interaction has been considered and, from (4.268), one can neglect the contribution Q'_{lm}, comparing the K-orbital transition rate directly with the electric multi-pole transition rate of (4.253), a crude approximation to the IC coefficient for K-orbital electrons is had,

$$\alpha_K \approx 16\left(\frac{Z^3}{r_\infty^4}\right)\left(\frac{l}{l+1}\right)\left(\frac{p_e}{\hbar c}\right)^{2l-3}\left(\frac{\hbar c}{k}\right)^{2l+1} \quad (4.288)$$

replacing $\hbar\omega$ with k. It is reasonable to assume that the nuclear excitation energy exceeds the binding energy of the K-orbital electrons, in which case, $p_e = \sqrt{2m_e k}$, and,

$$\alpha_K \approx \left(\frac{\hbar c}{m_e r_\infty}\right)^4 Z^3 \left(\frac{l}{l+1}\right)\left(\frac{2m_e}{k}\right)^{l+5/2} \quad (4.289)$$

This result is a reasonable approximation when the electron can be considered as nonrelativistic and the transition energy greatly exceeds the atomic electron binding energy. The main considerations of this formula are that IC increases strongly with atomic number and multi-pole order, but decreases with increasing transition energy. Hence, IC is important for high-Z nuclei in low-energy transitions of high multi-pole order. Figure 4.33 shows the IC coefficient for K-orbital electrons for zirconium as a function of IC electron kinetic energy as calculated from (4.289) for the electric multi-poles $l = 1, 2$. Full calculation of the IC coefficients would consider the total contributions of all electromagnetic interactions and, hence, would include the effects of the magnetic multi-pole moments. While the K-orbital electrons will dominate in IC, the L- and M-orbital electrons will make contributions, albeit with lower probability.

$0 \rightarrow 0$ Transitions

As discussed earlier, electromagnetic transitions between nuclear states with zero angular momentum are not possible as there are no $l = 0$ multi-poles in the radiation field. However, closer examination of the above derivation of the IC coefficient will demonstrate that such a transition is feasible in which the K-orbital electron takes away the energy. This statement, at first sight, contradicts the above result of (4.286) in which the multi-pole moment would go to zero for a $0 \rightarrow 0$ transition. However, the above derivation excluded the contribution to the matrix element when $R > R_n$, i.e., when the electron is within the nucleus. Inclusion of this contribution leads to the small probability of a $0 \rightarrow 0$ transition. The fact that this is possible demonstrates that IC cannot be interpreted as a photoelectric effect in which the photon emitted from the nucleus is absorbed by an atomic electron which is subsequently ejected.

4.4.4 Nuclear Isomerism

4.4.4.1 Introduction

The γ-transition selection rules described earlier can delay a γ transition significantly such that the excited nucleus can have a long half-life, up to years. Such nuclei are described as being in an *isobaric* state or as being *metastable*. Clearly, such isomeric transitions (ITs) are associated with large changes in nuclear angular momentum ΔJ and small transition energies. But we have also seen that these conditions are preferential for IC. ITs are frequently associated with β decay which leaves the nucleus with a high angular momentum, as shown schematically in Fig. 4.35.

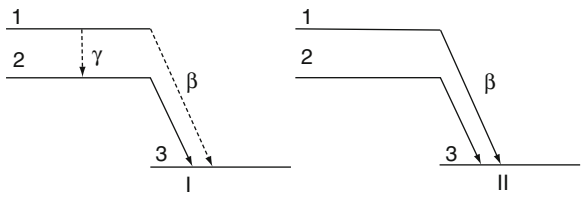

Fig. 4.35 Schematic representation of nuclear isomerism. In example I, level 1 decays predominantly through γ emission to level 2 which subsequently decays to level 3 through β decay. In example II, levels 1 and 2 undergo β decay independently to level 3

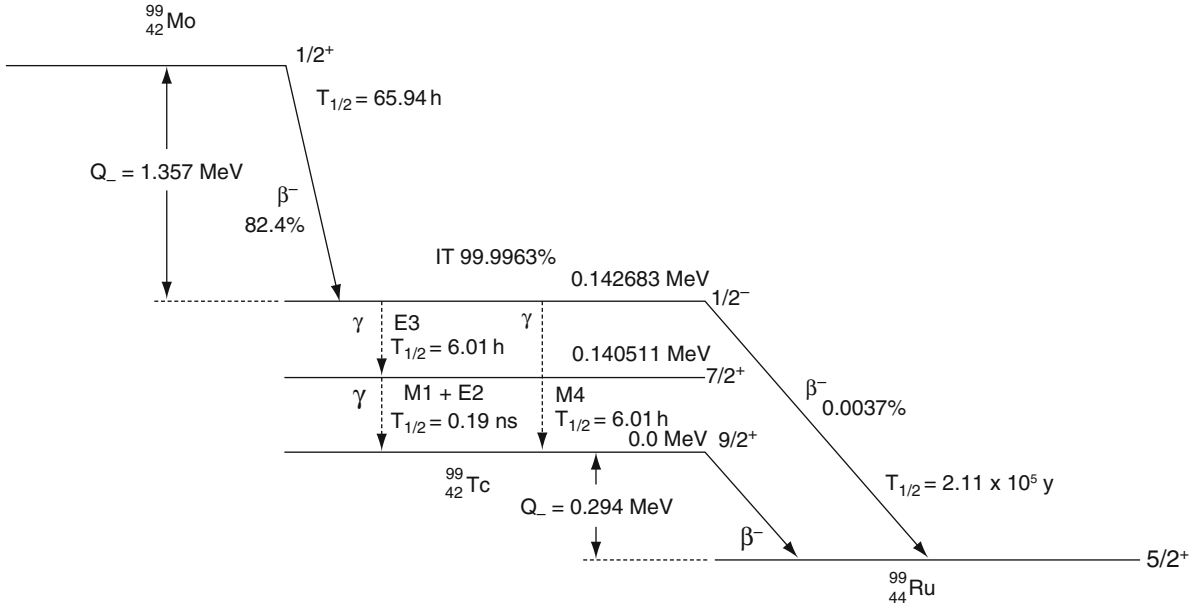

Fig. 4.36 Decay scheme ^{99}Mo→^{99,99m}Tc→^{99}Ru. (IT ≡ isomeric transition)

In Example I, the probability of level 1 decaying to level 2 through an IT exceeds the probability of it decaying to level 3 through β decay; in Example II, levels 1 and 2 transit to level 3 independently through β decay. If, in Example I, the transition rate for the γ transition from level 1 to level 2 is much greater or much less than that for the β-decay to level 3, then the β spectrum of level 2 with a transition rate equal to the IT of 1 → 2 is demonstrated. In the case of Example II, the levels 1 and 2 decay independently to level 3.

It was Weizsäcker who proposed the theory of nuclear isomers to explain the observation of long-lived γ-ray emitting isotopes. Equations (4.269) and (4.270) show that γ transitions with half-lives of a second or more for photon energies of about 0.1–0.5 MeV (typical for nuclear medicine) are between nuclear states with ΔJ = 3. A common example of an IT used in diagnostic nuclear medicine is the de-excitation of the ^{99m}Tc nucleus (the m superscript refers to its metastable state) to the ground state ^{99}Tc with a 6.01 h half-life (while ^{99m}Tc can undergo β^- decay to ^{99}Ru, the associated branching ratio is a negligible 3.7×10^{-5}); this is shown in Fig. 4.36. ^{99}Tc and ^{99m}Tc both result from the β^- decay of ^{99}Mo. The spin/parity (J^π) of the ^{99}Tc ground state is $9/2^+$ due to an unpaired proton in the $1g_{9/2}$ shell. The excited ^{99m}Tc nucleus is formed in the $J^\pi = 1/2$ level and can de-excite directly to the $9/2^+$ ground state via the emission of a 142.683 keV photon, with a branching ratio of about 3×10^{-4}. However, the difference in the angular momenta of the two states is significant: $\Delta J = 4$ and the transition is M4 (as there is also a change in parity) with a 6.01 h half-life. It can also de-excite with the same half-life to the intermediate $7/2^+$ excited state at the 140.511 keV level with $\Delta J = 3$ via an E3 transition (as there is no change in parity). This is followed by the de-excitation from this $7/2^+$ state to the $9/2^+$ ground state through a combination of M1 and E2 transitions ($\Delta J = 1$) with the emission of a 140.511 keV γ ray which is used for imaging.

References

Alvarez LW (1937) Nuclear K electron capture. Phys Rev 52:134–135

Anderson CD (1933) The positive electron. Phys Rev 43:491–494

Behrens H, Jähnecke J (1969) Numerische Tabellen für Beta-Zerfall und Elektronen-Einfang. In: Schopper H (ed) Landolt-Börnstein Gruppe I, Bd 4. Springer, Berlin

Blatt JM, Weisskopf VF (1979) Theoretical nuclear physics. Dover, New York

Bowkamp JJ, Casimir HBG (1954) On multipole expansions in the theory of electromagnetic radiation. Physica XX: 539–554

Condon EU, Gurney RW (1928) Wave mechanics and radioactive disintegration. Nature 122:439
Conversi M, Pancini E, Piccioni O (1947) On the disintegration of negative mesons. Phys Rev 71:209–210
Cox RT, McIlwraith CG, Kurrelmeyer B (1928) Apparent evidence of polarization in a beam of β-rays. Proc Nat Acad Sci 14:544–549
Danby G, Gaillard JM, Goulianos K, Lederman LM, Mistry NB, Schwartz M, Steinberger J (1962) Observations of high-energy neutrino reactions and the existence of two kinds of neutrinos. Phys Rev Lett 9:36–44
Fermi E (1934a) Tentativo di una teoria dei raggi β. Nuovo Cimento 11:1–19
Fermi E (1934b) Versuch einer theorie der β-strahlen I. Z Physik 1934:161–171
Gamow G (1928) Zur Quantentheorie des Atomkernes. Z Phys 51:204–212
Gamow G, Teller E (1936) Selection rules for the β-disintegration. Phys Rev 49:895–899
Gerward L (1999) Paul Villard and his discovery of gamma rays. Phys Perspect 1:367–383
Goldhaber M, Grodzins L, Scharff-Goldhaber G (1948) Identification of beta-rays with atomic electrons. Phys Rev 73:1472–1473
Goldhaber GL, Grodzins L, Sunyar AW (1958) Helicity of neutrinos. Phys Rev 109:1015–1017
Grotz K, Klapdor HV (1990) The weak interaction in nuclear, particle and astrophysics. Adam Hilger, Bristol
Hager RS, Seltzer EC (1968) Nucl Data A4:1–235
Jackson JD (1999) Classical electrodynamics. Wiley, New York
Kibédi T, Burrows TM, Trzhaskovskay MB et al (2007) Internal conversion coefficients – how good are they now? In: International Conference on Nuclear Data for Science and Technology 2007. http://nd2007.edpsciences.org/index.php?option=article&access=standard&Itemid=129&url=/articles/ndata/abs/2007/01/ndata07771/ndata07771.html. Accessed 2008
Kodama K, Ushida N, Anderopoulos C et al (2001) Observation of tau neutrino interactions. Phys Lett B 504:218–224
Lee TD, Yang CN (1956) Question of parity conservation in weak interactions. Phys Rev 104:254–258
Lipkin HJ (1962) Beta decay for pedestrians. North-Holland, Amsterdam
Marshak RE (1942) Forbidden transitions in β-decay and orbital electron capture and spins of nuclei. Phys Rev 61:431–449
Martins RA (1997) Becquerel and the choice of uranium compounds. Arch Hist Exact Sci 51:67–81
National Nuclear Data Center (2008) Chart of Nuclides. http://www.nndc.bnl.gov. Accessed 2005–2008
Neddermeyer SH, Anderson CD (1937) Note on the nature of cosmic-ray particles. Phys Rev 51:884–886
Particle Data Group (2004) Review of particle physics. Phys Lett B 592:1–1109
Perl ML, Abrams GS, Boyarski AM et al (1975) Evidence for anomalous lepton production in e^+–e^- annihilation. Phys Rev Lett 35:1489–1492
Reines F (1997) The neutrino: from poltergeist to particle. In: Ekspong G (ed) Nobel lectures, physics 1991–1995. World Scientific, Singapore
Reines F, Cowan CL Jr (1953) Detection of the free neutrino. Phys Rev Let 92:830–831
Rutherford E, Royds T (1909) The nature of the α-particle from radioactive substances. Phil Mag 17:281–286
Sargent BW (1933) The maximum energy of the β-rays from uranium X and other bodies. Proc Roy Soc (London) A139:659–673
Segrè E (1970) Enrico Fermi – physicist. University of Chicago, Chicago
Segrè E (1977) Nuclei and particles. Benjamin/Cummings, Reading
Smith EM, Harris CC, Rohrer RH (1965) Calculation of local energy deposition due to electron capture and internal conversion. J Nucl Med 7:23–31
Tsoulfanidis N (1995) Measurement and detection of radiation, 2nd edn. Taylor and Francis, Washington
Weisskopf VF (1951) Radiative transition probabilities in nuclei. Phys Rev 83:1073
Widman JC, Powsner ER (1970) Internal conversion coefficients for absorbed dose calculations. Phys Med Biol 15:99–106
Wilson D (1983) Rutherford – simple genius. Hodder and Stoughton, London
Wu CS, Ambler E, Hayward RW, Hoppes DD, Hudson RP (1957) Experimental test of parity conservation in beta decay. Phys Rev 105:1413–1415